NORTHWESTERN UNIVERSITY

Phase-Separated Elastomers: Novel Syntheses and Characterization

A DISSERTATION

SUBMITTED TO THE GRADUATE SCHOOL
IN PARTIAL FULFILLMENT OF THE REQUIREMENTS

for the degree
DOCTOR OF PHILOSOPHY
Field of Chemical Engineering

By
Elizabeth Ann Wilson Dhulst

EVANSTON, ILLINOIS
JUNE 2017

ABSTRACT

Phase-Separated Elastomers:
Novel Syntheses and Characterization

Elizabeth Dhulst

Phase separation in segmented polymers provides distinct challenges in regard to their chemical reaction kinetics and characterization. Well studied, it has been shown that structure, phase separation and non-covalent interactions are key factors in the design of elastomeric polyurethanes. Specifically, this dissertation is focused on two areas: the synthesis of novel materials that, through these factors, have potential for use as polyurethane replacements and the novel application of fluorescence to discern aromatic interactions in phase-separated polyurethanes.

In this work, two synthetic routes are employed to generate elastomers: multicomponent thiol reactions and amine-vinyl sulfone polymerizations. Using thiol-based click reactions, thiol-acrylate-epoxide hybrid polymers were produced by two simultaneous reactions at room temperature in a one-pot synthesis. Beyond good mechanical properties, some of the resulting phase-separated networks were very good shape memory polymers. Temperature and DBU catalyst loading were not found to influence the reaction-induced phase separation behavior in this system. Therefore, the spherical two-phase morphology is independent of cure conditions as thiol-acrylate reactions are much faster than thiol-epoxy reactions. Next, novel amine-vinyl sulfone networks were formed from oligomeric diamines and divinyl sulfone. Upon characterization of reaction kinetics and properties, it was found that these uncatalyzed reactions have rates that are competitive with both uncatalyzed polyurethane and non-isocyanate polyurethane reaction rates and the resulting polymers exhibited tensile properties comparable to polyurethanes and catalyzed

non-isocyanate polyurethanes.

Although phase separation in polyurethanes has been well studied for several decades, challenges remain in the experimental determination of aromatic interactions that exist between hard segments. Here, intrinsic fluorescence is applied to segmented polyurethanes with aromatic ring-containing hard segments to experimentally observe these interactions. Using emission spectra, the orientation and alignment of aromatic rings was characterized and quantified through monomer and excimer emission. Using excitation spectra, it can be observed that excimer formation originates from a ground-state dimer complex, which implies that the rings are specifically oriented in a sandwich-like configuration. In addition, the effects of confinement and substrate interactions are explored. Hydrogen bonding and rigidity at the substrate were observed to interfere with dynamic excimer formation, an effect that propagates some tens of nanometers into the film.

ACKNOWLEDGMENTS

First, I would like to thank my advisor, John Torkelson, for his advice and guidance during my time in graduate school. I am grateful for all of the time and effort that he has dedicated toward my development as an effective researcher and communicator. I would also like to thank my committee members and collaborators for their time and support: Justin Notestein, Mitchell Wang, Karl Scheidt, and Bill Heath.

I would like to thank past and present members of the Torkelson group: Mirian Diop, Emily Leitsch, Krishnan Iyer, Tian Lan, Anthony Tan, Shadid Askar, Goliath Beniah, Lanhe Zhang, Kailong Jin, Tong Wei, Lingqiao Li, Xi Chen and Mingxiao Li. Graduate school would not have been the same without you. Special thanks to the PU crew for support and helpful discussions in regard to exploring new research areas.

Lastly, I would like to thank my family for their infinite love and support. Thank you to my parents, Charles Dhulst and Kathy Wilson, who believed in me when I didn't believe in myself and for reminding me every Sunday to have some fun. There aren't enough words in the world to express my appreciation. To my friends in Chicago and around the country, I am truly grateful for your accompaniment through this entire process.

TABLE OF CONTENTS

LIST OF FIGURES

LIST OF TABLES

I. INTRODUCTION AND BACKGROUND

CHAPTER 1

INTRODUCTION

Polyurethanes, a well-known class of segmented polymers, are used in a wide range of applications due to their versatile structures and rapid reaction rates. Since World War II, polyurethanes have been used industrially as foams, fabrics, adhesives and elastomers (Oertel 1993). Synthesized from highly exothermic reactions between alcohol and isocyanate functional groups, polyurethanes are also used in field applications such as spray coatings and insulation. Recently, isocyanates have seen increased regulatory efforts against their use and transport due to health concerns. Because of these recent government policies, both academic and commercial research has begun to investigate alternative chemistries to produce materials that can potentially replace polyurethanes in certain applications (Guan 2011, Nair 2014, Nohra 2013). Because of the versatility of polyurethanes, efforts have not been focused a single chemistry alternative but rather application-specific alternatives that can achieve comparable reaction rates with minimal toxicity. This dissertation focuses on two alternative syntheses to replace segmented polyurethanes in field applications, elastomers and shape memory materials.

Polyurethanes have two desirable properties that any potential elastomer replacement would need to mimic to be commercially useful: easily-tuned structure and fast reactivity Prisacariu 2011). With condensation polymerizations, the functional groups participate in the reaction while the remainder of the molecule (R group) can be one of numerous structures. If the structure of the diol is vastly different than the structure of the diisocyanate, these are referred to as segmented polyurethanes. Segmented polyurethanes have the potential to phase separate due to thermodynamic incompatibilities between the structures of hard and soft segments. Phase-separated polymer systems often provide difficult challenges associated with their kinetics and thermodynamics. However, their distinctive properties are often advantageous both academically and commercially. Because phase separation can be induced during a polymerization reaction, it has been found that, in many cases, the extent of phase separation and final morphology are highly

influenced by chemical reaction kinetics (Girard-Reydet 1998). Because of this, extent of phase separation often determines the application as it controls thermal and mechanical properties of the material. While structure variation in polyurethanes is often the easiest method to change properties, the competition between phase separation and chemical kinetics is unique to every system and, if understood, can also be manipulated for property enhancement. In polymer networks, phase separation is further complicated by the increased presence of covalent bonds between incompatible segments (Williams 1997).

The second desired feature of polyurethanes, fast reactivity, has been more difficult to achieve in current potential polyurethane replacements. In the open literature, research has focused on alternative chemistries to produce either urethane-based polymers and urethane-like polymers. For example, Torkelson and coworkers investigated the reaction kinetics associated with cyclic carbonate aminolysis to produce polyhydroxyurethanes, a polymer containing repeat units of a urethane linkage and pendant hydroxyl group (Lombardo 2015). These reactions produced phase-separated materials but required extremely long reaction times even when catalyzed. However, rapid reaction rates are necessary for these polymers to be competitive with isocyanate-alcohol reactions in field applications. Recently, thiol reactions have been utilized in polymerizations to produce networks with the attributes of click chemistry, such as fast reaction times, high yield, and network uniformity (Hoyle 2010b). With typical two-component thiol-ene or thiol-acrylate reactions, the final product is limited to certain applications due to the thermal or mechanical properties of the material. To address these weaknesses, research has focused on using multi-component reactions to produce polymers with diverse structures and expanded mechanical properties. In the current literature, the addition of a third component to a thiol network has been shown to enhance thermal and mechanical properties (Carioscia 2007b, Jian 2013, Ortiz 2008a). These multi-component systems typically require complicated sequential UV and thermal steps with multiple initiators and catalysts. In addition to the synthesis, complications exist with radical homopolymerization of acrylates and/or incomplete thiol conversion which can negatively impact

the final properties of the network.

Section I of this thesis offers an introduction and background of relevant information required to appreciate the work presented in later chapters. Chapter 2 provides a discussion of the relevant chemical reactions in order to recognize the role of chemical kinetics in these phase-separated systems. It also provides an understanding of reaction-induced phase separation in segmented polymers based on thermodynamics and non-covalent interactions. An introduction to fluorescence is also presented as a basis for understanding its use as a technique for identifying aromatic interactions and molecular alignment in polymer systems.

Section II discusses the use of nucleophilic click reactions to produce novel phase-separated or segmented polymer networks with fast and efficient syntheses. With a focus on elastomeric materials that mimic polyurethane behavior, commercially available monomers are reacted together to produce polymers with both chemical and physical crosslinks on the same timescale as urethane reactions. In order to take advantage of property enhancements due to reaction-induced phase separation, the chemical kinetics are examined in order to understand their role in phase separation.

In Chapters 3 and 4, hybrid polymer networks are synthesized using thiol-, acrylate- and epoxide-functionalized reactants. The thiols are able to react with both acrylate and epoxide groups, but acrylate and epoxide groups are unreactive with each other. Past research efforts on this system have employed a combination of sequential photo-initiated and thermally-initiated reactions of thiols with (meth)acrylates and epoxides and have led to single-phase materials. Chapter 3 provides an analysis of reaction kinetics for these two reactions and shows that thiol-acrylate reactions are much faster than thiol-epoxy reactions. Consequently, we have developed a one-pot synthesis of thiol-acrylate-epoxy hybrid networks using room temperature reactions and 1,8-diazabicyclo[5.4.0]undec-7-ene (DBU) as catalyst. With some higher molecular weight reactants, e.g., 2000 g/mol diacrylate, novel phase separated thiol-acrylate-epoxide polymer networks are produced with properties that are highly tunable by composition and sequential

reaction order. Beyond good mechanical properties, some of the resulting phase-separated networks are excellent shape memory polymers, with shape recovery ratios of unity.

Phase separation in polymer networks is often difficult to induce because of the chemical crosslinks between incompatible segments. In thiol-acrylate-epoxide hybrid polymers, phase separated networks can be produced by adjusting structure design and synthesis methods. In Chapter 4, we show that variables commonly used to control reaction-induced phase separation have little to no impact on the thiol-acrylate-epoxide morphology. Here, we report that changes in temperature and DBU catalyst loading do not impact the final morphology of the network and similar to a room temperature synthesis, produce a dispersed-phase spherical morphology. These results are different than many modified epoxy thermosets presented in literature, in which morphologies, and therefore properties, are variable with different synthesis conditions. Multi-component materials synthesized by two distinct reactions with vastly different rates allow for gelation to occur after phase separation is complete or nearly complete and give spherical morphology (and elastomeric properties) under all synthesis conditions.

In addition to thiol reactions, the nucleophilic addition of an amine to a carbon-carbon double bond was investigated for its applicability to polymer synthesis. Chapter 5 discusses the chemical kinetics and mechanical properties of polymers synthesized from the reactions of diamines and divinyl sulfones. Using similar structures to traditional segmented polyurethanes, thermoset materials were synthesized in bulk by rapid room temperature reactions. Thermodynamically favorable, these reactions are efficient without the use of a catalyst. Reaction kinetics for amine-vinyl sulfone polymerizations show rapid reaction upon mixing. Polymerization rate parameters, reported for the first time for these reactants, of $k_{app} = 0.17\ M^{-1}\ min^{-1}$ show that these uncatalyzed reaction rates are greater than rates reported for uncatalyzed polyurethanes and certain catalyzed non-isocyanate polyurethanes. Tuning stoichiometry and reactant structure, these crosslinked materials have thermal and mechanical properties comparable to thermoset polyurethanes.

The second part of this dissertation focuses on the development of a novel fluorescence technique to characterize polyurethanes in both bulk and thin film geometries. Although isocyanate health hazards are a major concern for polyurethanes reacted by end-use consumers (such as spray foam insulation), with proper protective equipment, polyurethanes can be used safely in industrial settings, such as manufacturing facilities for electronics or medical devices. Most commonly, aromatic diisocyanates are employed as hard segments in segmented polyurethanes. Due to thermodynamic incompatibility, the aromatic rings may phase separate from the oligomeric soft segment. Phase separation and hydrogen bonding have been thoroughly investigated for their role in hard segment/hard segment interactions (Engels 2013). However, the roles of other non-covalent interactions, such as aromatic pi-pi stacking, have rarely been explored. Thermal and mechanical properties of segmented polyurethanes depend on orientation and packing of aromatic rings in the hard segments. For example, the microphase morphology impacts glass transition temperatures, strength of the material and optical properties. Relevant literature discusses the presence of aromatic interactions in hard segments through inference but currently there are no experimental techniques to detect these interactions in polyurethanes (Oertel 1993). Hydrogen bonding can easily be measured through both computational and experimental techniques. However, aromatic interactions, a loosely defined term, are based upon van der Waals interactions which have been deemed difficult to observe in any capacity (Dubey 2011, Martinez 2012).

In Section III, fluorescence is demonstrated to be useful as a tool for identifying aromatic interactions and molecular alignment of hard segments in thermoplastic phase-separated polyurethanes through the formation of complexes between aromatic rings. First, it is important to establish fluorescence as an experimental technique that can observe aromatic interactions. Using toluene diisocyanate-based polyurethanes, the intrinsic fluorescence of the aromatic rings can be used to quantify alignment and interactions of aromatic rings in the hard segments. In Chapter 6, polyurethanes were synthesized with identical hard segment content and different soft segment backbones in order to establish different degrees of phase separation. Using this novel application

of fluorescence, monomer and excimer fluorescence of the aromatic rings in polyurethanes can give information on the proximity and extent of aromatic ring alignment and allow for the observation of aromatic interactions that occur within the hard segments. Using excitation spectra, this technique can also give insight into the significance of aromatic interactions via ground-state dimer formation of aromatic rings in the hard domains. Reports of the experimental observation of these aromatic interactions is currently missing from polyurethane literature.

Another advantage of fluorescence is its applicability to polymer thin films. Chapter 7 explores the use of this technique with polyurethane thin films to understand the influence of confinement on the molecular orientation of the aromatic rings in the hard segment. Previously, there has been little work concerning polyurethane thin films as a function of confinement and attractive polymer-substrate interactions. This study revealed the importance of aromatic interactions and hydrogen bonding on molecular alignment in phase-separated polyurethanes. Using excimer to monomer intensity ratios, the extent of alignment of aromatic rings along the polymer-substrate interface can be inferred. Non-covalent interactions, specifically hydrogen bonding and rigidity at the substrate, can impede the alignment of the aromatic rings and this effect can propagate into the thin films up to tens of nanometers.

Finally, Chapter 8 summarizes the work completed in this thesis toward novel synthesis and characterization techniques for polyurethane and polyurethane-like materials. In addition, this chapter suggests future opportunities for research in these areas.

CHAPTER 2

BACKGROUND

This background will be divided into three sections. The first section discusses chemical reactions and kinetics that are relevant to this thesis. The second part examines the thermodynamics related to polymeric phase separation and final morphology. The final section explores fluorescence and its use to characterize polymers in bulk and thin films.

2.1 Chemistry and Synthesis Methods for Relevant Polymerizations

2.1.1. Segmented Polyurethane Chemistry

Polyurethanes are a diverse class of materials utilized in numerous thermoplastic and thermosetting applications (American Chemistry Council 2012). Polyurethanes are the products of reactions between alcohols and isocyanates (Engels 2013). With research dating back to World War II, polyurethanes are well studied materials (Oertel 1993). Studies have been performed on reaction kinetics, catalysts, structure-property relationships and uses in countless applications (Chang 1987, Chattopadhyay 2006, 2009, Elwell 1996a, Javni 2003, Król 2007a, Lu 2002, Petrovic 2008). Isocyanates, with their delocalized electrons, have high reactivity with nucleophiles such as alcohols, amines and water due to a partially positive charge on the carbon atom (Kathalewar 2013, Wicks 1999). Catalysts are often used commercially to accelerate reactions for room temperature applications. For example, aliphatic and aromatic amines, organometallic compounds, including dibutyltin dilaurate, and metal salts of phenols are among the most well-known catalysts (Delebecq 2013). Because step growth reactions are between functional groups, the possible backbone structures of the polyisocyanates and polyols are expansive and typically chosen based on desired properties. For example, aliphatic isocyanates are commonly employed in applications ranging from fibers to light-sensitive coatings while aromatic isocyanates are often used for rigidity in foams or elastomers.

For applications such as elastomers, segmented thermoplastic polyurethanes are synthesized using three components in a one- or two-step synthesis Prisacariu 2011). Most

commonly used, the two-step method begins with the synthesis of an isocyanate-endcapped prepolymer, through reactions between an oligomeric diol and excess diisocyanate (shown in Figure 2.1). This mixture is then chain extended with a small molecule diol to produce a segmented polyurethane with a soft segment (composed of the oligomeric diol with a polyester, polyether or polybutadiene backbone) and a polydisperse hard segment (diisocyanate and chain extender). Although fully reacted polyurethanes are inert, small molecule isocyanates possess potential health risks, including asthmatic symptoms, when people are exposed without proper protective equipment (Nohra 2013). As government regulations are increasingly restrictive on the transport and use of isocyanates in field applications, both commercial and academic research has been directed toward polymers that have the potential to replace polyurethanes.

2.1.2. Thiol Chemistry

Thiol reactions have been explored in organic chemistry since the early 1930s (Patai 1974). Photopolymerizations between thiol and -ene functional groups were developed largely through industrial processes in the 1970s by W.R. Grace and Armstrong for coatings and tiles (Morgan 1977). However, because of the strong odors associated with thiol chemistry and yellowed final products caused by the light instability of photoinitiators, industry turned away from thiol-ene chemistry. More recently, groups sponsored by the National Institute of Health have promoted renewed interest as new applications have been imagined (Hoyle 2004).

2.1.2.1. Thiol-Ene Reactions

With the popularization of "click" chemistry beginning in 2001 (Kolb 2001), the Michael addition, typically a reaction between an enolate-type nucleophilic reactant and α,β-unsaturated carbonyl functional group, reemerged with thiols as key reactants (Hoyle 2010b). These reactions can be classified as click reactions because they are efficient, thermodynamically favorable and yield highly selective products. The thiol-Michael reaction can occur between a thiol and any –ene that is electron-deficient, such as (meth)acrylates, unsaturated ketones, maleimides, or unsaturated esters. Because of the placement of sulfur on the periodic table, it is known that the element has

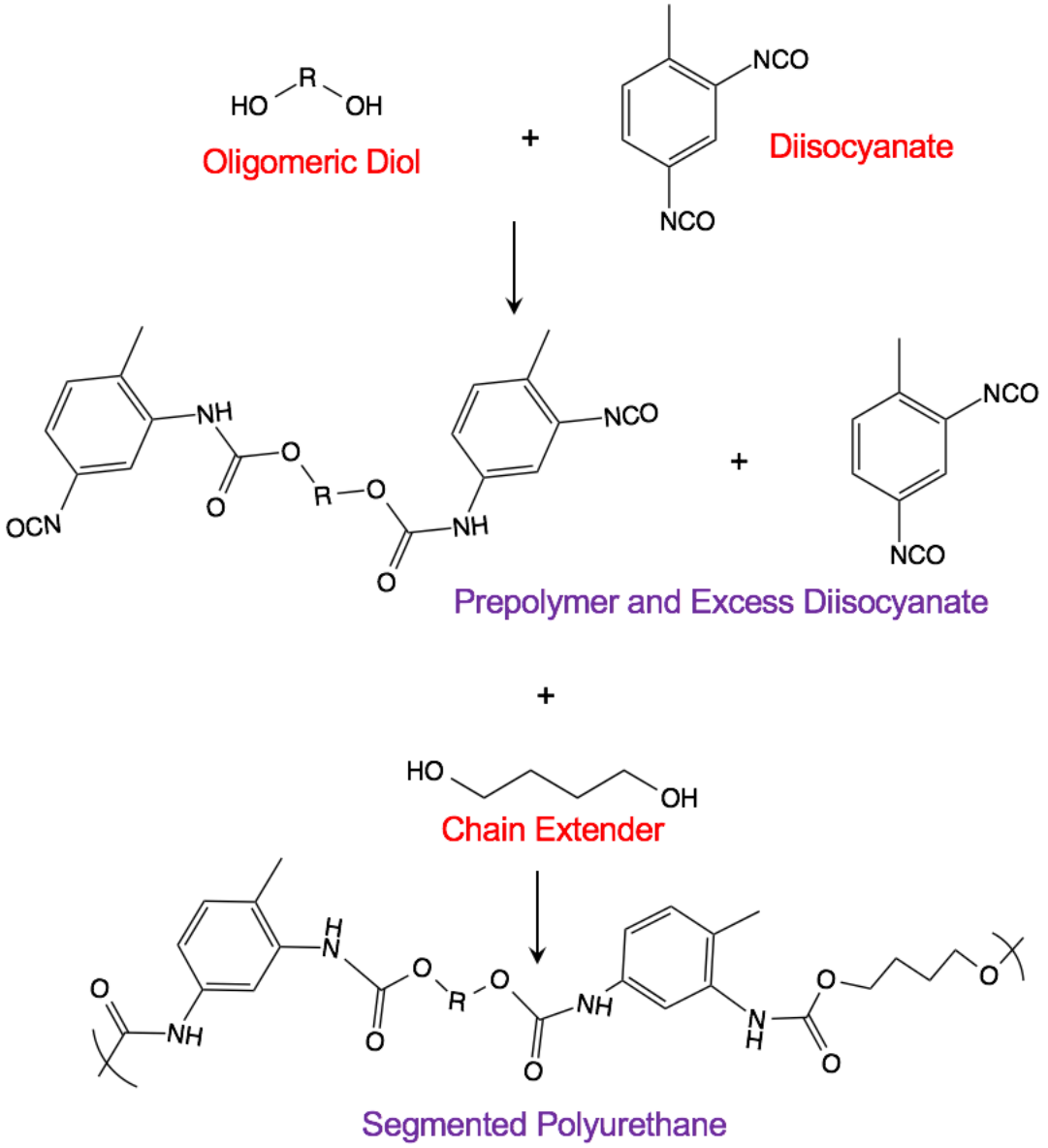

Figure 2.1. Reaction schemes for the two-step synthesis of a traditional segmented polyurethane, where R is an oligomeric polyester, polyether or polybutadiene backbone.

similar reactivity to oxygen but is less electronegative. Thiols have a weak bond dissociation energy when compared to alcohols, and with their high electron density, they are much more reactive as nucleophiles (Lowe 2010). Thiol reactivity is typically characterized by the structure of the "R" group: aromatic, thioacetates, thiopropionates, or aliphatic chains. These structures affect the pKa, or how easily a hydrogen atom can be abstracted.

Because the Michael reaction has been explored using other starting materials, including malonates and propionates, thorough research has been performed on the mechanism and effective catalysts. Certain catalysts can achieve high yields, including Lewis acids, methoxides, ionic liquids, and iodine (Lowe 2010). However, in order to produce fast reactions with minimal side products, base or phosphine catalysts must be used. Thiol reactions in this dissertation use a nitrogen-centered catalyst, but because the acting mechanism is unknown in current literature, both base-catalyzed and nucleophilic-initiated mechanisms will be described here (Chan 2009a, Li 2010).

In the base-catalyzed mechanism (Chan 2009a) (see Figure 2.2a), a base (B) abstracts a proton from a thiol to form a thiolate anion (S^-). Because of the low energy barrier, this hydrogen abstraction happens quickly and easily depending on the strength of the base used. The S^- then attacks the β-carbon of the electron-withdrawing group (EWG) to form an intermediate anion. This intermediate accepts a proton from either the protonated base or another thiol molecule (the former being more kinetically favored) to form the final product.

As previously mentioned, the acidity of the thiol is extremely important to the reaction rate and is suspected to play a role in which mechanistic path is initiated. Because thiols have a wide range of pKa values, the basicity of the catalyst must be chosen carefully in order to produce the highest concentration of thiolate anion. Chan et al. (Chan 2009b) investigated common catalysts in a model thiol-acrylate reaction system. They found that the higher the pKa of the catalyst, the larger the rate constant. However, after stricter characterization of the results, it was concluded that pKa is not the only factor. 1,5-diazabicyclo[4.3.0]non-5-ene (DBN) and 1,8-

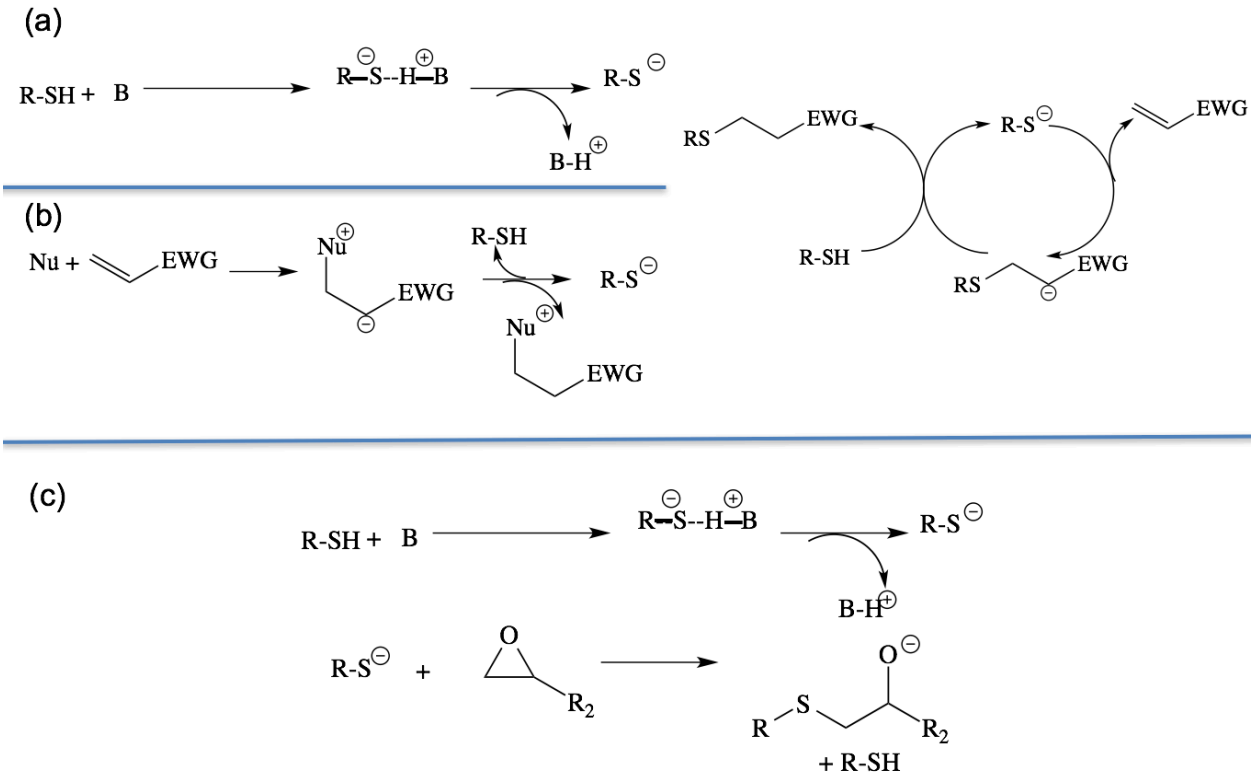

Figure 2.2. Proposed mechanisms for thiol-click reactions: (a) Base-catalyzed thiol-Michael addition, (b) Nucleophile-initiated thiol-Michael reaction and (c) Base-catalyzed thiol-epoxide reaction.

diazabicycloundec-7-ene (DBU) were found to have such dramatic increases in rates that it was postulated that the rate constants had a better correlation with catalyst nucleophilicity than pKa (Baidya 2008). Upon further investigation, it was found that high basicity of a catalyst initiates the base-catalyzed mechanism, while a high nucleophilic character of the catalyst (such as aza-aliphatic compounds) can lower the activation energy of the rate-limiting step. However, if the catalyst nucleophilicity is sufficiently high (such as aza-aromatic compounds), a different mechanism will be followed (Wang 2013).

The second proposed mechanism through which nitrogen-centered catalysts can facilitate the thiol-Michael addition is a nucleophile-initiated pathway (see Figure 2.2b). In the first step, the nucleophile-acting base attacks the β-carbon of the EWG to create a zwitterionic intermediate. The thiol donates a hydrogen to the intermediate. After S^- is formed, the remaining mechanistic steps are the final two steps of the base-catalyzed mechanism described above. However, in this mechanism, the nucleophile does not catalyze the reaction but rather reacts with the EWG to generate a strong base to catalyze the reaction (Chan 2009a, Liu 2013a).

Studies of the kinetics of small-molecule thiol-Michael addition to acrylates indicate that the reaction is second order overall when catalyzed by an amine and depends on the concentrations of S^- and the –ene acceptor (Mather 2006). The S^- concentration depends on the base strength, solvent and molecular structure (Connor 1938). Strong bases will increase the concentration of S^- and give a pseudo-first-order dependence on acrylate concentration (Clemens 1989). Solvent allows for stabilization of the charged intermediates, but it is possible for the reaction to be performed in bulk for ease of application. Molecular structure plays a large role in the reaction rate as strong nucleophiles (thiopropionates or thioacetates) can react faster with acceptors. The structure of the activated –ene is also important to the reaction rate. The more electron deficient the carbon-carbon double bond, the more susceptible it is to a Michael addition reaction (Chan 2009b, Lowe 2010). Maleimides have been shown to be the most reactive toward the addition, followed by fumerates, maleates, acrylates, and methacrylates. Thiol reactions in this dissertation

will focus on thiol-acrylate chemistry, as it is the most commonly used Michael addition in block copolymer synthesis (Bounds 2012, McEwan 2013, Rizzi 2005, Slavin 2012). Li et al. (Li 2010) and Chan et al. (Chan 2010) have done in-depth reaction rate studies on catalyst type, thiol acidity, and solvent for thiol-acrylate reactions.

2.1.2.2. Thiol-Epoxide Reactions

Another thiol reaction that is commonly used in the biomedical industry and for post-functionalization is the thiol-epoxy (or thiol-oxirane) reaction (Guzmán 2015, Harvison 2011a, 2011b). The thiol-epoxy reaction occurs by nucleophilic ring-opening, where the proton capture can occur from the thiol or the catalyst (see Figure 2.2c). Like the thiol-Michael mechanisms described above, the mechanistic pathway is determined by the thiol acidity and basic strength of the catalyst and can be catalyzed by Lewis acids as well as bases (Amantini 2003, Bouyahyi 2012, De 2012, Fringuelli 2003, Lowe 2010, Rahane 2012). Although commonly used in industry, few kinetic studies have been performed on this reaction (Binder 2014, Jin 2015, Loureiro 2015, Stuparu 2016). For the base-catalyzed mechanism, Khan and coworkers (Binder 2014) designed an AB-type monomer with thiol and epoxide functional groups and screened basic catalysts in a solvent-based reaction. They found that tetrabutyl ammonium fluoride, lithium hydroxide (LiOH) and DBU were excellent catalysts for reactions with high selectivity and yield. Khan and coworkers (Brändle 2012) also used difunctional thiols and epoxides to produce linear polymer chains with LiOH as a catalyst. Cook et al. (Cook 2012) used differential scanning calorimetry (DSC) and Fourier-transform infrared spectroscopy (FTIR) to investigate the reaction times of the thermal cure of a multifunctional thiol and difunctional epoxy network. Torkelson and coworkers (Jin 2015) have demonstrated an autocatalytic effect from the product that changes the reaction order when using DBU.

2.1.3. Multi-component Hybrid Networks

Thiol-ene networks are employed in a wide range of applications in biomedical, optical, sensing, and industrial fields because of their high yields and rapid reaction rates. However,

because of the inherent flexibility of their chemical structure, thiol-Michael networks exhibit low glass transition temperatures (T_g's), which limit their applications. In order to promote this chemistry into other applications, research groups have attempted to couple thiol-ene chemistry with additional reactions to enhance the overall strength of the material. Epoxy resins, on the other hand, are known for their high mechanical strength and chemical robustness (Rozenberg 1986). However, when cured without a co-monomer, they are extremely brittle. To utilize polymers in a wide range of applications, it is possible to incorporate multiple reactions to achieve a synergistic effect with regard to mechanical properties. Hybrid chemistry, systems where one or more of the monomers contain functional groups which are reacted by multiple curing methods to achieve a networked polymeric structure, is one method to achieve these materials (Itoh 1996). Similarly, interpenetrating networks (IPNs), which are polymer networks that are cured using separate polymerization mechanisms to achieve a physically and/or chemically interlocking system, are used to achieve these goals (Sperling 1996).

In literature, there are numerous examples of attempts to increase the mechanical robustness of a thiol-ene network (Carioscia 2007b, Kade 2010, Lee 2007, Matsushima 2010, McNair 2013, Nair 2012, Sangermano 2009, Schreck 2011, Shin 2010, Ye 2011). Hoyle and coworkers (Matsushima 2010, Shin 2010) were successful in improving mechanical properties related to hardness by incorporating a thiol-isocyanate reaction into the thiol-ene system. Nair et al. (Nair 2012) were able to achieve different mechanical properties by creating a two-step polymerization process with different monomeric thiol and acrylate structures. They observed that the component concentrations and monomer structures were key variables in the adjustment of mechanical properties. Kade et al. (Kade 2010) stated that the use of thiol-ene chemistry in combination with other reactions would allow for more sophisticated polymer structures without increased synthetic requirements. Most commonly reported in the literature for hybrid synthesis is the two-step approach or sequential syntheses (Carioscia 2007a, 2007b, Lee 2007, McNair 2013, Ye 2011). These complex syntheses often require multiple methods of curing (such as UV and

thermal) and the addition of both initiator and catalyst for reactions in both steps. Specifically, this dissertation employs the combination of thiol-ene and thiol-epoxy reactions to produce hybrid phase-separated materials.

2.1.4. Vinyl Sulfone Chemistry

As an alternative to acrylates, vinyl sulfone has been employed as an electrophile in Michael additions (Chatani 2013, Nair 2014). Using similar mechanisms for reactions with nucleophiles, vinyl sulfone is useful as an intermediate in organic synthesis. Fuchs and coworkers (Meadows 2006) were pioneers for the use of vinyl sulfones as Michael acceptors which allowed for highly substituted bicyclic structures and complex diastereomers. Most known for their ability to introduce carbon-X bonds into polymers, vinyl sulfone has recently been employed in thiol-Michael additions for biomedical applications (Morales-Sanfrutos 2010). In this work, vinyl sulfones are reacted with amines to produce chemically crosslinked polymer networks. Small molecule amine-vinyl sulfone reactions reported in the literature investigate conversion levels and yield with different reactant structures (Esteves 2007, Wang 2015). Because of the inherent basicity of the amine reactants, this reaction can often occur in the absence of an external catalyst (dependent on reactant structure). However, it can also occur in acidic or basic conditions. It was found that secondary amines, due to their higher nucleophilicity, react more quickly than primary amines (Mather 2006).

Most research done with vinyl sulfone chemistry is application-focused in protein chemistry or biomedical uses. Vinyl sulfone has been utilized in biological systems because they were found to reversibly inhibit different types of cysteine proteases as well as other enzymes (Meadows 2006). Therefore, research has been dedicated to bio-conjugation and medicinal chemistry. In literature, very little is reported in regard to polymerizations with these two reactants. Further, there are no polymerization kinetics reported. Vinyl sulfone will react with an active hydrogen (Simpkins 1990). Classifying a single active hydrogen as a functional group, a common diamine with two primary amines will have a functionality of four. Under stoichiometric balance,

this will produce a network. In literature, crosslinked systems have not been fully explored. There have been reports of using imbalanced stoichiometry to produce linear and branched polymers with this chemistry. For example, Gao and coworkers (Gao 2001) used divinyl sulfone and 1-(2-aminoethyl)piperazine (trifunctional) to produce branched polymers. Ueda and coworkers (Imai 1981) also found that product molecular weight from the polyaddition of piperazine to divinyl sulfone is highly dependent on solvent choice.

2.2. Phase Separation in Polymer Systems

2.2.1. Thermodynamics Associated with Phase Separation in Polymers

This portion of the background will briefly introduce and discuss the thermodynamics that ultimately govern phase behavior in polymer systems, specifically the segmented polymers relevant for this thesis. Solution thermodynamics, used for polymer-solvent systems, is a solid basis for understanding polymer-polymer mixing and block copolymer behavior. The solubility of one component in another is quantitatively controlled by the Gibbs free energy of mixing:

$$\Delta G_{mix} = \Delta H_{mix} - T\Delta S_{mix}, \qquad \text{(Eq. 2.1)}$$

where ΔG_{mix} is the change in Gibbs free energy of mixing, ΔH_{mix} is the enthalpy of mixing, T is temperature and ΔS_{mix} is the entropy of mixing (Koretsky 2004). In the simplest case, miscibility occurs when ΔG_{mix} is less than zero. With polymeric materials, the entropic term is small and therefore temperature does not contribute to solubility as greatly as with small molecules. Enthalpy of mixing, typically positive, is calculated by the energy change that occurs when polymer-solvent interactions replace pure component interactions and can be represented by:

$$\Delta H_{mix} = n_1 \varphi_2 \chi \, RT, \qquad \text{(Eq. 2.2)}$$

where n_1 is the number of moles of solvent, φ_2 is the volume fraction of polymer and R is the gas constant. When the interaction parameter, χ, is multiplied by $k_B T$ (where k_B is Boltzmann's constant), it is a per-molecule representation of the energy change between a solvent molecule in pure solvent and pure polymer (Shibanov 1985, Shultz 1952).

In this dissertation, segmented polymer phase behavior is examined and characterized.

Segmented block copolymers follow the same laws of thermodynamics, however, the segment miscibility is influenced by other factors such as covalent connectivity, segment sizes, segment size distribution, non-covalent interactions and chemical reaction kinetics (Bates 1990, 1999, Fasolka 2001, Fredrickson 1987, Leibler 1980). Because the incompatible blocks are covalently connected, block copolymers do not undergo macroscopic phase separation. Instead, the blocks undergo local phase separation to produce nanophases and/or microphases. Most commonly, the phase behavior of symmetric block copolymers is described by morphology changes instead of polymer-solvent phase diagrams such as Figure 2.3 (Bates 1999). Here, phase morphology is controlled by degree of polymerization, volume fraction of components and the Flory-Huggins interaction parameter. The morphology of the phase-separated material is dependent on the monomer composition as it must minimize the unfavorable interactions while stretching the chains into separate phases (causing entropic penalty).

2.2.2. Non-Covalent Interactions in Polymers

Molecular interactions are crucial to many biological and chemical processes from protein folding to nanoparticle aggregation (Hotze 2010). Chemical bonds can be divided into two categories: covalent bonds and non-covalent interactions (Odian 2004). Monomer units are connected covalently to form polymers. In certain systems, repeat units also have the the ability to interact through more disperse forces such as electrostatic interactions (ionic or hydrogen bonding), van der Waals or pi-effects. These interactions play a large role in determining polymer properties including phase separation and morphology as well as T_g (Bissantz 2010, Calvo-Castro 2016, Pukánszky 2008, Waters 2004, Wojtecki 2015, Yilgör 2015).

In this dissertation, two interactions will be explored and characterized: hydrogen bonding and aromatic interactions. Hydrogen bonding is the attractive force between a hydrogen attached to an electronegative atom (typically amine NH or alcohol OH) and an electronegative atom of a different molecule (Sami 2014). This is typically the strongest dipole force between molecules but weak in comparison to a covalent bond. In polymer systems, hydrogen bonding can occur through

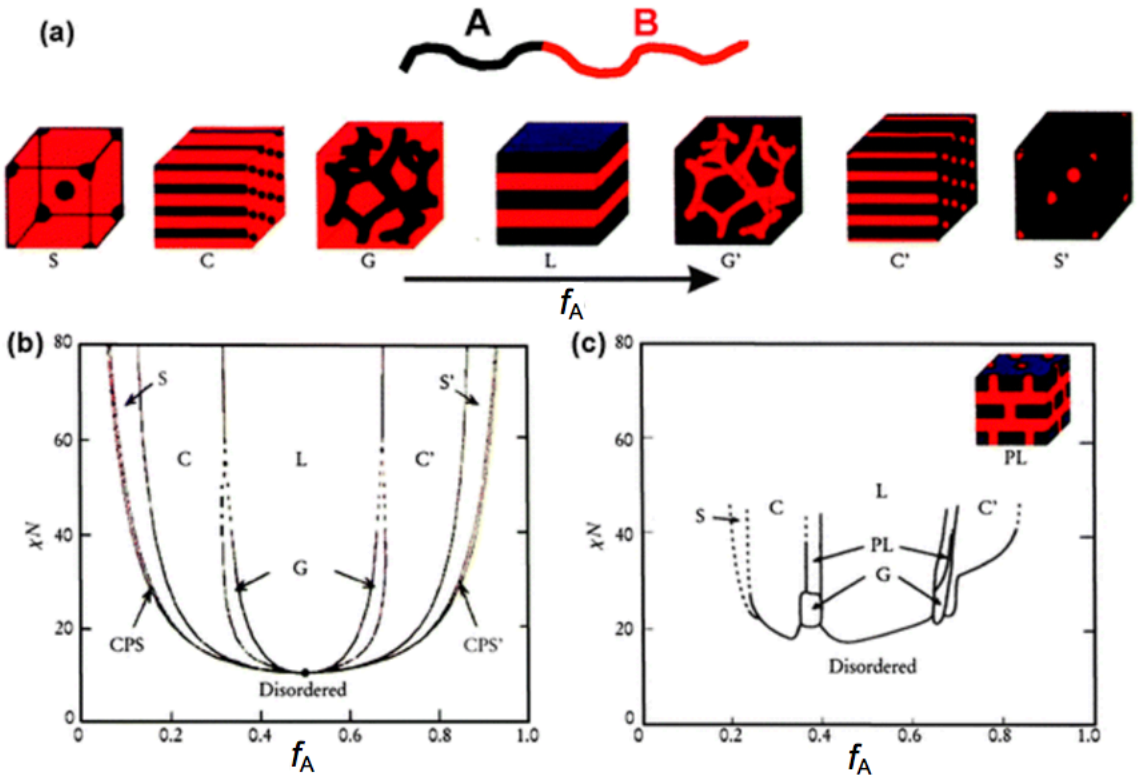

Figure 2.3. Phase diagrams for linear AB block copolymers (a) Equilibrium morphologies of copolymers: spherical (S and S′), cylindrical (C and C′), gyroid (G and G′) and lamellar (L) dependent on composition (f) and combination parameter, χN, where χ is the Flory–Huggins interaction parameter and N is the degree of polymerization (b) Theoretical phase diagram of AB diblocks based on; CPS and CPS′ = closely packed spheres. (c) Experimental phase diagram of polyisoprene-polystyrene diblock copolymers, in which f_A represents the volume fraction of polyisoprene, PL = perforated lamellae. Reproduced from (Bates 1999) with the permission of the American Institute of Physics.

intramolecular or intermolecular interactions as it is a medium-to-long range bond with strength that varies based on binding energy, distance, donor-acceptor pair and medium. Aromatic interactions, including π-π stacking, CH-π, anion-π, are the attractive interactions that involve systems with π electrons (Dubey 2011). The π-π stacking interactions are debated in literature as they are difficult to observe and characterize, and therefore the underlying foundation for the interactions is not well understood (Hunter 1990, Martinez 2012). In the most fundamental case, benzene rings can form dimers because of these interactions. When two benzene rings are in a certain conformations (sandwich, T-shaped or displaced), it is said that dispersive forces are responsible for these interactions. Most notably, aromatic interactions are seen in biopolymers, including base stacking to form double helical structures seen in DNA and RNA (Waters 2004). Because dispersive forces are challenging to discern with common techniques, aromatic interactions, especially in polyurethane literature, are often inferred rather than observed.

2.2.3. Reaction-Induced Phase Separation

An added level of complexity in polymer phase separation arises when phase separation occurs simultaneously with the polymerization reaction. There are numerous commercial materials that rely on reaction-induced phase separation (RIPS) to achieve application-based properties, such as liquid-crystal displays or high-impact polystyrene (Kim 1995, Williams 1997, Yamanaka 1989). Reaction-induced phase separation (also referred to as polymerization-induced phase separation) is caused by an increase in molecular weight of the polymer, which results in a reduction in entropy of mixing, and possible variations in χ (Jaffrennou 2006). The phase separation process is determined by the ratio of the rate of reaction and the rate of phase separation. Each reaction begins as a homogenous mixture of components and phase separates with time and conversion of the monomers.

During RIPS, both the chemical reaction and phase separation proceed under non-equilibrium conditions as they are occurring simultaneously. Once a certain conversion is reached in a crosslinking system, the phase separation will be impeded and the system will remain in this

non-equilibrium state. The reverse situation could also occur. If the phase separation occurs too rapidly, the chemical reaction will be in a state of quasi-equilibrium and the two phases will be of various compositions. Often, it is useful to consider the well known time-temperature-transformation (TTT) diagram for a single-phase system, which highlights three key independent events: liquid-to-solid transformation, gelation, and vitrification (Enns 1983). However, for most complicated RIPS systems (or for novel RIPS systems), these diagrams do not exist or do not provide information useful for the details of morphology.

Pascault and coworkers (Bonnet 1999, Girard-Reydet 1998, Williams 1997) studied the RIPS associated with modified thermosets. In these systems, a thermoset reaction, typically between an epoxy and amine, occurs in the presence of a non-reacting polymer, such as polystyrene. Phase separation of a ternary mixture is more complicated to characterize than a binary mixture as each component will have different solubility in the changing reaction medium. Research methods to track morphology and phase segregation include light scattering as a function of time, transmission electron microscopy (TEM) and cloud point measurements (Park 2012). Ryan and coworkers (Bras 1995, Li 2002b, Sutton 2004) have produced numerous systems including both reactive and non-reactive modifiers in epoxy systems to influence final product morphology.

2.2.4. Nanophase Separation in Segmented Polyurethanes

Segmented polyurethanes are a type of multi-block copolymer synthesized by the reaction of a diisocyanate and a balance of a long chain diol and short chain diol. They are known for their phase-separated structure in which hard (glassy or crystalline) domains are dispersed in a soft (rubbery) domain (Kwei 1982, Pukánszky 2008, Yilgör 2015). Phase separation in these systems allows for physical crosslinking which, although weaker, acts in a manner similar to covalent crosslinking and chain entanglement. These physical crosslinks allow the thermoplastic to have rubber-like and elastomeric qualities such as high elongation with good shape recovery. Because these are not permanent crosslinks, the materials can be heated and deformed, which is sometimes

advantageous over thermoset materials.

Most commonly, oligomeric diols utilized as soft segments have polyester, polyether, or polybutadiene backbones, with molecular weights ranging from 400 to 7,000 g/mol (Oertel 1993, Yilgör 2007). For elastomer synthesis, aromatic diisocyanates such as toluene diisocyanate (TDI) or methylene diphenyl diisocyanate (MDI) are most commonly employed. After this reaction, segmented polyurethanes are formed with nanophase or microphase separated morphologies due to the thermodynamic incompatibilities of the two segments. The oligomeric diol acts as a flexible soft segment with a T_g well below room temperature while the rigidity of the aromatic rings and chain extender in the hard segment allows for a domain with T_g typically well above room temperature. Heavily studied in literature, the structures employed as soft and hard segments, as well as the compositions of each segment, are observed to influence the thermodynamics, and therefore extent of phase separation (Castagna 2012, Petrović 1998, Sheth 2005, Yilgör 2015).

Hydrogen bonding in polyurethanes has a large impact on phase separation, morphology, and mechanical properties (Bagdi 2012, Sami 2014, Wang 1994, Zhang 2010, 2014). Shown in Figure 2.4, the urethane linkage has the ability to hydrogen bond through multiple functional groups in the hard segment (amide NH, carbonyl C=O) and in certain soft segments (such as ether COC). Interurethane hydrogen bonding in segmented polyurethanes has been shown to stabilize and assist in the physical crosslinks to promote elastomeric behavior. However, any interactions between hard and soft segments (for example, amide-ether hydrogen bonding) can result in the prevention of urethane group segregation and an increase in phase mixing.

Studies have shown that the choice of soft segment backbone is a key variable in the degree of phase separation because of thermodynamic incompatibility and hydrogen bonding potentials. When used as a soft segment, polybutadiene (PBD) produces extremely well phase-separated polyurethanes because it is non-polar and there is no potential for non-covalent interactions between the butadiene segments and urethane linkages. In a study by Schneider et al. (Schneider 1979), oligomeric PBD was employed as the soft segment with either TDI or MDI and 1,4-

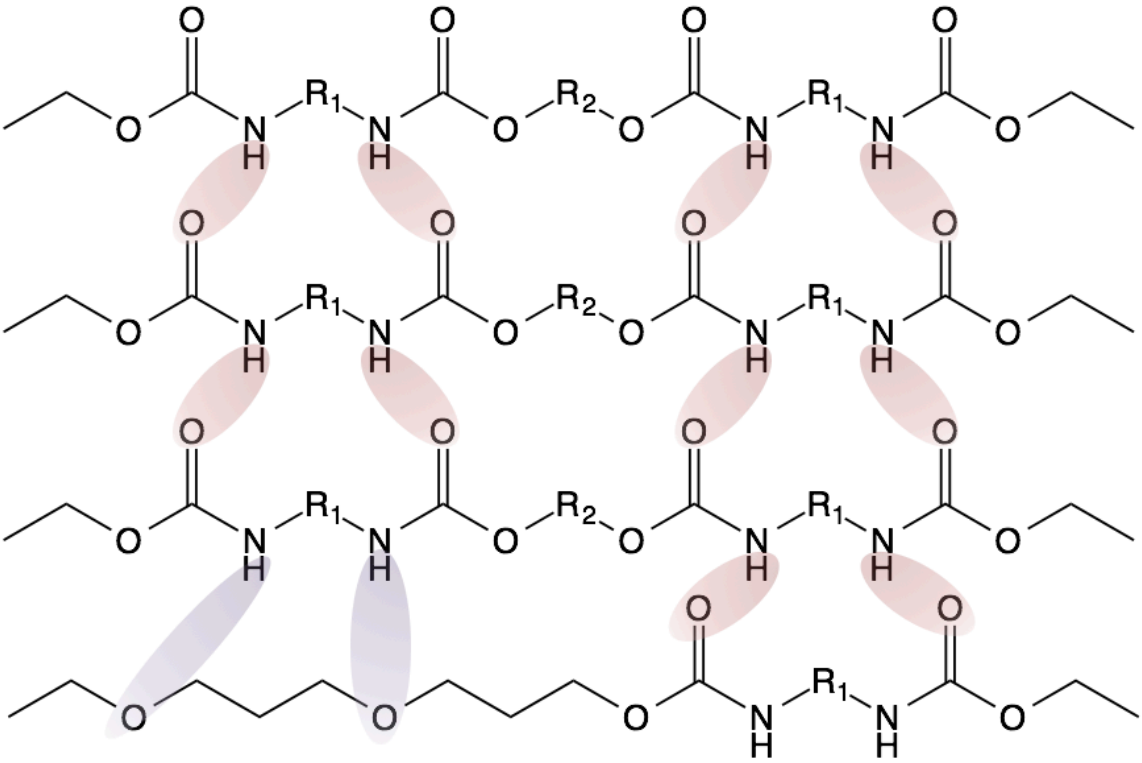

Figure 2.4. Hydrogen bonding of the urethane amide group in polyurethane materials. Highlighted in red, the representation of the expected hydrogen bonding interaction between hard segments in polyurethanes; the urethane carbonyl group hydrogen bonds to neighboring urethane amide hydrogen in the hard-segment regions. Shown in purple, the expected interaction of amide hydrogens with soft-segment ether oxygens in polyether-based polyurethanes.

butanediol (BDO) as a chain extender over a range of hard-segment contents. It was found that regardless of the hard segment structure or composition, the soft segment T_g showed little variation from the pure PBD T_g. This is indicative of an extremely well phase-separated material as the two segments have little impact on each other's thermal properties. When polyesters are used, such as polycaprolactone (PCL), the soft segment has repeat units of ester groups. These ester groups can hydrogen bond with the amide hydrogens in the urethane linkage. In a study by Seefried et al. (Seefried 1975), PCL diols of various molecular weights were employed in a reaction with MDI and BDO as the hard segment. All synthesized polyurethanes exhibited a soft segment T_g at least 20 °C higher than the T_g of neat PCL. This result indicates a less phase-separated system because the interactions between hard and soft segments (due to polarity and hydrogen bonding) cause phase mixing.

Common techniques used to investigate phase separation in segmented polyurethanes include Fourier-transform infrared spectroscopy (FTIR), differential scanning calorimetry (DSC), and small-angle X-ray scattering (SAXS) (Boyard 2005, Camberlin 1983, Chu 1992, Elwell 1996b, Teo 1997, Wang 1994, Yilgör 2000). Infrared spectroscopy can give information on the extent of hydrogen bonding in a sample. As the electronics of the functional groups change with interactions, the peak area and location will shift in the spectrum. Well studied in literature, the amide hydrogen and urethane carbonyl have well known peak positions for free (non H-bonded) and H-bonded functional groups (Teo 1997, Wang 1994, Yilgör 2000). Thermal transitions can also be employed to investigate the extent of phase separation by comparing each polymer phase T_g to its pure starting material (Camberlin 1983). For example, the difference in T_g's between a pure soft segment diol and the rubbery phase in the segmented polymer will reveal the extent of hard segment dissolved in the soft segment matrix.

2.3. Fluorescence as a Tool for Polymer Characterization

2.3.1. Basics of Fluorescence Spectroscopy

Fluorescence is a form of luminescence, which is the emission of light from a material

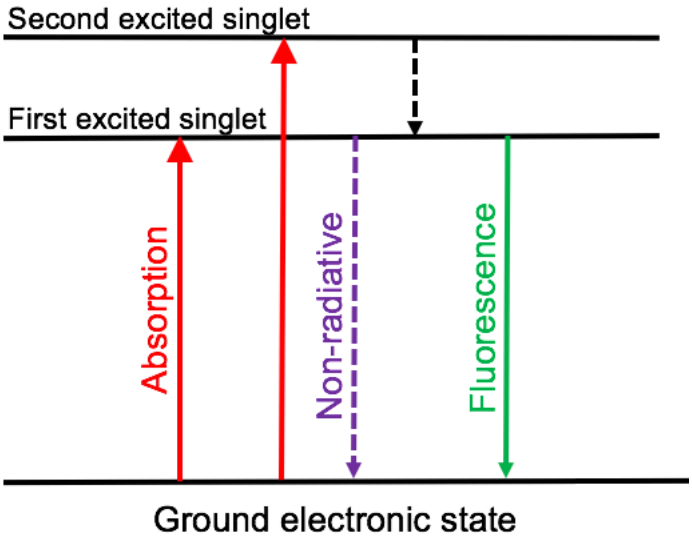

Figure 2.5. Simplified Jablonski diagram illustrating energy pathways associated with absorbance, fluorescence, internal conversion, and non-radiative decay of a dye molecule.

(Lakowicz 2007). More specifically, after a photon is absorbed by a molecule and is raised to an excited electron state, it can return to its ground state by two processes: radiative and non-radiative decay. Radiative decay, or fluorescence, is the emission of light from this excited-singlet state. Non-radiative decay is the relaxation through bond vibrations or rotations. The absorption and fluorescence processes are best shown in the Jablonski diagram (Figure 2.5) (Guilbault (Ed.) 1990). In this simplistic diagram, the ground, first and second electronic states are shown. Upon the absorption of light, the molecule is excited to a certain vibrational level in the first or second electronic state. After internal conversion to the lowest vibrational level, relaxation to the ground state will either occur through vibrational loss or fluorescence. A molecule can also undergo a spin conversion to the triplet state and undergo phosphorescence. For the purposes of this work, fluorescence will be the only pathway discussed. From Figure 2.5, other details about fluorescence can be understood. For example, the energy of absorbance is greater than the energy of fluorescence. Because of this difference, fluorescence emission will occur at lower energy (longer wavelength). It can also be seen that the shape of the fluorescence emission spectrum will be constant and independent of the absorption and excitation wavelength as it always occurs from the lowest vibrational level of the excited state.

Fluorophores are molecules that can undergo this fluorescence process. Typically, fluorophores contain aromatic rings or multiple pi bonds (Procházka 2016). These molecules contain delocalized electrons that can be excited and maintain a certain stability in the excited state. Pyrene, a molecule containing four aromatic rings, is a common fluorophore, while benzene, a single aromatic ring, can also be used as a flourophore (Dawson 1968). Therefore, any polymer than contains a phenyl ring has the potential for intrinsic fluorescence. Polystyrene, a commodity polymer, can intrinsically fluoresce through its phenyl side group (Khan 2005). Different fluorophores are more common based on their quantum yields. Quantum yield is the ratio of light emitted by fluorescence to the total of both radiative and non-radiative decay. The impact of temperature on the fluorescence intensity can be explained through quantum yield. Non-radiative

decay is heavily influenced by the thermal motions of molecules, and therefore, increases with increasing temperature. As a result, increased temperature causes a decrease in the fluorescence quantum yield of a sample.

Fluorimeters use a wide range of techniques to give information on the fluorescence of a sample (Lakowicz 2006). Emission spectra are generated by holding an excitation wavelength constant and scanning through emission wavelengths. Emission spectra are the most commonly reported in literature as they reveal the emitted light from the sample excited at a particular wavelength. The structure of the emission is not typically affected by excitation wavelength, but the intensity will be impacted. Emission can be influenced by any light absorption of the sample. For example, PBD contains pi orbitals that absorb light and decrease the absorption of any attached dyes (Lakowicz 2007). Excitation spectra can also be generated for a given sample. Excitation spectra, in which the emission wavelength is fixed (typically at the maximum emission for that sample), are generated as the monochromator scans through the excitation wavelengths. Excitation spectra are similar to absorption spectra, in that they give details on the wavelength (or species) that is absorbing light.

2.3.2. Excimer Fluorescence

In fluorescence, the mirror rule can be applied to most fluorophores. The mirror rule states that the emission spectrum is a mirror image of the absorption spectrum (Balzani 1991, Guilbault (Ed.) 1990). However, there are exceptions to the mirror rule that can occur with excited-state molecular association. Some fluorophores containing aromatic rings, such as pyrene or polystyrene, can form complexes that will change the emission spectrum from that of the isolated fluorophore. These complexes, termed excimer (excited-state dimer), emit fluorescence at longer wavelengths (Birks 1963a, 1963b, 1963c, Gordon (Ed.) 1975). Förster et al. (Förster 1969) were the first to comment extensively on the concept of excimers in pyrene. It was found that adjacent conjugated fluorophores have the ability to share their pi electrons equally in the excited state, but not in the ground state. In later work, it was found that conjugated polymers can have pi electrons

that are delocalized between bonds in both the ground and excited states (Winnik 1993). Because conjugated polymers can interact in countless ways and also undergo processes like charge transfer, the literature for excited-state species is vast. For the purposes of this dissertation, only the relevant literature on equally-shared pi electrons between conjugated species will be discussed.

To more specifically describe excimer excitation and emission, this section will focus on the formation of excimers in single phenyl rings. In the excited state, intermolecular interactions are stronger due to the enhanced electron affinity. However, in order to share electrons equally, aromatic rings require intense orbital overlap that occurs when the distance between two identical molecules is 3 – 4 Ångstroms (Gordon (Ed.) 1975). The interaction is largely determined by the concentration and sterics of the aromatic rings. There is also a requirement of orientation of the molecules for excimer formation. In aromatic rings, this is a parallel, sandwich-like (face-to-face) geometry for two rings. This orientation can occur in both intramolecular and intermolecular species, dependent on the polymer. For example, intramolecular excimers are formed in aromatic polymers with flexible carbon backbones of lengths of $-(CH_2)_3-$ between rings (Hirayama 1965). Typically, a chain length longer than n = 3 will not produce any excimer due to conformational entropy. Although this rule has been found to describe most aromatic polymer species, there are exceptions in regard to rigidity and other interactions between backbones and side chains (Zacharaisse 1991).

2.3.3. Excimer Formation Pathways

Most commonly explored, and discussed here, are the interactions between molecules in the lowest excited state and the ground state. An excimer, in the original and strictest definition, is an excited-state dimer that is associated in the excited state but dissociated in the ground state (Birks 1962). However, the definition has been revised to include species that are associated in the ground state in the absence of external restraints (Winnik 1993). With this definition, species from crystal structures, viscous solutions, as well as from intramolecular interactions, like those studied here, can be included (Mei 2005).

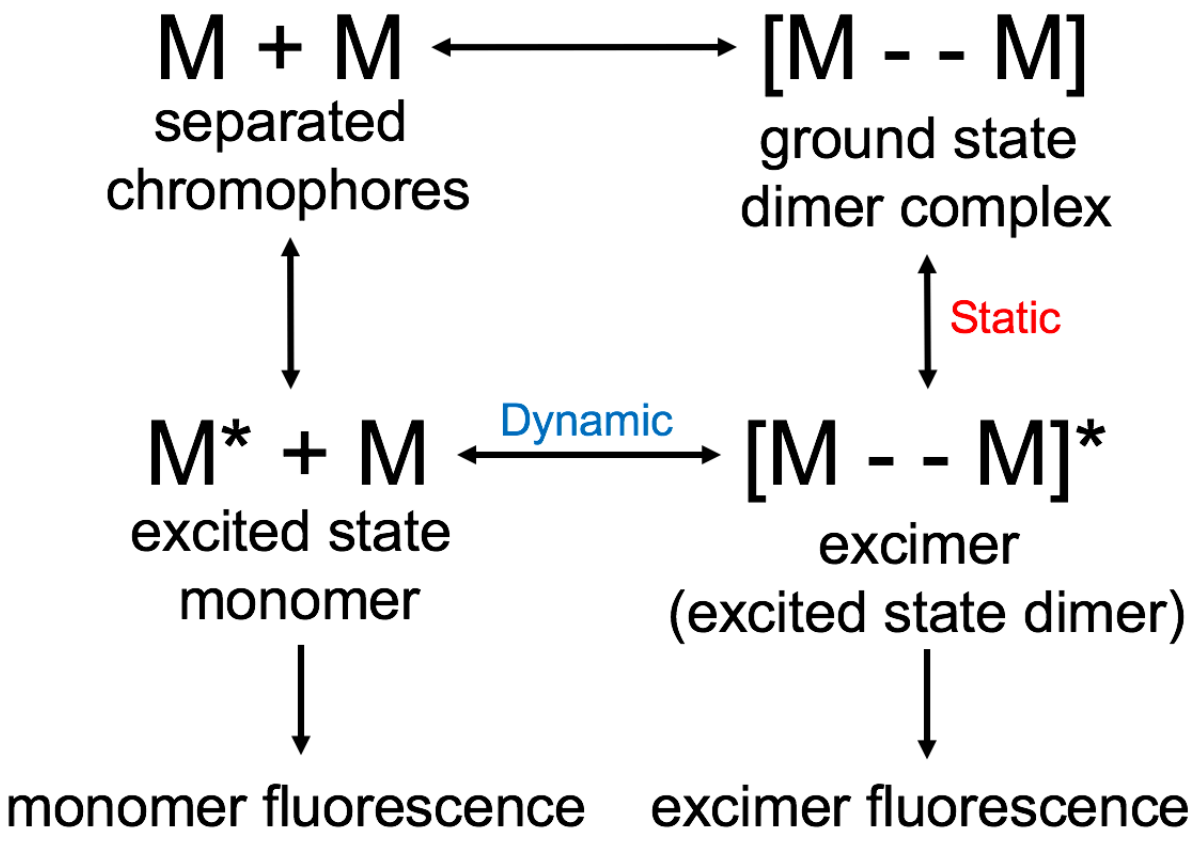

Figure 2.6. Fluorescence pathways for monomer, static excimer and dynamic excimer, where M is ground state monomer and M* is excited state monomer.

In relevant literature, excimer species have become more specific and are classified according to their formation: dynamic excimer and static excimer. Dynamic excimer, most closely related to Birks' definition, is an excited-state dimer that is only associated in the excited state. A static excimer is an excited-state dimer that is associated in both the ground and excited state. Figure 2.6 shows the formation pathways for static and dynamic excimers. From these pathways, a few details about their fluorescence can be noted. First, that excited-state monomer has two competing pathways for fluorescence: monomer and dynamic excimer fluorescence. Second, that static and dynamic excimer fluoresce as the same species, and will therefore be identical in their emission profiles. Finally, that static and dynamic excimer fluorescence are from non-competing pathways because they are formed by unique ground-state species. The use of excitation spectra to identify the absorption profile of the absorbing species is a method of distinguishing between the two pathways.

2.3.4. Sensitivity to Polymer Properties

Fluorescence of a species is largely determined by the fluorophore, its covalent connectivity and surrounding medium. For example, polystyrene, an aromatic ring containing polymer, displays both monomer and excimer intensity that changes with concentration as well as solvent (Gelles 1982b). The solvent molecules have the mobility to reorient during the lifetime of the excited state species. This reorientation will lower the energy of the excited state and produce an emission at a longer wavelength. The polarity of the solvent will determine the extent of this effect (Khan 2005). Although solvent is the only example explored here, fluorescence is largely influenced by mobility as well as polymer structure, temperature, viscosity and interfaces (Guilbault (Ed.) 1990, Healy 2007, Morris 2016).

Because of its sensitivity to the local environment, fluorescence can be used to investigate properties in polymeric systems. Both intrinsic and extrinsic fluorescence can be employed in polymeric systems to examine polymerizations, chemical degradation, morphology changes, self-assembly and thermal transitions (Bosch 2005a). Fluorescence is a powerful tool for these

measurements because it is non-destructive, has high sensitivity and selectivity, and a fast timescale. For example, Torkelson and coworkers (Ellison 2002) have demonstrated fluorescence as a method for probing the T_g of polymer systems through the impact of density changes on fluorescence emission. Conversions for polymerizations of systems such as poly(methyl methacrylate) (PMMA) can be measured extrinsically using monomer and excimer intensity ratios of the pyrene-labelled polymer. The gel point of this system can also be determined through a sudden increase in pyrene emission and its emission insensitivity after that increase. In this dissertation, the properties of segmented polyurethanes in bulk and thin films are investigated by fluorescence. Previously, fluorescence has been used to explore properties in polyurethanes such as micelle formation, dispersion, electric potential, and mechanical strain, as well as cure progression (Bosch 2005a, Goda 2001, González-Benito 2002, Karthikeyan 2009, Lupu 2007, Sun 1996, Wang 2002). Water uptake in polymer films and coatings can be quantified through fluorescence. Peinado and coworkers leverage the plasticizing effect of water on polymer coatings by relating the changes in fluorescence emission to Fickian diffusion to model water absorption in humid conditions (Bosch 2005b).

2.3.5. Confinement Behavior of Polymer Films

Polymers in confined geometries are employed in numerous technological applications including lithography, composite materials, and coatings. As polymers are forced into confined states, their bulk physical properties (i.e. T_g, diffusion, morphology) often do not scale proportionally (Dalnoki-Veress 1998, Despotopoulou 1996, Fasolka 2001, Napolitano 2011, Priestley 2007). Because of the complex nature of confinement behavior, many techniques have been developed to probe polymer properties, including fluorescence, ellipsometry, and atomic force microscopy (AFM). In confined geometries, polymer properties are largely determined by interfaces. For example, a generally accepted model to describe supported polymers in thin films is the three-layer model (Keddie 1994). The polymer-air interface (or free surface) is the top region of the film in which the polymer has greater mobility relative to the bulk polymer. Dependent on

the polymer film thickness, the middle region is considered to be bulk polymer and will have properties similar to those in a non-confined state. The third region, the polymer-substrate interface, can impact polymer properties due to rigidity as well as attractive interactions. For example, studies have shown that PMMA supported on silica show an enhancement in T_g with decreasing film thickness due to hydrogen bonding interactions between the PMMA side group and the hydroxyl groups of the native silicon dioxide layer which causes decreased mobility at the substrate (Keddie 1994).

While the field of polymer-confinement effects has been studied for over two decades, most property-confinement research is limited to addition-type polymers, such as PS and PMMA. Recently, more research has been performed on the confinement behavior of block copolymers (Fasolka 2001). Typically, these studies investigate morphology and self-assembly rather than polymer properties. Confinement behavior of polyurethanes has only been investigated in a few studies. Kojio et al. (Kojio 2007, 2009) examined the microphase separation in bulk and thin film polyurethanes using AFM, optical microscopy and X-ray photoelectron spectroscopy. They reported that for films with thickness greater than 200 nm, the morphology was similar to bulk polyurethanes. However, upon confinement to thicknesses equal to or below bulk domain spacing, the samples exhibited homogenous structures.

II. SYNTHESIS AND CHARACTERIZATION OF NOVEL, CROSSLINKED POLYMER NETWORKS FROM CLICK REACTIONS

CHAPTER 3

HYBRID THIOL-ACRYLATE-EPOXY POLYMER NETWORKS: COMPARISON OF ONE-POT SYNTHESIS WITH SEQUENTIAL REACTIONS AND SHAPE MEMORY PROPERTIES

3.1. Introduction

Thiol reactions have been studied in organic chemistry since the early 1930s (Jacobine 1993, Patai 1974). With the popularization of "click" chemistry beginning in 2001 (Kolb 2001), the Michael addition emerged using thiols as key reactants (Hoyle 2010a). The thiol-Michael addition reaction can be classified as a click reaction because it is efficient, thermodynamically favorable and yields highly selective products. The thiol-Michael reaction can occur between a thiol and any carbon–carbon double bond that is electron-deficient, such as (meth)acrylates, unsaturated ketones, maleimides, or unsaturated esters (Chan 2010, 2009, Chatani 2013, Li 2010, Mather 2006, Nair 2014, Tunca 2014). This reaction achieves high yields with certain catalysts, including Lewis acids, methoxides, ionic liquids, and iodine (Alleti 2008, Lowe 2010, Lowe (Ed.) 2013, Moghaddam 2005). However, in order to produce fast reactions with minimal side products, base or phosphine catalysts must be used (Chan 2009b, Hoyle 2010a, Liu 2013a). The acting mechanism for certain nitrogen-centered catalysts is currently unknown in literature but is reported to be base-catalyzed or nucleophile-initiated (Baidya 2008, Lowe 2010, Mather 2006, Nair 2014, Watts 2001).

Another thiol reaction that has recently gained popularity due to potential applications is the thiol-epoxy (or thiol-oxirane) reaction. Thiol-epoxy polymers are known for high chemical resistance and mechanical strength. Commonly used in biosynthetic and biomedical applications (Baidya 2008), this reaction is said to occur by nucleophilic ring-opening, where the proton capture can occur from the thiol or the catalyst. The thiol-epoxy reaction can be initiated by Lewis acids as well as bases (Watts 2001). In literature, few kinetics studies have been performed on this reaction (Amantini 2003, Fringuelli 2003, Lowe 2010) and, like the thiol-ene Michael addition,

knowledge about the mechanism is just emerging (Binder 2014, Brändle 2012, Jin 2015). In this work, 1,8-diazabicyclo[5.4.0]undec-7-ene (DBU), a nitrogen-centered catalyst, is used to catalyze thiol reactions with acrylate as well as epoxide functional groups.

Multifunctional thiols and multifunctional vinyls have been utilized to form highly uniform and homogenous networks (Hoyle 2010a). Thiol-Michael polymerizations are step-growth reactions. This fact eliminates common issues associated with thiol-acrylate reactions such as oxygen inhibition or acrylate homopolymerization (Mather 2006). However, due to typical reactant structures and the step-growth polymerization mechanism, thiol-Michael networks exhibit low glass transition temperature (T_g) and low crosslink density, which limit their applications (Kwisnek 2009, Nair 2014, Rydholm 2008, Shin 2009). Recently, there has been interest in using multi-component systems to produce structurally diverse polymers. Hybrid polymer chemistry, where one or more monomers contain functional groups which are reacted by multiple curing methods, is one approach to achieve these materials (Wei 2007). Specifically, this work will focus on the combination of thiol-ene and thiol-epoxy reactions to produce hybrid phase-separated materials. In the literature, these reactions have only been performed under different reaction conditions, such as UV initiation, with the goal of producing single-phase, high T_g materials (Carioscia 2007a, 2007b, Flores 2013, Itoh 1996, Jian 2013, Li 2017, Nair 2012, Ortiz 2008a, 2007, 2014, 2008b, Sangermano 2010, 2015, Shin 2010).

Bowman and coworkers (Carioscia 2007b) were the first to study hybrid polymers produced by thiol-ene and thiol-epoxy reactions. They aimed to combine the benefits of the thiol-ene network (fast reaction, lack of oxygen inhibition, and high selectivity) with those of thiol-epoxy resins (chemical resistance, high T_g, and mechanical strength). They investigated the effects of monomer ratios and reaction conditions on final material properties of a photo-initiated thiol-ene reaction and base-catalyzed thiol-epoxy reaction. Their findings established that the order of sequential reactions significantly affects final conversion, as monomer mobility is a key factor in reaction conditions of network formations. Ortiz and coworkers (Ortiz 2007, 2014, 2008a,

Sangermano 2010, 2015) approached a similar synthesis by introducing a cationic thiol-epoxy reaction into a photopolymerizable thiol-ene formulation. This synthesis is made possible through the use of a photoinitiator that undergoes photolysis to protonate the epoxy monomer. Jian et al. (Jian 2013) used both a free-radical photoinitiator and photo-base generator to prepare thiol-ene/thiol-epoxy hybrid systems.

Thus, based on results in the open literature, thiol-ene/thiol-epoxy hybrid materials have been produced only via use of two synthesis techniques, UV and thermal initiation, performed sequentially. With sequential reactions, full conversion cannot always be achieved as the initially cured network can hinder the formation of the second network. Here, we present results of the first study to undertake a one-pot, single-catalyst approach to the synthesis of thiol-ene-epoxy polymers. This approach provides synergistic property enhancements through a synthesis that is much simpler and more efficient than the multi-step or multi-catalyst approaches currently presented in literature. In the cases studied here, the network is formed with all three components. With DBU as a catalyst, both reactions can achieve full thiol conversion under ambient conditions. Through characterization of reaction kinetics and study into structure design, the first phase-separated thiol-acrylate-epoxy polymer was synthesized. From these phase-separated materials, a novel type of thermally induced shape memory polymer with good thermal and mechanical properties was synthesized and characterized.

3.2 Experimental Section

3.2.1. Materials

Trimethylolpropane tris(3-mercaptopropionate) (TMPTMP) (Aldrich, > 95%), Bisphenol A diepoxide DER 383 (The Dow Chemical Company), 1,6-hexanediol ethoxylate diacrylate (314 g/mol, Aldrich) and the catalyst, 1,8-diazabicyclo[5.4.0]undec-7-ene (Aldrich) were used as received. Difunctional urethane acrylates of various molecular weights (1000, 2000, and 4000 g/mol) were synthesized by The Dow Chemical Company from a poly(propylene oxide)

urethane prepolymer end-capped with acrylate functional groups and used as received.

3.2.2. Simultaneous Polymer Synthesis

A mixture of epoxide-containing monomer and acrylate-containing monomer were placed in a FlackTek cup, and a stoichiometric amount of thiol-containing monomer (pre-mixed with 0.5 mol % DBU with respect to SH) was added and mixed in a high-speed mixer (FlackTek, DAC 150.1 FVZ-K) for 30 s at 2000 rpm. The reaction proceeded at room temperature (23 °C). The studied stoichiometries were 1.0:0.5:0.5 eq. thiol:epoxide:acrylate functional groups and 1.0:0.9:0.1 eq. thiol:epoxide:acrylate functional groups.

3.2.3. Sequential Polymer Synthesis

Thiol-acrylate then thiol-epoxide: 1.0 eq. thiol (pre-mixed with 0.5 mol % DBU with respect to SH) was mixed with 0.5 eq. acrylate in a high-speed mixer for 30 s at 2000 rpm and reacted until complete conversion (confirmed by Fourier-transform infrared spectroscopy (FTIR)) at 23 °C. 0.5 eq. epoxide was then added and hand-mixed for 15 s. Thiol-epoxide then thiol-acrylate: 1.0 eq. thiol (pre-mixed with 0.5 mol % DBU with respect to SH) was mixed with 0.5 eq. epoxide in a high-speed mixer for 30 s at 2000 rpm and reacted until 50% epoxide conversion (before gelation) at 23 °C and then 0.5 eq. acrylate was added and hand-mixed for 15 s.

3.2.4. Nomenclature

Polymer samples are prepared in stoichiometric balance between nucleophile (thiol functional groups) and electrophiles (epoxide and acrylate functional groups). Because of this and for ease in mechanical property discussion, the samples will be referred to by the weight percent of the thiol-epoxide phase (X%E) and weight percent of thiol-acrylate phase (X%(Yg/mol A)), followed by sim or seq for simultaneous or sequential reactions, respectively. For example, a simultaneous reaction between 1.0 eq. thiol, 0.9 eq. epoxide and 0.1 eq. acrylate of 2000 g/mol is designated 74(E)/26(2000A)/sim. A sequential reaction between 1 eq. thiol, 0.5 eq. epoxide and 0.5 eq. acrylate of 314 g/mol is designated 52(E)/48(314A)/seq. The mass and mole percentages are clearly labeled for each sample in Table 3.1.

3.2.5. Monomer Conversion via FTIR

Attenuated total reflectance FTIR spectra were taken on a Bruker Tensor 37 FTIR spectrometer. The resolution for all infrared spectra was 4 cm^{-1}; there were 32 scans for each spectrum. To measure conversion, the thiol (wavenumber 2550 cm^{-1}), the vinyl of the acrylate (1620 cm^{-1}) and the alcohol formation (wavenumber 3500 cm^{-1}) peaks were used. Isothermal kinetics measurements were made from thin polymer films at room temperature (23 °C).

3.2.6. Analysis of FTIR Data

Functional group conversion was calculated with the following equation:

$$\text{Conversion (\%)} = \{[(A_x/A_{ref})_0 - (A_x/A_{ref})_t] / (A_x/A_{ref})_0\} \times 100\% \qquad \text{(Eq. 3.1)}$$

where A_x is the area of the functional group peak (x = ~2550 cm^{-1}, 1620 cm^{-1} and 3500 cm^{-1} for S-H, C=C and O-H stretches, respectively), and A_{ref} is the area of the internal standard peak.

3.2.7. Differential Scanning Calorimetry

Samples were characterized using a Mettler-Toledo DSC822e. A sample of ~8 mg was placed into a 40 μl aluminum pan and annealed for 10 min at 200 °C to erase the thermal history. After cooling at −40 °C/min to −80 °C, the heat flow was measured upon heating at 10 °C/min to 200 °C. The reported T_g is by the half-ΔC_p method. Extent of phase separation can be quantified through the comparison of the heat capacities for the thiol-epoxide phase and pure thiol-epoxide system. Phase separation % is estimated by the following equation:

$$\text{\% Phase Separated} = [(Cp_{T\text{-}E\text{-}A} / x_{T\text{-}E}) / Cp_{T\text{-}E}] \times 100\% \qquad \text{(Eq. 3.2)}$$

where $Cp_{T\text{-}E\text{-}A}$ is the heat capacity of the thiol—epoxide phase in a three-component polymer, $x_{T\text{-}E}$ is the theoretical weight fraction of thiol-epoxide phase and $Cp_{T\text{-}E}$ is the pure thiol-epoxide heat capacity measured by DSC.

3.2.8. Turbidity via UV-Vis Absorbance Spectroscopy

After 30 s mixing in FlackTek high-speed mixer, the reaction mixture was placed in a disposable cuvette (polystyrene, 10 mm path length, 2.5–4.5 mL). Light transmission at 800 nm was recorded with a UV–Vis absorbance photo-spectrometer (PerkinElmer, Lambda 35) as a

function of time at 23 °C. The relative change in transmitted light was used to estimate the onset of phase separation.

3.2.9. Tensile Testing

Samples were cured at T_g + 20 °C in a hot press until complete conversion was achieved and confirmed by FTIR. Dumbbell-shaped specimens (1 mm × 2.5 mm x 20 mm) were cut from films using a Dewes-Gumbs die. Mechanical properties were measured using a Sintech 20/G following ASTM 1708 (100 N load cell; crosshead speed 130 mm min^{-1}). Young's modulus was determined from the initial slope of the linear portion (the first 3–6% elongation) of the stress–strain curves. Elongation at break and yield strength were also determined.

3.2.10. Dynamic Mechanical Testing

Dynamic mechanical analysis (DMA) samples were cured in the same manner as for tensile testing and cut to dimensions of 3 mm × 10 mm × 30 mm. The storage modulus and tan delta curves were determined using a TA RSA3 DMA over a temperature range of −80 to 100 °C at a frequency of 1 Hz and a heating rate of 3 °C/min.

3.2.11. Shape Memory Testing

A shape memory test was conducted using a Sintech 20/G (100 N load cell; crosshead speed 130 mm min^{-1}; 350 Hz data acquisition frequency) instrument equipped with an Instron temperature chamber and liquid nitrogen. Dumbbell-shaped samples (30 mm length, 2 mm thickness) were prepared by the same method as the tensile samples. Results are the average of five trials. Shape fixity (R_f) and shape recovery (R_r) values were calculated as follows:

$$R_f = \varepsilon/\varepsilon_{max} \text{ x } 100 \text{ (\%)} \qquad \text{(Eq. 3.3)}$$

$$R_r = \varepsilon_{final}/\varepsilon_{max} \text{ x } 100 \text{ (\%)} \qquad \text{(Eq. 3.4)}$$

where ε, ε_{max}, and ε_{final} are the strain after shape-fixing, the maximum strain and the final strain after the shape recovery cycle, respectively. The sample characterized with this method was 74(E)/26(2000A)/sim, as this was the optimized composition of reactants according to preliminary bending test evaluations. The sample was clamped into the Sintech 20/G and elongated to ε_{max} (10–

20%) after heating to a temperature 60 °C (~T_g + 30 °C). This strain was maintained for 3 min to allow for relaxation of polymer chains. While being held under constant stress, the temporary shape was fixed by controlled cooling (−6 °C/min) to 0 °C. After 3 min, the strain was reduced until a stress-free condition was achieved at 0 MPa. The polymer was then heated to 60 °C while the stress was held constant at 0 MPa, resulting in the contraction of the sample to its permanent shape.

3.3. Results and Discussion

3.3.1. Polymer Synthesis, Reaction Kinetics and Phase Separation

For the simultaneous synthesis of a thiol-acrylate-epoxy polymer, a system was chosen in which a multifunctional thiol was able to react with both acrylate and epoxide, each of which act as an electrophile, under the same conditions. The model reactants are shown in Figure 3.1. The trifunctional thiol (TMPTMP) and DBU are added to a mixture of diacrylate and diepoxide. With the use of DBU catalyst, a thiol can react with both diacrylate and diepoxide. In recent literature, these components have only been combined sequentially using UV and thermal approaches to produce hybrid polymers (Carioscia 2007a, Jian 2013, Ortiz 2008b).

In order to characterize the reactivity of these components and how the polymer network is formed, the kinetics of the three-component reactions were studied at room temperature. The conversion of each functional group was tracked as a function of reaction time using FTIR. Figure 3.2 shows the thiol conversion over the course of the reaction for 1.0:0.5:0.5 eq. thiol:epoxide:acrylate sample in the presence of 0.5 mol% DBU (52(E)/48(314A)/sim). The thiol-acrylate reaction occurs rapidly (<5 min) and is complete before the thiol-epoxy reaction, which occurs at a much slower rate. This difference in reaction rate is evident under different catalyst loadings as well as different relative stoichiometries of reactants. Additional experiments show that the thiol-epoxide reaction is more sensitive to increases in temperature while the thiol-acrylate reaction is more sensitive to increases in catalyst. (Future work focused on the quantification of these different reaction rates is warranted.) Room temperature reactions were characterized here

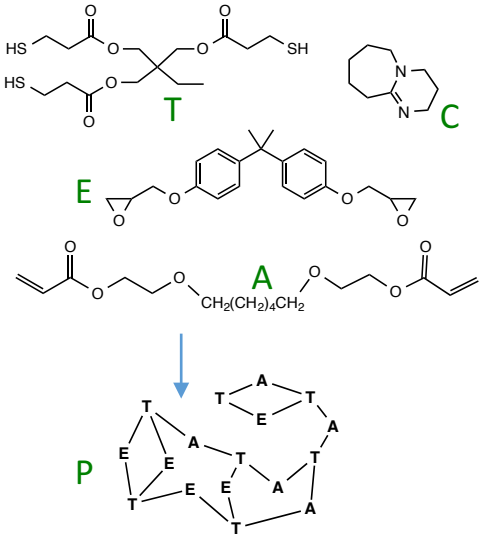

Figure 3.1. Model hybrid thiol-acrylate-epoxy reactants: T: Trimethylolpropane tris(3-mercaptopropionate), E: Bisphenol A epoxy resin, A: 1,6-Hexanediol ethoxylate diacrylate, C: 1,8-Diazabicyclo[5.4.0]undec-7-ene. P: Proposed network product for 1.0:0.5:0.5 T:E:A (sample 52E/48(314A)/sim).

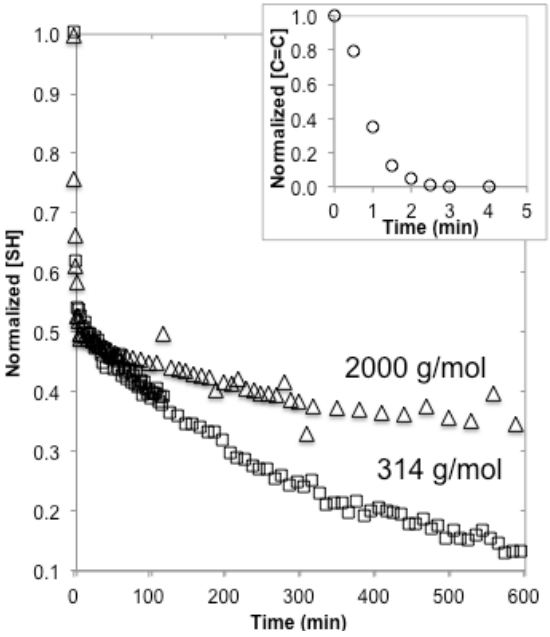

Figure 3.2. Fractional conversion as a function of time for simultaneous room temperature reaction of 1.0 eq. thiol, 0.5 eq. epoxide and 0.5 eq. acrylate in the presence of 0.5 mol% DBU. (square) SH conversion for reaction with 314 g/mol diacrylate to produce sample 52(E)/48(314A)/sim. (triangle) SH conversion for reaction with 2000 g/mol diacrylate to produce sample 24E/76(2000A)/sim. (circle) Acrylate group conversion in inset**.**

in order to monitor the rapid thiol-acrylate reaction as well as to maintain a reasonable rate for the thiol-epoxide reaction.

To investigate the behavior of these materials as phase-separated elastomers, a high molecular weight (MW) soft-segment diacrylate (2000 g/mol poly(propylene oxide) urethane diacrylate) was used at the same 1.0:0.5:0.5 stoichiometry (24(E)/76(2000A)/sim). Figure 3.2 shows the reaction conversion of thiol in the presence of 0.5 mol% DBU as a function of time at 23 °C for these multi-component reactions. As expected, the functional groups are diluted in the high MW system and cause a decreased reaction rate. The thiol-acrylate reaction nevertheless proceeds to completion in 10 min whereas the thiol-epoxide reaction does not reach full conversion during the 600 min reaction time scale shown in Figure 3.2 (within error, full conversion is achieved in 26 h). At a temperature of 50 °C, all reactions are complete in less than 20 min. Table 3.1 indicates that all of the hybrid polymers made with a 1.0:0.5:0.5 stoichiometry are single-phase materials as determined by the appearance of a single T_g by DSC, as well as lack of turbidity.

To increase the incompatibility of the components and induce phase separation, a different stoichiometry (1.0:0.9:0.1 eq. thiol:epoxide:acrylate with 0.5 mol% DBU) was used, with the resulting material being a novel phase-separated thiol-acrylate-epoxy polymer (sample 74(E)/26(2000A)/sim), the first reported in the literature. As shown in Figure 3.3, the conversion-time profile is different than that for the 1.0:0.5:0.5 eq. thiol:epoxide:acrylate discussed previously. Thiol concentration decreases rapidly when reacting with the acrylate, followed by a slow (almost plateaued after ~10% conversion) reaction with the epoxide. At 345 min, phase separation occurs (measured by the onset of the decrease of light transmittance through the reacting mixture). We hypothesize that once the thiol-epoxide blocks reach and exceed a critical MW, the thiol-epoxide and epoxide monomers phase separate from the thiol-acrylate blocks. After phase separation, the reaction rate increases as the local concentrations of thiol- and epoxide-containing monomers have increased by being in an epoxy-rich phase.

Table 3.1. Thermal and mechanical properties for hybrid thiol-ene-epoxy polymers produced by simultaneous or sequential thiol-epoxide then thiol-acrylate reactions. Shaded row indicates material tested for shape memory.

Nomenclature	MW_A	E_{phase}:A_{phase} (wt%/mol frac)	Modulus (MPa)	Elongation at Break (%)	Ultimate Strength (MPa)	T_g (°C)	Phase Separated (%)
52(E)/48(314A)/sim	314	52:48 / 0.5:0.5	6.1 +/- 0.4	50 +/- 13	1.7 +/- 0.1	-6	No
52(E)/48(314A)/seq	314	52:48 / 0.5:0.5	7.2 +/- 1.5	25 +/- 12	2.1 +/- 0.8	-6	No
35(E)/65(1000A)/sim	1000	35:65 / 0.5:0.5	3.2 +/- 0.2	210 +/- 25	1.6 +/- 0.8	-10	No
35(E)/65(1000A)/seq	1000	35:65 / 0.5:0.5	3.0 +/- 0.3	185 +/- 30	1.2 +/- 0.5	-12	No
83(E)/17(1000A)/sim	1000	83:17 / 0.9:0.1	180 +/- 10	35 +/- 10	9.7 +/- 0.8	-44, 27	Yes, 93%
74(E)/26(2000A)/sim	2000	74:26 / 0.9:0.1	140 +/- 12	85 +/- 15	11 +/- 2.0	-47, 28	Yes, 94%
56(E)/44(2000A)/sim	2000	56:44 / 0.8:0.2	13.5 +/-0.3	140 +/- 10	6.7 +/- 2.5	-49, 25	Yes, 72%
24(E)/76(2000A)/sim	2000	24:76 / 0.5:0.5	1.6 +/- 0.2	310 +/- 10	1.7 +/- 0.9	-49	No
24(E)/76(2000A)/seq	2000	24:76 / 0.5:0.5	Too adhesive to tensile test after compression molding			-48, 12	Yes, 24 %
61(E)/39(4000A)/sim	4000	61:39 / 0.9:0.1	23 +/- 3	135 +/- 25	8.2 +/- 1.4	-55, 29	Yes, 91%

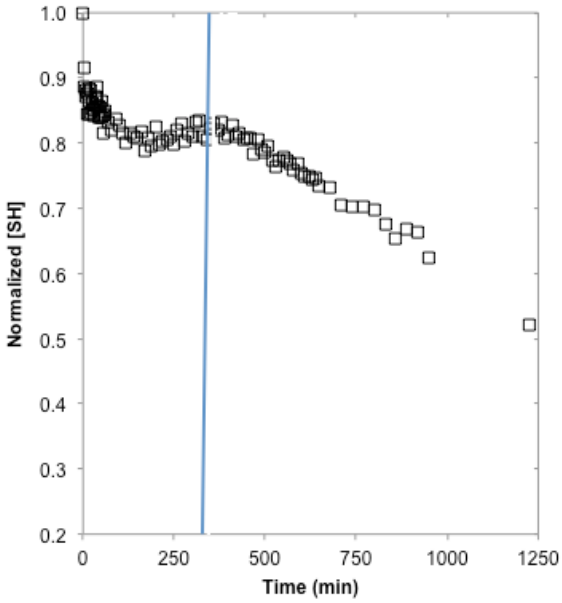

Figure 3.3. Fractional conversion as a function of time for simultaneous room temperature reaction of 1.0 eq. thiol, 0.9 eq. epoxide and 0.1 eq. acrylate (2000 g/mol diacrylate) in the presence of 0.5 mol% DBU, (sample 74E/26(2000A)/sim). Line represents onset of phase separation from turbidity measurements.

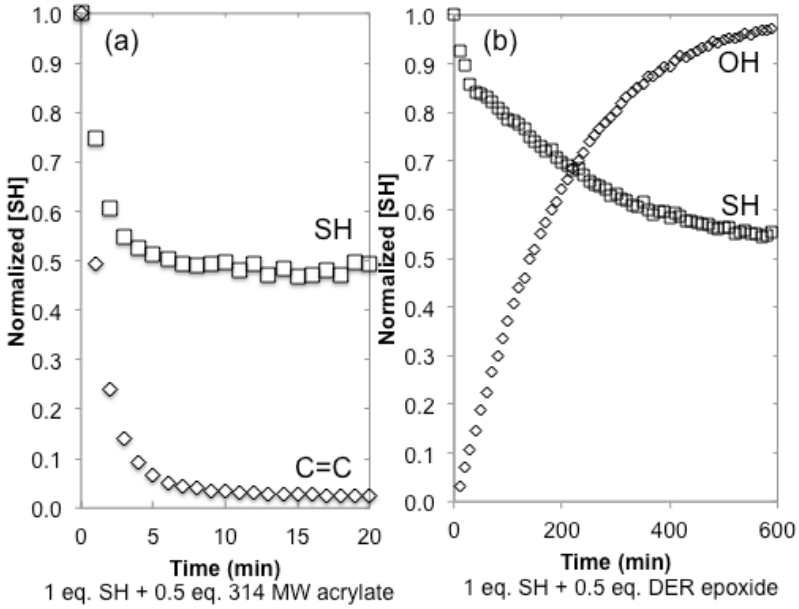

Figure 3.4. Two-component fractional conversion as a function of time for 1.0 eq. thiol in the presence of 0.5 mol% DBU and a) 0.5 eq. acrylate (314 g/mol diacrylate) or b) 0.5 eq. epoxide. Reactions occur at room temperature.

3.3.2. Comparison of Simultaneous and Sequential Reactions

In addition to the novel simultaneous synthesis of hybrid thiol-acrylate-epoxy polymers described above, a sequential synthesis approach was also employed. Because there are two electrophiles in this polymerization, it is possible to perform the sequential reaction two ways: first thiol-acrylate and then thiol-epoxide, or first thiol-epoxide and then thiol-acrylate. To investigate the reactions of the sequential addition, the kinetics of two-component mixtures (thiol-acrylate and thiol-epoxide) were characterized. Figure 3.4 shows the separate reaction conversions as a function of time for 1.0 equivalence of thiol reacted with 0.5 equivalences of acrylate and epoxide in the presence of 0.5 mol% DBU. The two-component reaction kinetics are indicative of the first step of each of the sequential reactions. From the simultaneous reaction kinetics described above, it is known that the thiol-acrylate reaction reaches nearly complete conversion before significant thiol-epoxide conversion occurs, which is comparable to the first thiol-acrylate and then thiol-epoxide sequential reaction. All syntheses performed with this type of sequential addition showed reaction kinetics that were the same within error as the kinetics of the simultaneous addition. In addition, the mechanical properties of the hybrid polymers were identical within error when synthesized by these two reaction types.

In contrast, relative to the results for the simultaneous reactions, some similarities as well as differences are apparent when sequential reactions are done as first thiol-epoxide then thiol-acrylate additions. Similarities are shown in cases where low MW acrylates are used as reactants. After the thiol-epoxide reaction is underway, the addition of either 314 g/mol or 1000 g/mol diacrylate results in a single-phase reaction mixture, which allows for the thiol to reach complete conversion. Figure 3.5 (curve a) shows the fractional conversion as a function of time for the first thiol-epoxide then 314 g/mol diacrylate addition in the presence of 0.5 mol% DBU. Upon the addition of the acrylate, the thiol, catalyzed by DBU, preferentially undergoes the thiol-Michael addition. After completion of the thiol-Michael reaction, the thiol-epoxide reaction continues to full conversion. Table 3.1 shows that all materials that maintain a single phase throughout the

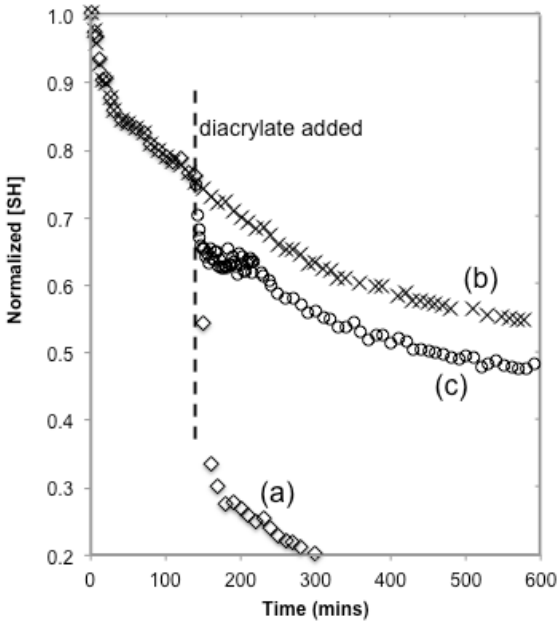

Figure 3.5. Fractional conversion as a function of time for sequential addition of 0.5 eq. epoxide to 1.0 eq. thiol in the presence of 0.5 mol% DBU, followed by the addition of 0.5 eq. acrylate after 25% thiol conversion: (a) 314 g/mol diacrylate added which results in a single-phase system (sample 52E/48(314A)/seq) (b) 2000 g/mol diacrylate added which results in a two-phase system (sample 24E/76(2000A)/seq), and (c) premixed 2000 g/mol diacrylate and 0.1 mol % DBU added which results in a two-phase system.

reaction will produce similar thermal and mechanical properties.

The difference between the simultaneous reaction and the first thiol-epoxide then thiol-acrylate sequential addition is highlighted in the systems in which phase separation can occur. With 1000, 2000, 4000 g/mol reactants forming the soft segments, incompatibility plays a large role in the reaction chemistry. In the simultaneous reactions using a 1.0:0.5:0.5 eq. thiol:epoxide:acrylate with 2000 g/mol diacrylate, there is no apparent phase separation (sample 24(E)/76(2000A)/sim). With sequential addition (first, thiol-epoxide then thiol-acrylate using the same stoichiometry), the addition of the acrylate immediately results in phase separation (sample 24(E)/76(2000A)/seq). Phase separation is made apparent in two ways: the appearance of two T_g values (one associated with the thiol-acrylate-rich phase and the other with the thiol-epoxide-rich phase) and the presence of sample turbidity. In Figure 3.5 (curve b), the conversion of the thiol is unaffected by the addition of the diacrylate and the thiol appears to not participate in the thiol-Michael addition. This result can be explained by the thiol molecules entering the epoxide molecule phase or that DBU catalyst enters the epoxide molecule phase. Without the significant presence of thiol or DBU in the acrylate phase, the thiol-acrylate reaction will proceed slowly, if at all. An experiment that supports this explanation, in which another 0.1 mol % DBU was premixed with diacrylate before addition, was performed (See Figure 3.5 (curve c)). With the additional DBU, there was a rapid 10% thiol conversion due to the acrylate addition, but phase separation dominated and the overall reaction was incomplete. Additional experiments were performed at higher temperatures in which complete conversion was achieved in both phases as the thiol-acrylate reaction can be thermally-initiated.

The first simultaneous synthesis approach for producing thiol-acrylate-epoxy polymer networks was presented with the use of a single base catalyst DBU. Sequential reactions can also be used to produce these materials with results dependent on the phase behavior. Phase separation of multi-component systems plays a large role in the final conversion, morphology and properties

of the material.

3.3.3. Thermal and Mechanical Properties of Hybrid Polymer Networks

The hybrid polymers described above were synthesized in order to combine two distinct polymer networks and enhance thermal and mechanical properties. Here, using thiol, acrylate and epoxide, the resulting polymer has the typical advantages associated with thiol-ene networks but with a higher T_g usually associated with epoxy polymers. The T_g's of the synthesized polymers, however, are limited by the flexibility of the chosen monomers. For example, stoichiometric reaction of a two-component trifunctional thiol and the difunctional epoxide leads to a material with a T_g of 31 °C, which represents the upper limit of any polymer containing this flexible thiol monomer and explains why the higher of the two T_g's in our phase-separated hybrid polymer networks are only several degrees above room temperature.

Because of the many variables (e.g. stoichiometry of electrophiles, MW of diacrylate, type of addition, etc.), the potential thermal and mechanical properties associated with this hybrid polymer system are vast. Table 3.1 summarizes the structure–property relationships of the hybrid polymers synthesized in this study. These materials were tested after full (>99%) conversion. When comparing heat capacities of thiol-epoxide phases in the polymer and material made using only thiol and epoxide (see experimental section), extent of phase separation can be estimated quantitatively. For example, the 74(E)/26(2000A)/sim sample exhibits nearly complete (94%) phase separation, whereas the 56(E)/44(2000A)/sim sample is only partially (74%) phase separated. The partial phase separation of 56(E)/44(2000A)/sim is also supported by comparison of T_g's. Sample 24(E)/76(2000A)/seq, which exhibits an estimated 24% phase separation, have an upper T_g that is well below room temperature (12 °C) due to the incomplete phase separation caused by the sequential addition technique.

With phase-separated systems which have a phase with T_g above room temperature, tensile properties can be optimized by adjusting either molar equivalences or MW of the acrylate soft segment. For example, elongation at break can be enhanced from 85% (74(E)/26(2000A)/sim) to

310% (24(E)/76(2000A)/sim) with an increase of the high MW acrylate reactant from 10 to 50 mol %. In accordance with the kinetics described above, the mechanical and thermal properties of single-phase materials are independent within error of reaction sequence. This result makes the one-pot simultaneous synthesis the simplest and best option for producing single-phase thiol-acrylate-epoxide networks. With reactions resulting in two-phase materials, robust properties are developed only from the simultaneous synthesis. For example, the 24(E)/76(2000A) polymers exhibit very different behavior when cured sequentially (first, thiol-epoxide then thiol-acrylate) compared to when cured simultaneously. After the sequential cure, the polymer exhibited qualitatively strong adhesion to the polyimide substrate on which it was cured but elastomeric behavior after the simultaneous cure with little adhesion to the substrate. Future studies are warranted to address the potential of these hybrid materials in adhesive applications (Leitsch 2016).

3.3.4. Use as Shape Memory Materials

Beyond the good tensile properties associated with the two-phase materials, some of these samples also exhibited good shape memory behavior. Such behavior is described below for the 74(E)/26(2000A)/sim sample (thiol-epoxide phase T_g = 28 °C). Shape memory polymers are able to form a temporary shape and recover rapidly to the permanent shape after a stimulus is applied (in this case, temperature) (Atli 2009, Behl 2007, Beloshenko 2007, Ge 2012, Huang 2010, Lendlein 2002, Liu 2007, Liu 2013b, Luo 2013, Mather 2009, Ratna 2008, Tcharkhtchi 2014, Xie 2011, Yan 2012). Most commonly, polymers rely on either physical or chemical crosslinks in their molecular structure to hold a temporary shape and to recover to the permanent shape. In this work, shape memory polymers take advantage of both the physical crosslinks provided by phase separation and the chemical crosslinks of network formation to provide a permanent structure with a flexible transition. First, qualitative testing (Lendlein 2002) was used to investigate the shape memory programming and recovery. As shown in Figure 3.6, a semi-circle was formed during the reaction curing step. Following that, the semi-circle was heated to 60 °C and deformed into one of

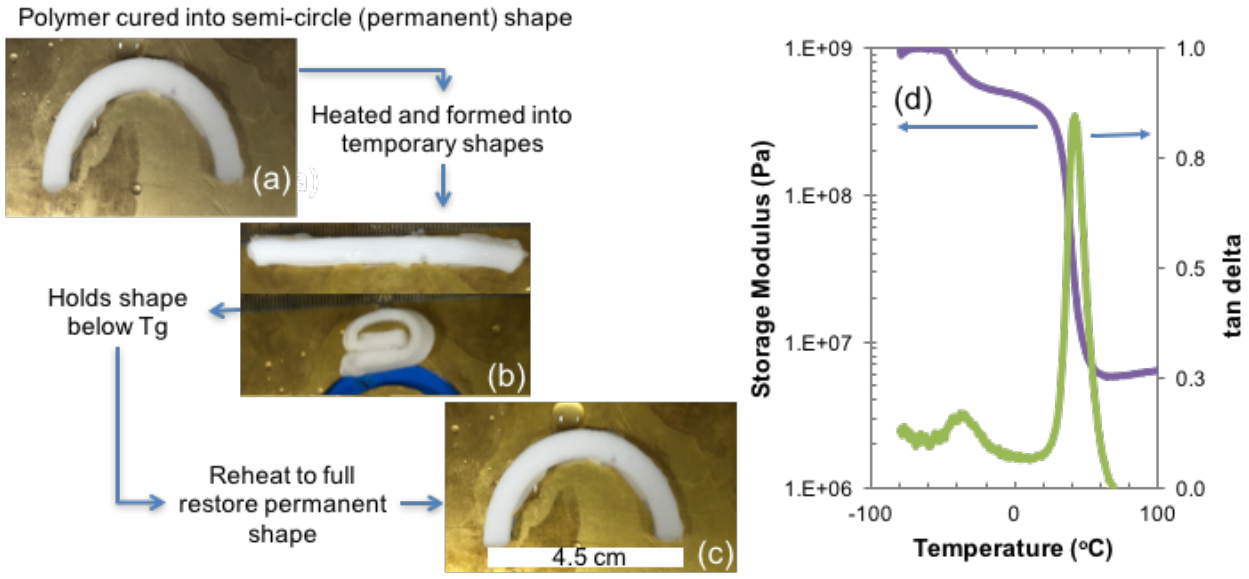

Figure 3.6. After cured into semi-circle shape (a) and heated above T_g, polymer is molded into rectangular slab or coil and cooled in ice bath to form temporary shape (b). After reheating above T_g, (c) sample fully recovers semi-circle shape. (d) Storage modulus and tan delta as a function of temperature curves for sample 74(E)/26(2000A)/sim.

two temporary shapes: rectangular slab and coil. The polymer was then cooled in an ice bath (0 °C) for 1 min and held its temporary shape. Upon reheating to 60 °C, the polymer was able to fully recover its original, semi-circular shape.

Shape memory polymers are typically characterized by a modulus that spans about two orders of magnitude as the temperature is varied (Behl 2007). As shown in Figure 3.6d, the thiol-epoxide phase glassy modulus is ~500 MPa at 0 °C and is reduced dramatically to ~6 MPa at 60 °C. The rigidity from the aromatic epoxide structure allows for the complete fixing of the temporary shape without creep. The thiol-epoxide domains exhibit a sharp transition region that allows for rapid recovery upon heating. Quantitatively, shape memory can be characterized through a stress-controlled programming cycle over a relevant temperature range (discussed in experimental section) (Atli 2009, Behl 2007, Beloshenko 2007, Huang 2010, Liu 2007, Luo 2013, Mather 2009, Ratna 2008, Tcharkhtchi 2014, Yan 2012). For the optimized composition, sample 74(E)/26(2000A)/sim (shown shaded in Table 3.1), the shape memory
properties are centered around a useful temperature transition (T_g = 28 °C), which could be convenient for applications switching between room (23 °C) and body temperature (37 °C). For samples strained to 10%, the average shape-fixity (R_f) was measured to be 91.5% and the average shape-recovery (R_r) was 99.2%. When ε_{max} = 20%, the average shape memory properties increased (R_f = 93.8% and R_r = 99.6%). It is possible that the shape-fixity is affected by the thiol-acrylate phase as that phase (with T_g = −47 °C) is mobile at the temperatures used during the testing cycle. These samples were also tested for multiple programming cycles, and the shape fixity and recovery results were consistent for three consecutive trials. The shape recovery values are comparable to other chemically crosslinked shape memory networks whereas the shape fixity values are slightly above these typical networks (Behl 2007, Lendlein 2005). Further studies to optimize shape memory properties are warranted.

3.4. Conclusion

The first simultaneous syntheses of hybrid polymers using catalyzed thiol-acrylate and thiol-epoxide reactions have been performed. To date, this is the only single-catalyst synthesis that combines these chemistries simultaneously to achieve full conversion of materials. Sequential syntheses with the overall same reactant composition were also performed, and properties of the resulting network polymers were compared to the polymers made by simultaneous reactions. For one-phase materials, both sequential and simultaneous reaction orders produce mechanically similar polymers. However, with two-phase materials, the simultaneous synthesis is the simplest technique and provides the best mechanical properties. In addition to the ease of synthesis, these polymers can be tailored to show shape memory behavior. The evident advantages of the thiol-acrylate-epoxide system are its facile synthesis, design versatility, and potential for new materials.

CHAPTER 4

EXPLOITING DISSIMILAR REACTION RATES TO MAINTAIN MORPHOLOGY IN SIMULTANEOUSLY CURED THIOL-ACRYLATE-EPOXY THERMOSETS

4.1. Introduction

Thermosetting polymers, polymer networks that cannot reach a fluid-like state at high temperatures due to chemical crosslinks, are employed in a wide range of applications including as shape memory materials, rubbers, coatings and foams (Brazel 2012). When designed for high mechanical strength and robustness, thermosetting polymers, such as epoxy resins, can be extremely brittle (Williams 1997). Heavily studied in literature, the toughening of epoxy resins can be done through structural variation of the starting materials or by the inclusion of a toughening phase such as a thermoplastic or rubber. In the latter category, rubber modified epoxy resins have been studied for decades, with research exploring structure, molecular weight and functionality of the rubber (Inoue 1995, Liu 2013b, PascaultJ. P. 2010, Ruiz-Pérez 2008). A common technique to produce these materials is reaction-induced phase separation. Reaction-induced phase separation involves a homogeneous mixture that undergoes liquid-liquid phase separation (Williams 1997). As the reaction progresses, the thermodynamics of homogeneity become unfavorable and the components begin to phase separate due to a reduction of entropy of mixing with increasing molecular weight and a changing reaction medium. To toughen epoxy resins, typically modifiers are added during the initial stages of the epoxy cure and allowed phase separate from the resin over the course of the reaction.

Widely studied in epoxy systems, reaction-induced phase separation has been observed to be sensitive to temperature, initiator/catalyst loading, composition and modifier type (Lipatov 2007, Meng 2006, Saito 1990, Szczepanskia 2012, Yamanaka 1989, Yu 2012, Zhang 2008). Because phase separation is occurring during the reaction, its extent is largely determined by gelation and vitrification of the system. Gelation limits the mobility of the polymer chains and

halts diffusion into separate phases from thermodynamic incompatibilities. Gelation is adjusted through kinetic parameters such as temperature and inherent rates of reactivity. In the literature, there are a number of factors controlling extent of phase separation, morphology and overall properties of the final materials, including structure compatibility of the phases (χ parameter), reaction rate, composition, mobility of chains (crosslink density) and degree of polymerization at gelation (Liu 2013b, Williams 1997). The competition between rate of polymerization and rate of phase separation controls the extent of phase separation. The dominant rate will largely determine the morphology and properties of the materials.

Research in reaction-induced phase separation has largely been focused on revealing the relationship between morphology and mechanical properties on model systems as the morphology can dramatically change as a function of the cure conditions. For example, Inoue and coworkers observed morphology changes between uniform spheres to cocontinuous structures dependent on the temperature of the first cure (Kim 1993, 1995, Yamanaka 1989). In these studies, the morphology-property relationships of these rubber modified epoxy resins were also examined and differences in modulus, vibrational damping, elongation and yield points were observed. Lemstra and coworkers also examined the effect of temperature on morphology and found that a stepwise cure was necessary for the desired properties. They employed a low temperature cure for the fixation of the desired spherical morphology followed by a high temperature cure to ensure complete conversion of the starting materials (Jansen 1999). The use of a two-step synthesis is not ideal for industrial applications because it is time and energy intensive compared to a one-step procedure. Research has also shown that block structure in copolymers can impact the morphology as the monomer structure can influence the overall reactivity of the functional group (Meng 2006, Yamanaka 1989). Another factor that can disrupt the ratio of reaction rate to phase separation rate is catalyst. In literature, it is observed that increased catalyst loading can cause changes in morphology due to increased reaction rate (similar to increased temperature) (Klempner 1985, Suthar 1995).

Literature has reported that changes in morphologies of modified epoxy resins produce materials with a wide range of thermal and mechanical properties. With the different extents of phase separation (caused by structure and rate changes described above), modified epoxy resins have been observed with single phase, lamellae, cocontinuous or spherical morphologies. Bates and coworkers designed nanostructured materials using different architectures of amphiphilic block copolymers (Grubbs 2000, Liu 2010). A popular method of achieving spherical domains is the use of specially designed AB and ABC block polymers (Girard-Reydet 1997, 1999, Liu 2010, Ritzenthaler 2002). This is possible as A is soluble in the thermosetting polymer while B is insoluble and thus leads to B being expelled from the network while still covalently attached. This procedure produces epoxide polymers that are less brittle than the original network. In addition to the use of thermoplastics, research has also incorporated reactive sites into the epoxy-miscible blocks in order to fix the desired morphology. However, the design of such monomers is multi-step and tedious.

Hybrid polymer networks, networks formed through multicomponent or multiple reaction mechanisms, have recently been used to incorporate thiol-ene networks into epoxy resins to decrease the observed brittleness (Carioscia 2007b, Jian 2013, Narayanan 2012, Sangermano 2010). Previously, in these hybrid systems with thiol, acrylate and epoxide starting materials, phase separation is difficult to achieve because of the reactant symmetry and compatibility. In previous works by our group, these hybrid components were mixed together using a simultaneous synthesis to produce one- and two-phase materials (Dhulst 2016, Jin 2016). The single phase materials showed properties that were a weighted average of rigid epoxy resins and flexible thiol-ene networks whereas the two-phase materials showed segmented behavior with both glassy and rubbery phases. Two-phase materials were able to capitalize on the flexibility of the thiol-acrylate network and the rigidity of the thiol-epoxy network in order to achieve elastomeric response and shape memory properties. These materials were able to phase separate through reaction-induced phase separation.

Previously, we generated a one-pot simultaneous synthesis of elastomeric materials at room temperature. Here, we investigate the cure variables of temperature and DBU catalyst concentration to show their minimal effectiveness on changing system morphology and properties. The purpose of this work is to demonstrate the ease of reaction-induced phase separation in these hybrid systems with two distinct reactions to produce toughened epoxy resins. In this work, properties and nanostructures in the thermosets were investigated by means of tensile testing and scanning electronic microscopy (SEM).

4.2. Experimental Section

4.2.1. Materials

Trimethylolpropane tris(3-mercaptopropionate) (Aldrich, > 95%), bisphenol A diepoxide DER 383 (The Dow Chemical Company), and the catalyst, 1,8-diazabicyclo[5.4.0]undec-7-ene (DBU, Aldrich) were used as received. Difunctional urethane acrylates of various molecular weights were synthesized by The Dow Chemical Company from a poly(propylene oxide) urethane prepolymer end-capped with acrylate functional groups and used as received. Structures of all reactants are shown in Figure 4.1.

4.2.2. Network Polymer Synthesis

A mixture of epoxide-containing monomer and acrylate-containing monomer were placed in a FlackTek cup, and a stoichiometric amount of thiol-containing monomer (pre-mixed with various wt % DBU with respect to SH) was added and mixed in a high-speed mixer (FlackTek, DAC 150.1 FVZ-K) for 30 sec at 2000 rpm. The reaction proceeded at various reaction temperatures (23, 30, 50, 70, 90 °C). The studied stoichiometry was 1.0:0.9:0.1 eq. thiol:epoxide:acrylate functional groups which produces 74(E)/26(2000A)/sim.

4.2.3. Monomer Conversion via FTIR

Attenuated total reflectance FTIR spectra were taken on a Bruker Tensor 37 FTIR spectrometer. The resolution for all infrared spectra was 4 cm^{-1}; there were 32 scans for each

spectrum. To measure conversion, the thiol (wavenumber 2550 cm^{-1}) and the vinyl of the acrylate (1620 cm^{-1}) peaks were used. Isothermal kinetics measurements were made from thin polymer films at room temperature (23 °C). Functional group conversion was calculated with the following equation:

$$\text{Conversion (\%)} = \{[(A_x/A_{ref})_0 - (A_x/A_{ref})_t] / (A_x/A_{ref})_0\} \times 100\% \qquad \text{(Eq. 4.1)}$$

where A_x is the area of the functional group peak (x = ~2550 cm^{-1} and 1620 cm^{-1} for S-H and C=C, respectively), and A_{ref} is the area of the internal standard peak. Epoxide conversion referenced in figures was calculated from thiol conversion after acrylate conversion was complete (assumed that no thiol-epoxide reaction happens during thiol-acrylate reaction).

4.2.4. Turbidity via UV-Vis Absorbance Spectroscopy

After 30 sec mixing in a FlackTek high-speed mixer, the reaction mixture was placed in a disposable cuvette (polystyrene, 10 mm path length, 2.5-4.5 mL). To characterize turbidity, light transmission at 700 nm was recorded with a UV-Vis absorbance spectrophotometer (PerkinElmer, Lambda 35). The relative change in transmitted light was used to estimate the onset of phase separation.

4.2.5. Morphology Characterization

Morphologies of hybrid samples were determined via field-emission scanning electron microscopy (FE-SEM) using an S-4800 II instrument (Hitachi) after sputtering (Denton Desk III) with gold/palladium.

4.3. Results and Discussion

Here, hybrid materials were synthesized from reactions between a trifunctional thiol and a balance of diacrylate and diepoxide. Shown in Figure 4.1, the three components with majority thiol-epoxy (74 wt % thiol-epoxide phase, 26 wt % thiol-acrylate phase and a stoichiometry of 1 eq. thiol, 0.9 eq. epoxide and 0.1 eq acrylate) formed an initially homogeneous mixture. Upon mixing base catalyst, 1,8-diazabicyclo[5.4.0]undec-7-ene (DBU), the reaction began

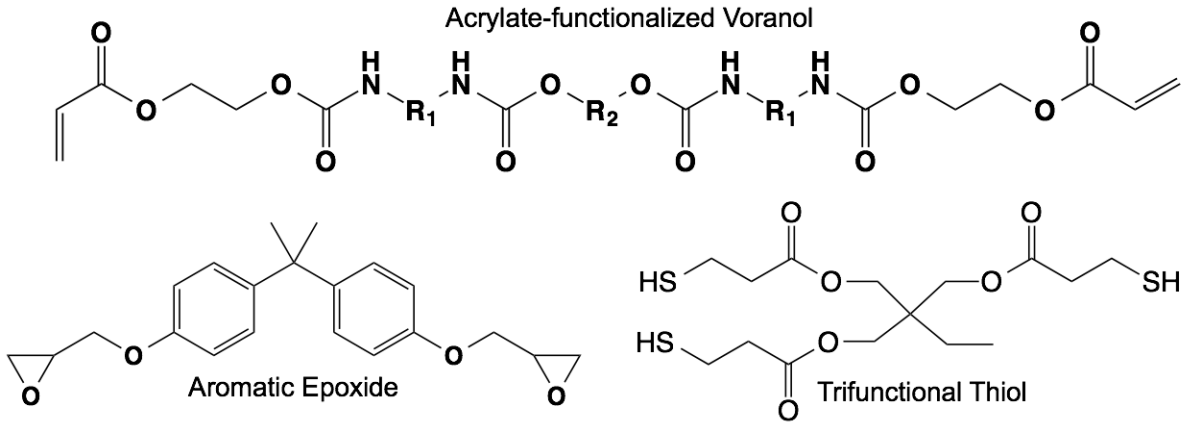

Figure 4.1. Hybrid thiol-acrylate-epoxide reactants: Acrylate-functionalized Voranol diol with R_1 = toluene and R_2 = 2000 g/mol poly(propylene oxide):, Aromatic epoxide: Bisphenol A diglycidyl ether, Trifunctional thiol: Trimethylolpropane tris(3-mercaptopropionate).

instantaneously and proceeded under ambient conditions. Previous studies have shown that, in the presence of DBU, thiol-acrylate reactions are rapid and thiol-epoxide reactions are much slower in comparison (Dhulst 2016, Hoyle 2010a, Jin 2016). In this work, the system undergoes reaction-induced phase separation as the oligomeric poly(propylene oxide) diacrylate phase separates from the crosslinking thiol-epoxide reaction. However, because of its reactive end-groups, the diacrylate participates in the thiol reactions and covalently connects to the thiol-epoxide network. As the reaction progresses, the crosslinking leads to formation of a stable morphology.

As the material cures and the thiol-epoxy phase reaches a critical molecular weight, the reaction mixture becomes turbid. Turbidity is often used as an indication of phase separation in mixtures. Here, turbidity is measured as a function of time, temperature and catalyst loading to obtain information of the reaction-induced phase separation of this system. To quantify the timescale of phase separation, the cloud point time (the time at which the reaction mixture becomes turbid) will be used to indicate the onset of two-phase formation. Two reactions (thiol-acrylate and thiol-epoxide) are involved in the overall conversion of thiol. It is known that both reaction rates can be tuned by reaction variables such as temperature and catalyst loading, but the impact on each rate will be different. With reaction-induced phase separation, any change in the reaction rate has the potential to change the morphology and therefore the thermal and mechanical properties of the network. Figure 4.2 shows the cloud point times as a function of catalyst loading and temperature. These onset times reveal that phase separation occurred in all studied systems. With increased catalyst loading, there is a non-linear decrease in phase separation onset times.

4.3.1. Effect of Catalyst Loading on Morphology

In previous studies, it was shown that at this functional group concentration, the thiol-acrylate reaction is complete or near completion before the thiol-epoxide reaction (Dhulst 2016). Therefore, it is the thiol-epoxide reaction that is at low conversion at the point of phase separation. The unreacted thiol and epoxide will both phase separate into a distinct phase due to their mobility

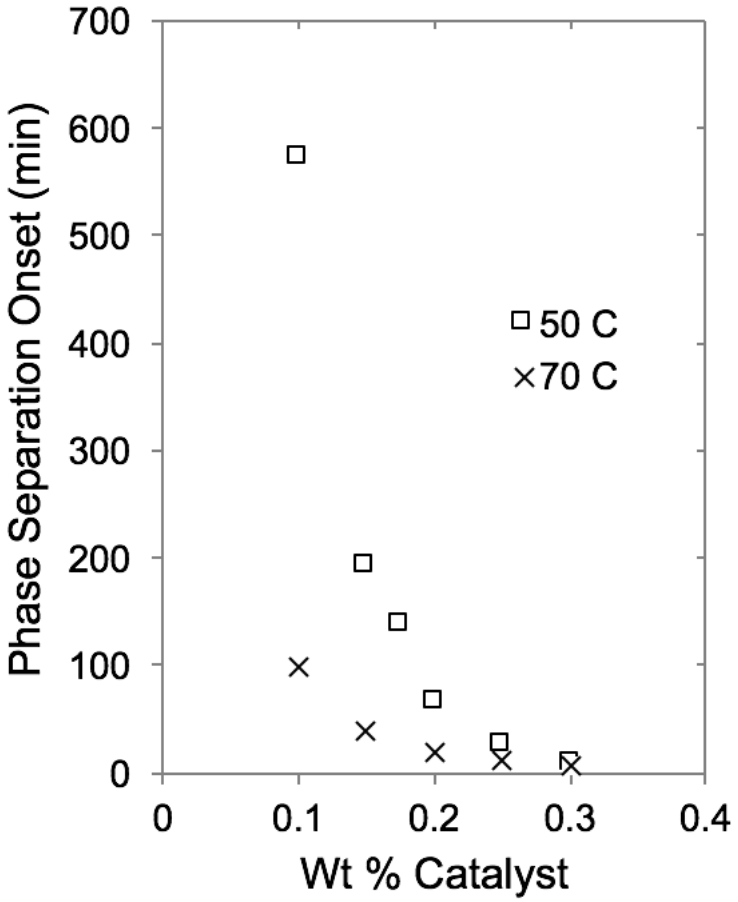

Figure 4.2. Phase separation onset times at different temperatures and DBU catalyst loadings for a reaction of 1.0 eq. thiol, 0.9 eq. epoxide and 0.1 eq. acrylate (2000 g/mol diacrylate) (74 wt % epoxide phase, 26 wt % acrylate phase). DBU wt % is relative to thiol concentration.

as small molecules, as well as their incompatibility with the oligomer chains. Because of this, we examine phase separation conversion levels through epoxide conversion. In order to understand which reaction is responsible for the changes in timescale of phase separation, each factor was investigated separately with respect to epoxide conversion. First, catalyst loading was examined for its effect on phase morphology. Figure 4.3 shows the impact of catalyst loading on the epoxide conversion at the onset of phase separation. With increased catalyst loading, both thiol reactions had increased rates. Although the thiol reactions are faster with increased catalyst loading, the epoxide conversion at which the phase separation occurs is independent (or nearly so) of catalyst loading over the range 0.15 wt % to 0.30 wt %. Conversions that are independent of catalyst loading reveal that the rate of phase separation is faster than the rate of reaction associated with gelation time at all tested levels of catalyst. Figure 4.4 shows the SEM images of thiol-acrylate-epoxide hybrid networks at selected catalyst loadings. According to SEM, the domain sizes of the epoxide phase remained very similar as a function of catalyst loading. Catalyst loading does not impact the gelation time and therefore the epoxide domains are able to reach a uniform size in all tested cases.

4.3.2. Effect of Temperature on Morphology

The most common method for increased reaction rate in the reaction-induced phase separation literature is to increase temperature. Specifically, in certain modified epoxy resins, changes in temperature and cure conditions led to changes in morphology and mechanical properties (Cho 1993, Jansen 1999, Varley 1996). In the hybrid system, a change of temperature will modify the rates of both reactions. Figure 4.5 shows the relationship between epoxide conversion at onset of phase separation and temperature. This temperature-conversion transformation plot gives us insight into the specific relationship of temperature with this phase-separated hybrid system. In particular, an increase in temperature leads to an increase in conversion at the cloud point. This behavior is indicative of a system with an upper critical solution

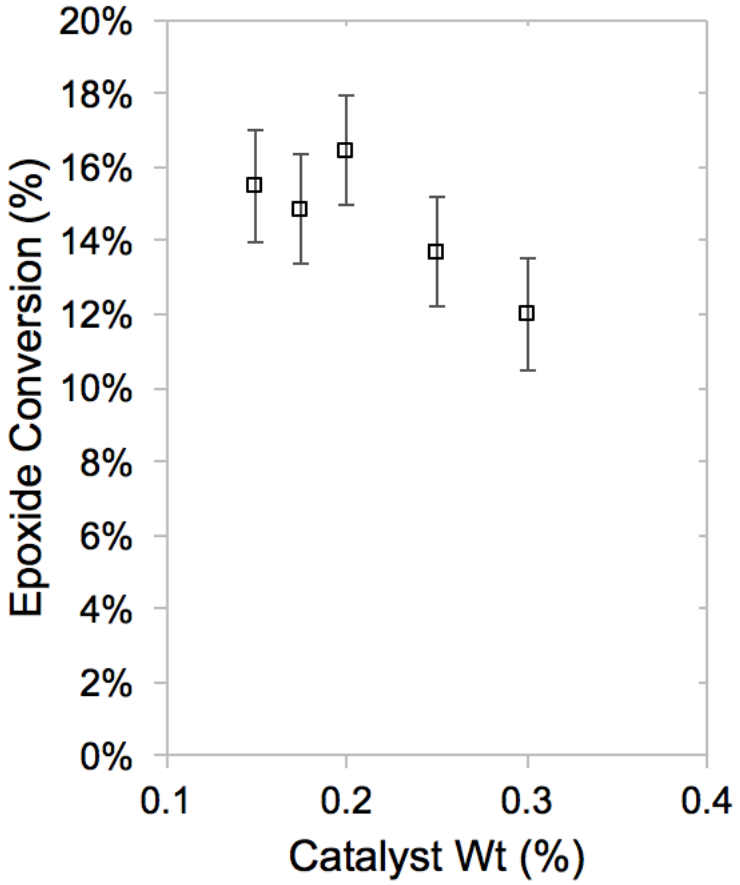

Figure 4.3. Epoxide conversion of a 1.0 eq. thiol, 0.9 eq. epoxide and 0.1 eq. acrylate (2000 g/mol diacrylate) (74 wt % epoxide phase, 26 wt % acrylate phase) reacting system at different catalyst loadings at 50 ºC at which phase separation onset occurs (determined by UV-Vis turbidity measurements). DBU wt % is relative to thiol concentration.

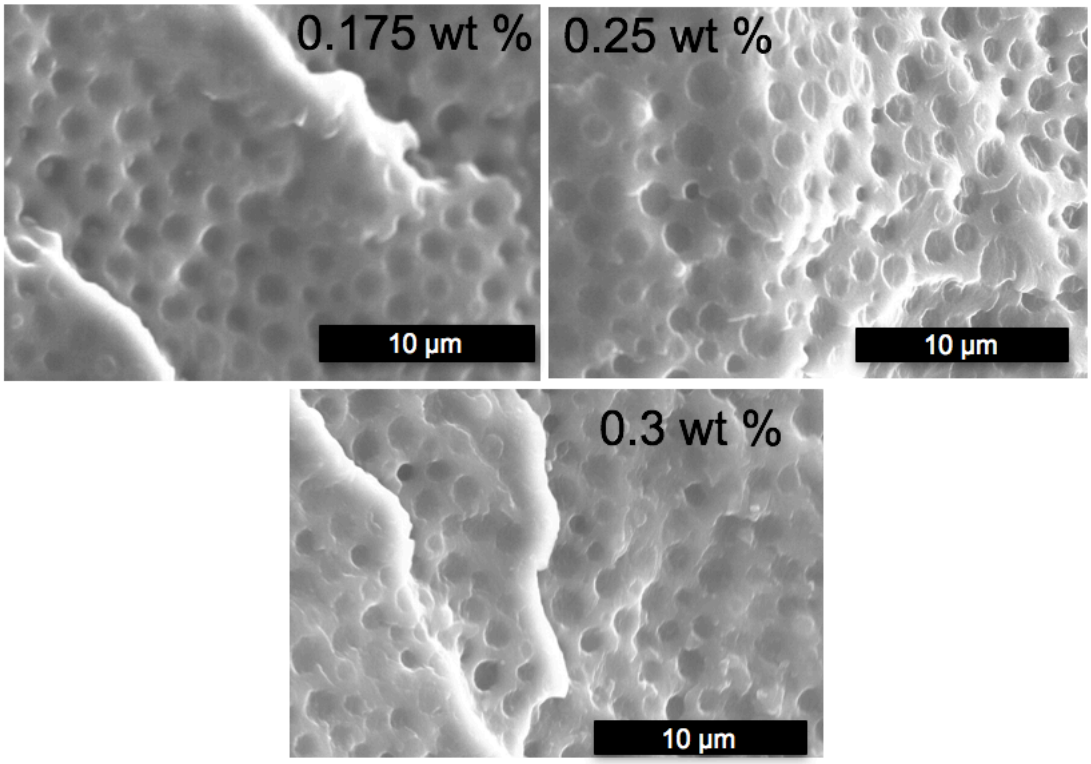

Figure 4.4. SEM images of thiol-acrylate-epoxide hybrid networks with 1.0 eq. thiol, 0.9 eq. epoxide and 0.1 eq. acrylate (2000 g/mol diacrylate) (74 wt % epoxide phase, 26 wt % acrylate phase) reacting system at different catalyst loadings at 50 ºC. DBU wt % is relative to thiol concentration.

temperature (UCST). With a higher reaction temperature, higher conversion levels are required for the system to phase separate as the reacting materials and products have an increased level of miscibility in the polymerizing medium.

With differences in cloud point conversion, the morphology has the potential to change as gelation can occur before phase separation is complete. To examine the effect of temperature on the morphology, hybrid samples were cured at both room temperature and 50 °C and examined by SEM. Figure 4.6 shows the resulting SEM images of thiol-acrylate-epoxide hybrid networks. It appears that when cured at different temperatures, the samples retain the spherical morphology. However, a notable difference between the two samples is the domain size of the thiol-epoxide phase. For hybrid samples, the domain size of the spheres apparently decreases with increasing temperature. As the reaction temperature is increased, the cure rate is accelerated and an increase in temperature will decrease the gelation time. With decreasing gelation time, the spheres do not have time to coarsen before their size is fixed.

As previously shown, the final thermal and mechanical properties of a modified epoxy resin are largely determined by the morphology (Cook 1996, Giannotti 2005, Mimura 2000, Ruiz-Pérez 2008). Table 4.1 gives a comparison of mechanical properties for a selection of thiol-acrylate-epoxide hybrid samples at the various temperature and catalyst conditions chosen. It can be seen that these samples have properties that are identical within error to the room temperature cured system with a standard loading of catalyst. These results show that the hybrid thiol-acrylate-epoxide system is in a distinctive class of modified epoxy resins in which an increased reaction rate does not change the overall properties. Most commonly, controlled cure conditions are the only way to achieve a desired morphology through reaction-induced phase separation. The hybrid systems produced the desired spherical morphology and matched previously seen tensile properties to produce a useful shape memory material under all conditions.

It is hypothesized that these materials, made under dramatically different reaction

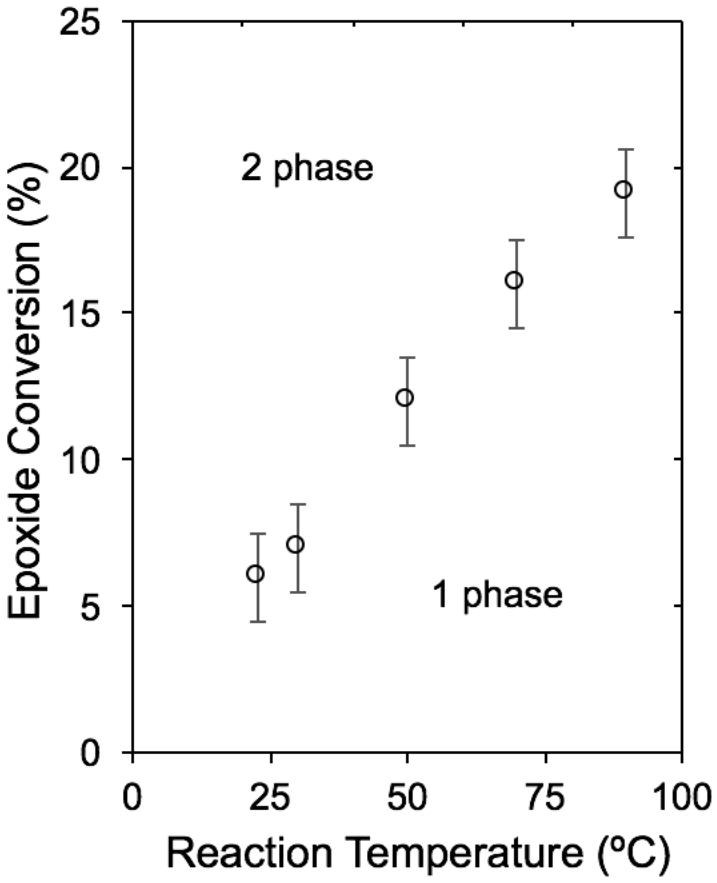

Figure 4.5. Temperature-conversion transformation diagram showing phase separation for a 1.0 eq. thiol, 0.9 eq. epoxide and 0.1 eq. acrylate (2000 g/mol diacrylate) (74 wt % epoxide phase, 26 wt % acrylate phase) system at constant DBU loading (0.3 wt % relative to thiol concentration).

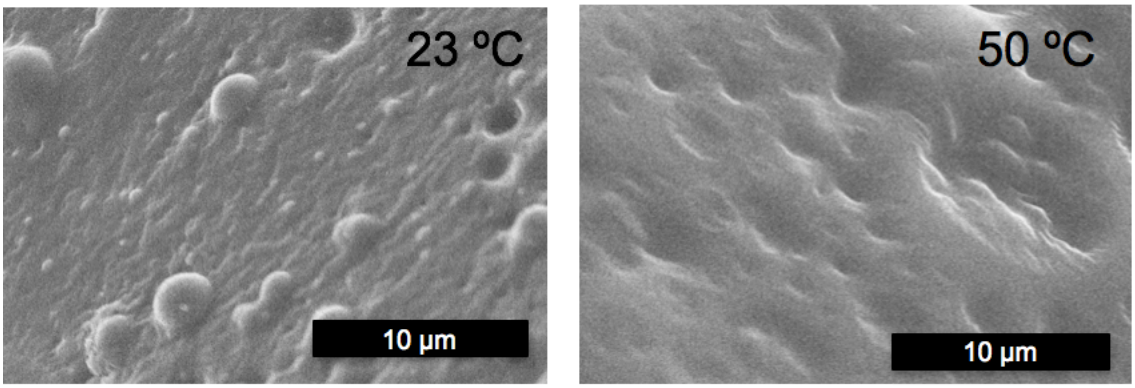

Figure 4.6. SEM images of thiol-acrylate-epoxide hybrid networks with 1.0 eq. thiol, 0.9 eq. epoxide and 0.1 eq. acrylate (2000 g/mol diacrylate) (74 wt % epoxide phase, 26 wt % acrylate phase) reacting system at different curing temperatures with 0.15 wt % catalyst relative to thiol concentration.

Table 4.1. Comparison of mechanical properties for 1.0 eq. thiol, 0.9 eq. epoxide and 0.1 eq. acrylate (2000 g/mol diacrylate), (74 wt % epoxide phase, 26 wt % acrylate phase), cured under different temperature and catalyst conditions. DBU wt % relative to thiol concentration.

Cure Temperature (°C)	Catalyst Loading (wt %)	Modulus (MPa)	Elongation at break (%)	Ultimate Strength (MPa)
23	0.15	138 +/- 5	60 +/- 9	13.7 +/- 3.1
50	0.15	140 +/- 12	85 +/- 15	11.0 +/- 2.0
50	0.30	141 +/- 5	72 +/- 15	9.2 +/- 0.8
70	0.15	146 +/- 4	66 +/- 3	12.9 +/- 1.0

conditions, produce identical morphologies and properties because of the highly dissimilar reaction rates of the thiol-acrylate and thiol-epoxide reactions. With the polymerization of the thiol-acrylate reactants, the flexible chains (thiol-acrylate) have reacted and not introduced any level of gel formation because of the off-balance stoichiometry. This essentially causes those chains to act as thermoplastic modifiers during the thiol-epoxide reaction. After the thiol-epoxide reaction begins, at a certain conversion, the epoxide-containing chains will phase separate from the system. However, because of the end-group functionality, at full conversion the immiscible chains are covalently attached to the thiol-epoxide network allowing for further fixation of the phase separated morphology. This approach is similar to AB/C thermoplastic modifiers but with a simple, one-pot synthetic method.

4.4. Conclusion

Reaction-induced phase separation is often used to induce nanostructures or microstructures into materials in order to enhance mechanical properties such as toughness. In hybrid systems with thiol, acrylate and epoxide starting materials, phase separation is difficult to obtain because of reactant symmetry and compatibility. Here, with the incompatibility of an oligomeric component as well as the rigidity of an aromatic epoxide, phase separation was shown to be achievable at room temperature. Often with reaction-induced phase separation, there is a trade-off between complete phase separation (to achieve a desired morphology) and complete conversion of a system. Here, we demonstrated that this hybrid system, through its use of two distinctly different reaction rates, can produce materials with essentially identical morphologies, and therefore essentially identical mechanical properties, under a wide variety of cure conditions. With a simple, one-pot synthesis, the oligomeric component phase separates but is still covalently attached to the network and fixes the phase separated morphology.

CHAPTER 5
NOVEL NETWORK ELASTOMERS SYNTHESIZED BY AMINE – VINYL SULFONE REACTIONS

5.1. Introduction

Polyurethanes are known for their versatility and wide applicability (Ahmad 2012, American Chemistry Council 2012, Andersson 2010, Engels 2013, Meier-Westhues 2007). However, exposure to isocyanates has been found to cause negative health effects and there has been increasing regulatory pressure by governmental agencies to find replacements (Guan 2011). Because of the fast and efficient isocyanate-alcohol reaction, there is a high benchmark of rapid reactivity for any potential polyurethane replacements. In recent research, focus on the synthesis and use of non-isocyanate polyurethanes (NIPUs) has led to the application of reactions well known in small-molecule organic chemistry to polymerizations (Cornille 2016, Guan 2011, Kathalewar 2013). Thermoset polyurethanes are chemically crosslinked networks with thermo-mechanical properties specific to their applications (Dušek 1969). Because of their lack of reprocessability, crosslinked polymers are sometimes synthesized at their application site. For example, coatings and adhesives are often applied as reactants and cured directly on a surface. Due to this necessity for speed, these materials are required to be fast reacting, as well as to have the ability to achieve high conversion under ambient conditions. Recently, the use of click reactions has led to synthesis of valuable materials with reaction rates that are competitive with isocyanate-alcohol reactions (Besse 2013, Dhulst 2016, Guan 2011, Jin 2016, Kathalewar 2013). However, the typical commercially available structures associated with these click reactants, e.g. mercaptopropionates, create difficulties in achieving mechanical robustness and high glass transition temperatures (T_gs) in the products (Hoyle 2010a). In addition, many click reactions require thermal activation to achieve fast reaction timescales (Leonards 2015, Nair 2012, Uygun 2010).

Vinyl sulfone is a well-studied functional group in small-molecule organic chemistry that is often used for post-functionalization in protein chemistry to produce water-stable products or as a method of bio-conjugation (Chatani 2013, Lopez-Jaramillo 2012, Podgórski 2014, Rizzi 2005, Simpkins 1990). Vinyl sulfone has high reactivity that is attributed to the extreme electron-withdrawing nature of the sulfone group, which allows for the vinyl to be a good electrophile (Esteves 2007). This electrophilicity allows for the group to be reactive toward nucleophiles. The sulfone group imparts flexibility into the backbone, similar to ethers or esters. In addition, sulfone lends solvent resistance that is usually missing from these functional groups.

Vinyl sulfones are reactive with functional groups such as alcohols, thiols and amines (Mather 2006). Only recently has vinyl sulfone been explored as a reactant in polymerization reactions. For example, the reactivity of vinyl sulfone toward nucleophiles has made them a promising alternative to (meth)acrylates in many reactions. The Michael addition, a thermodynamically controlled reaction between a nucleophile and an electrophile, has been recently used for polymerizations with thiols as reactants (Chan 2009a, Chatani 2013, Li 2010, Liu 2013a, Lutolf 2001, Nair 2014). Thiol-Michael reactions are rapid when catalyzed by either base or phosphine catalysts and are efficient with a number of electrophiles, including acrylates and maleimides (Wang 2013). However, the use of a thiol reactant for field-based applications has the disadvantage of the offensive thiol odor and lack of shelf stability (Hoyle 2010b).

Although recent interest has been shown in thiol-vinyl sulfone reactions, relatively little has been reported in regard to amine-vinyl sulfone polymerizations. The aza-Michael addition is similar to the thiol-Michael addition with an amine as the nucleophile (Esteves 2007, Magnier-Bouvier 2006, Mather 2006, Saidi 2009). Because of the inherent basic character of the amine, an external catalyst is not necessary for reaction with electrophiles. However, catalysts, such as Lewis acids, have been employed to increase the reactivity of certain sterically and/or electronically hindered amines (Wabnitz 2003, 2004). Other things being equal, secondary amines are more nucleophilic than primary amines and will be more reactive toward a vinyl sulfone in the aza-

Michael addition (Nguyen 2013, Wu 2004, Zheng 2005).

Most reported amine-vinyl sulfone reactions are utilized as an intermediate step to the final product (Jung 1991). For example, in the synthesis of macrocycles, two or three segments are vinyl sulfone functionalized and can be joined together through nucleophilic additions (Teyssot 2003). This reaction has also been successfully used in the field of protein chemistry to functionalize proteins that have thiol- or amine-containing residues, such as lysine (de Castries 2007, Li 2002a, Lopez-Jaramillo 2012, Masri 1988, Morpurgo 1996) or to covalently attach a protein to a vinyl sulfone functionalized substrate (Tosatti 2003, Wang 2015). However, in the field of polymer science, only three research teams have provided literature reports on this reaction to polymerize macromolecules (Gao 2001a, 2001b, 2001c, 2001d, 2002, 2001e, 2001f, Glória 2011, Halimehjani 2016, Wang 2012, Yan 2000). For example, Gao and coworkers have taken advantage of the reactivity difference between primary and secondary amines to produce a series of non-crosslinked branched polymers. In particular (Gao 2001e, 2001f), they used divinyl sulfone (A_2) and N-methyl-1,3-propanediamine (BB'_2) as monomers. The BB'_2 molecule contains both primary and secondary amines, and when synthesis was performed in a polar solvent, such as water or dimethyl sulfoxide, a linear polymer was obtained. However, upon altering the solvent polarity, as with the use of chloroform, a hyperbranched polymer was obtained. They suggested that the reaction mechanism differs as a function of solvent but did not provide a detailed discussion as the primary focus of their work was to produce branched polymers. Currently, there is no report of the reaction kinetics (reaction order, apparent rate parameters, etc.) for amine-vinyl sulfone polymerizations.

Here, reported for the first time, crosslinked elastomeric materials are synthesized with divinyl sulfone and diamines in solventless reactions without catalyst or thermal initiation. The electronic properties of the sulfone allow for fast reactions and the rapid synthesis of mechanically robust elastomers at room temperature. Reaction kinetics for amine-vinyl sulfone polymerizations and thermal and mechanical properties of the resulting polymers are presented. The elastomeric materials produced in this study exhibit competitive reaction kinetics and promising tensile

properties when compared with currently reported NIPU elastomers.

5.2. Experimental Section

5.2.1. Materials

Soft segments (~1750 g/mol polyether diamine Elastamine HE1700, PTMO) were obtained from Huntsman Chemical. Divinyl sulfone, 1,3-cyclohexane bis(methyl amine) and m-xylylene diamine were obtained from Sigma Aldrich. All reagents were used as received.

5.2.2. Polymer Synthesis

Divinyl sulfone (DVS) was added to a mixture of the polyether diamine and chain extender. For nomenclature, each functional group will be denoted via a letter: vinyl (C=C, A), secondary amine (NH, B). The amine hydrogens can be further divided into those located on the oligomeric PTMO (B_{PTMO}) and on the chain extender ($B_{Extender}$). For crosslinked materials with the highest crosslink density, the stoichiometry was calculated based on secondary amine functionality, with 1.0:1.0 A:B and in particular 0.25:1.0:0.75 B_{PTMO}:A:$B_{Extender}$, with 4 NH groups per diamine. The reactants were mixed without solvent and allowed to react at 23 °C for 2 h and heated to 60 °C for 2 h to ensure complete conversion within error (confirmed by FTIR). For crosslinked materials reacted at room temperature, the stoichiometry was 1.0:1.3 A:B or 0.5:1.0:0.8 B_{PTMO}:A:$B_{Extender}$, with 3 NH groups per diamine (complete conversion considered to be depletion of vinyl groups within error). For example, 0.54 g phenyl was dispersed into 3.00 g PTMO. Then, 1.01 g DVS was added and mixed for 1 min. This mixture was allowed to react at room temperature until full depletion of vinyl groups (< 1 day) as determined via FTIR.

5.2.3. Fourier-transform Infrared Spectroscopy

Attenuated total reflectance FTIR spectra were taken on a Bruker Tensor 37 FTIR spectrometer. The resolution for all infrared spectra was 4 cm^{-1}; there were 32 scans for each spectrum. Full conversion of reactions was verified by disappearance of vinyl peak (1610 cm^{-1}) or amine peak (3200 cm^{-1}).

5.2.4. Solubility Testing

Materials were tested for chemical crosslinks by confirming insolubility in tetrahydrofuran and dimethylformamide (0.5 g material in 10 mL solvent). If samples were not completely dissolved after 24 h at 40 °C, they were considered to be networks.

5.2.5. Tensile Testing

Samples were cured in a press (60 °C for stoichiometry of 1.0:1.0 A:B and 23 °C for 1.0:1.3 A:B) until complete conversion (within error) was achieved as confirmed by FTIR. Dumbbell-shaped specimens were cut from films using a Dewes-Gumbs die. Mechanical properties were measured using a Sintech 20/G following ASTM 1708. Young's modulus was determined from the initial slope of the linear portion (the first 3-6 % elongation) of the stress–strain curves. Strain at break and ultimate strength were also determined.

5.2.6. Dynamic Mechanical Testing

Dynamic mechanical analysis (DMA) samples were cured in the same manner as for tensile testing and cut to dimensions of 3 mm x 10 mm x 30 mm. The moduli and tan delta curves were determined using a TA RSA3 DMA over a temperature range of -80 to 100 ºC at a frequency of 1 Hz and a heating rate of 3 ºC/min.

5.2.7. Differential Scanning Calorimetry

Samples were characterized using a Mettler-Toledo DSC822e. A sample of ~8 mg was placed into a 40 µl aluminum pan and annealed for 10 min at 150 °C to erase thermal history. After cooling at -40 °C /min to -100 °C, the heat flow was measured upon heating at 10 °C/min to 125 °C. The reported T_g is by the half-ΔC_p method.

5.3. Results and Discussion

In this work, both the reactivity and structure of the reactants are investigated in order to produce crosslinked materials. Figure 5.1 shows the monomer structures that were employed in this study. Typically, polyurethane elastomers are designed with a soft segment, often an

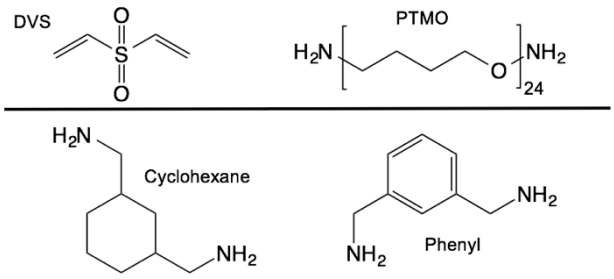

Figure 5.1. Monomer structures employed for the synthesis of crosslinked materials: divinyl sulfone (DVS), poly(tetramethylene oxide) diamine (1750 g/mol, PTMO) and chain extenders (1,3-cyclohexane bis(methyl amine) (Cyclohexane) and m-xylylene diamine (Phenyl).

oligomeric polyether with a glass transition temperature (T_g) well below room temperature, and a hard segment, composed of the rigid isocyanate component and a short chain extender. Here, a ~1750 g/mol poly(tetramethylene oxide) diamine (called PTMO in Figure 5.1) and a chain extender were reacted with divinyl sulfone (DVS). 1,3-cyclohexane bis(methyl amine) (called cyclohexane in Figure 5.1) was chosen as the model chain extender with a non-aromatic, yet rigid, cyclohexane ring. To determine the effect of a more rigid structure, m-xylylene diamine (called phenyl in Figure 5.1) was used as a chain extender.

In addition to the reactant structures, the stoichiometry is important to the final architecture of the polymer. Each of the amine-containing structures used in this study contained two primary amine functional groups. Similar to an epoxide-amine reaction, due to the presence of two active hydrogens on a primary amine (Girard-Reydet 1995, Mijovic 1992), vinyl sulfone can react twice with each primary amine in the absence of catalyst. Figure 5.2 shows a reaction scheme for the crosslinking of divinyl sulfone with a primary amine. In the first step, the vinyl group (A) can react with one active hydrogen (B) of the primary amine. After this, the next reaction can occur between A and either B of the secondary amine or B of another primary amine. In this work, the reaction is done in bulk and crosslinked polymers are produced. The stoichiometry can be adjusted to produce polymers of various crosslink density. For example, if 1 B is fed for every 1 A and nearly all functional groups were converted, the polymer crosslink density would be high. However, if 1.5 B is fed for every 1 A, the reaction will be incomplete (in terms of the amine functionality) but still produce a network polymer.

5.3.1. Reaction Kinetics of Room Temperature Amine-Vinyl Sulfone Polymerizations

Analysis of room temperature reaction kinetics was performed on a three-component reaction in which DVS was added to 1750 g/mol diamine-capped PTMO and m-xylylene diamine (phenyl) in 1.0:1.0 A:B stoichiometric balance. In order to characterize reaction kinetics, concentrations of A and B (not differentiating between primary and secondary amines) were monitored by FTIR over the course of the room temperature reaction. Figure 5.3a shows

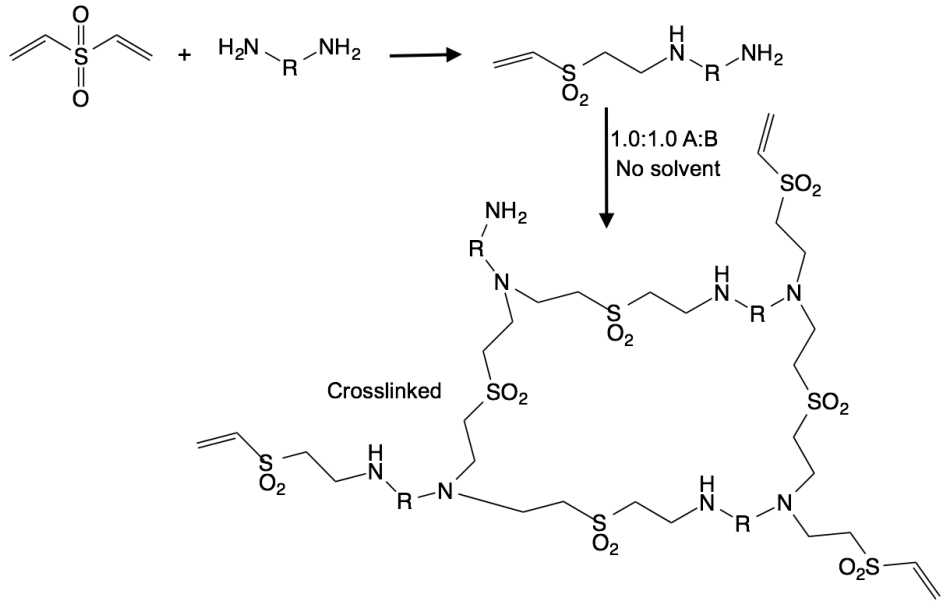

Figure 5.2. Reaction pathway for diamines and divinyl sulfones. Initially, the vinyl group (C=C, A) can react with amine group (NH, B) to produce a reactant with both primary and secondary amine functionalities. In bulk, crosslinked polymers are formed through the next reaction between a vinyl and a secondary amine.

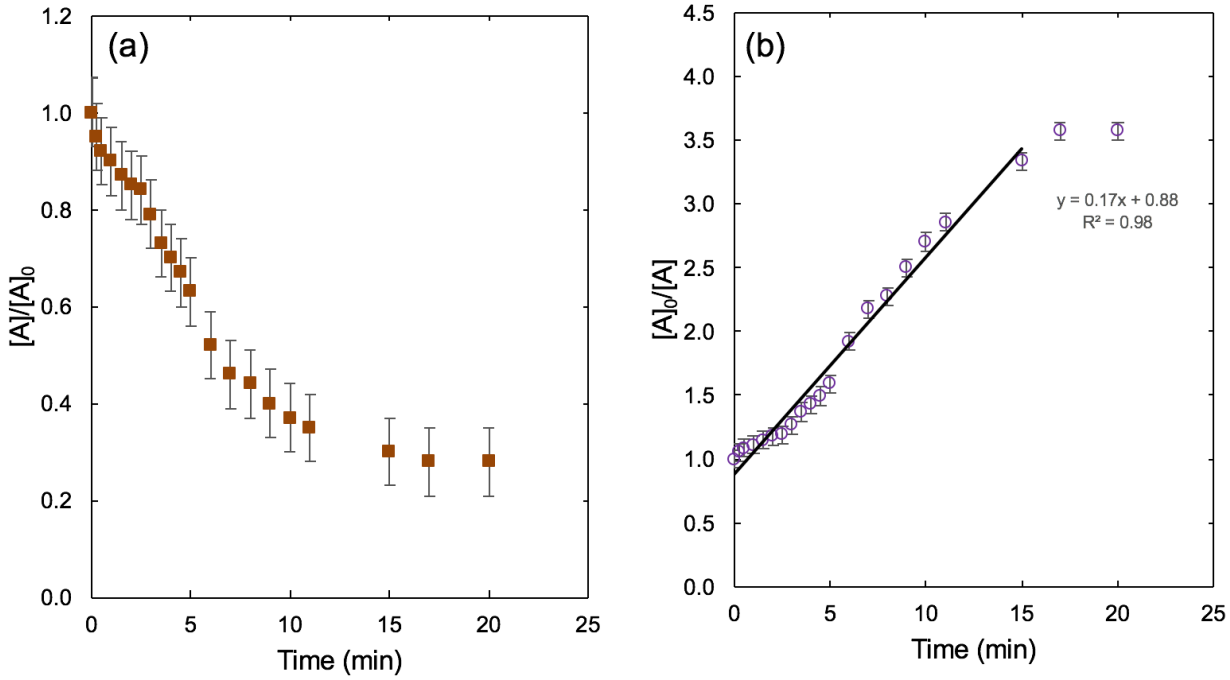

Figure 5.3. Reaction kinetics plots for solventless, room temperature amine-vinyl sulfone polymerizations with DVS, PTMO and phenyl at 1.0:1.0 A:B stoichiometry: (a) Vinyl (C=C, A) conversion as a function of time and (b) Vinyl group (C=C, A) conversions fit to an integrated second-order rate equation for a balanced stoichiometry of 1.0:1.0 A:B. Slope provides *k* value for the reaction: k_{app} = 0.17 M^{-1} min^{-1} with $[A]_0$ = 4.8 M.

conversion of the vinyl group for a bulk, room temperature reaction. Seen here, the initial stages of reaction occur rapidly without catalyst at room temperature. The reaction conversion is ~ 67% after 10 min. At this stoichiometry, the material forms a network with high crosslink density and the mobility of the functional groups is limited at high conversion in a bulk reaction. Because of this limited mobility, the reaction continues slowly after network formation. Although the rate slows, the reaction reaches 81% conversion after 24 h reaction time.

Figure 5.3b demonstrates that, up to conversion of ~ 70%, the room temperature reaction with 1.0:1.0 A:B stoichiometry provides a reasonable fit to results expected for second-order reactions. Second-order reactions with balanced stoichiometry should obey the following equation (Houston (Ed.) 2001):

$$[A]_0/[A] = 1 + k_{app}t \qquad \text{(Eq. 5.1)}$$

where $[A]_0$ is the initial vinyl concentration and [A] is the vinyl concentration at reaction time t, k_{app} is the apparent second-order reaction rate parameter and t is the reaction time. The slight deviation from linearity could be attributed at least in part to the fact that the observed [B] concentrations are from both primary and secondary amines on both oligomeric and small molecule diamines, as reactions with primary amines have different rate parameters than reactions with secondary amines. With step-growth reactions, it is also known that the rate parameter can sometimes change over the course of the reaction as the polarity of the medium will change (Flory 1939). Even with the polarity changes and the combination of different reactant reactivities, the approximate linearity of this plot reveals that the reaction is consistent with an apparent second order overall. It was also confirmed that these concentrations were not a better fit with 1.5 or 2.5 reaction orders. This reaction was done in the absence of catalyst and was still particularly rapid (k_{app} is 0.17 $M^{-1}min^{-1}$ calculated from the slope) in comparison to reactions of other NIPUs, including those involving catalyzed cyclic carbonate aminolysis (Guan 2011, Kathalewar 2013, Lombardo 2015). This rate was also impressive compared to an uncatalyzed model polyurethane polymerization reaction between commonly used toluene diisocyanate and castor oil with a k =

0.09 $M^{-1}min^{-1}$ (reaction at 30 °C) (Ajithkumar 1998). This study is the first to determine a rate parameter or reaction order for a polymerization using amine-vinyl sulfone reactions.

A room temperature reaction was also evaluated for a stoichiometry of 1.0:1.3 A:B (complete conversion was considered to be the depletion of all vinyl groups). Under these conditions, a crosslinked polymer with a lower crosslink density formed as the vinyl concentration was depleted. Conversion and kinetics analysis for this system can be seen in Appendix A. It can be seen that this reaction is also consistent with being second order. The apparent rate parameter (k = 0.11 $M^{-1}min^{-1}$) differs from that obtained with the 1.0:1.0 A:B stoichiometry because the polarity of the medium is different with additional chain extender in the medium.

5.3.2. Thermal and Mechanical Properties Associated with Crosslinked Amine-Vinyl Sulfone Networks

Thermoset materials were synthesized using bulk reactions with varying stoichiometries. With complete conversion within error of both functional groups (1.0:1.0 A:B), the maximum crosslink density for this material was obtained. Upon analysis via FTIR, it was found that complete conversion was not achieved at room temperature due to limited functional group mobility after network formation. However, conversion could be pushed to a virtual complete conversion (99+ % for vinyl group) at a higher temperature (< 30 min at 60 °C); the material properties of the resulting networks with cyclohexane and phenyl chain extenders were evaluated.

The tensile properties for networks made from starting stoichiometries of 1.0:1.0 A:B and 1.0:1.3 A:B and run to virtually complete conversion are summarized in Table 5.1. The networks resulting from the balanced stoichiometry reactions exhibited substantially higher Young's modulus and ultimate stress values as compared to those of the off-stoichiometry reactions. Additionally, the phenyl-based networks resulted in much higher Young's modulus and ultimate stress values as compared with those of cyclohexane-based networks. The best overall properties are those of the phenyl-based networks resulting from the balanced stoichiometry reactions, resulting in room temperature Young's modulus and ultimate stress values of 5.1 +/- 1.6 MPa and

Table 5.1. Room temperature tensile properties for crosslinked amine-vinyl sulfone materials reacted in the limit of full conversion at various stoichiometries with an aliphatic cyclohexane or aromatic phenyl chain extender. [+]Values measured upon heating after samples had been cooled to -100 °C and cold crystallization had occurred. [*]Values measured at room temperature after samples had been cured at 60 °C.

Network	Stoichiometry	T_g [+]	T_m [+]	Young's Modulus[*]	Ultimate Stress[*]	Strain At Break[*]
	A:B	°C	°C	MPa	MPa	%
Phenyl-based	1.0:1.0	-24	20	5.1 +/- 1.6	0.75 +/- 0.10	73 +/- 25
Cyclohexane-based	1.0:1.0	-25	18	0.80 +/- 0.07	0.26 +/- 0.06	55 +/- 8
Phenyl-based	1.0:1.3	-45	19	1.11 +/- 0.04	0.34 +/- 0.06	187 +/- 32
Cyclohexane-based	1.0:1.3	-46	20	0.55 +/- 0.08	0.18 +/- 0.04	201 +/- 12

0.75 +/- 0.10 MPa, respectively. With traditional polyurethane network elastomers, Young's modulus values typically fall in the range of 3.5 – 4.5 MPa (Tsai 1998), which are comparable to the value associated with the phenyl-based network developed here. However, traditional polyurethane network elastomers exhibit ultimate stress values of 10 – 40 MPa (Tsai 1998), more than a factor of ten higher than that exhibited by the phenyl-based network from balanced stoichiometry.

The fact that the phenyl-based networks exhibit substantially higher modulus and ultimate stress values than cyclohexane-based networks can result from two factors. First, the enhanced stiffness can be attributed to the rigidity of the phenyl chain extender. Second, although the functional group stoichiometries are equivalent, the reactivities of the amine functional groups are dissimilar in the aromatic and aliphatic structure. Dependent on reactivity, the crosslink densities (where the crosslinks are located) of the materials may change (Król 2007b).

The thermal properties of these polymers are reported in Table 5.1 and Figure 5.4, which show the T_g's and melt temperatures from DSC measurements as well as DMA curves for the phenyl-based network made with balanced stoichiometry. This material showed a robust rubbery plateau at temperatures above the melt transition of the PTMO chain segments that is competitive with crosslinked polyurethanes. These polymers also showed interesting crystallization behavior with cold crystallization occurring in both systems around -55 °C and melting occurring at ~19 °C. These values are consistent with pure semi-crystalline PTMO. From DSC and DMA, the T_g was difficult to observe due to the cold crystallization peaks. With measurements taken upon heating, cold crystallization of the PTMO chains occurred which could cause the remaining amorphous network to be more rigid. These materials also have large glass transition breadths due to the network heterogeneity. As this was the first study to examine the application of amine-vinyl sulfone polymers as elastomers, there was limited investigation into the thermal and mechanical properties as a function of chain extender. However, the comparison of the cyclohexane- and phenyl-based networks demonstrated the structure-property tunability of this chemistry.

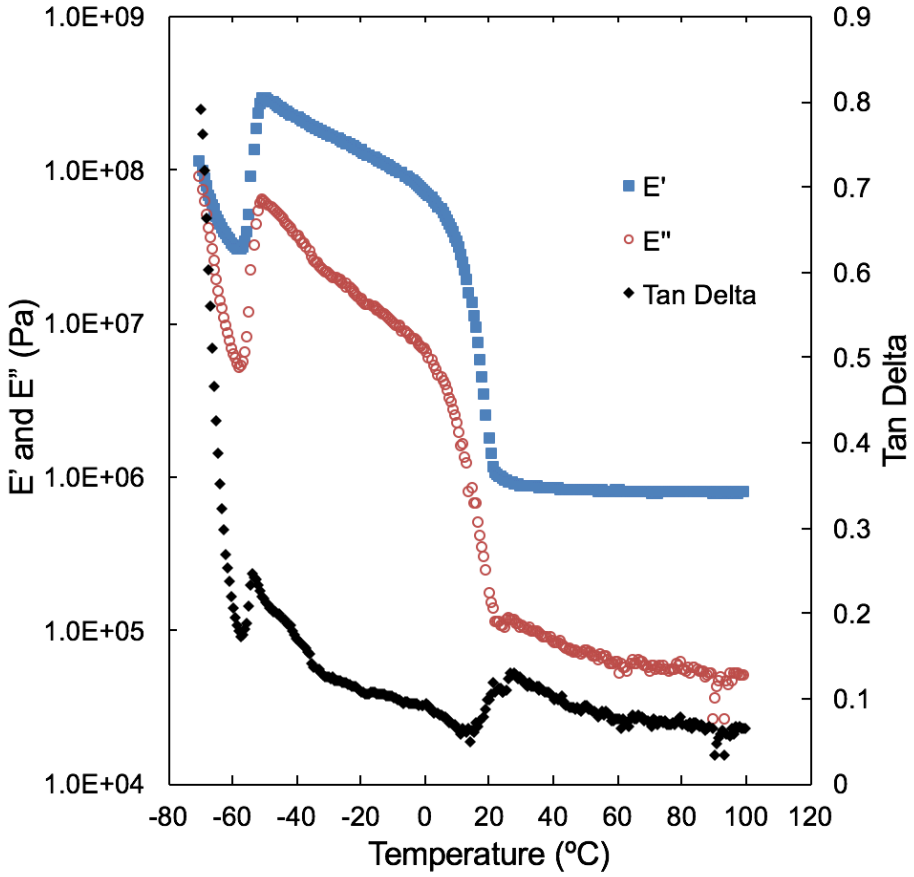

Figure 5.4. Dynamic mechanical analysis of amine-vinyl sulfone networks at 1.0:1.0 A:B stoichiometry synthesized with aromatic phenyl chain extender.

To eliminate any issues associated with the semi-crystalline nature of the networks, future studies should be done with an amorphous oligomeric diamine component. Future studies are also needed to explore the stoichiometries and structures of reactants to reveal the full extent of properties and applications of this reaction. Investigation into the use of a catalyst with this system could be beneficial to the synthesis of highly crosslinked materials that can achieve complete conversion at room temperature.

5.4. Conclusion

In this study, segmented crosslinked materials were synthesized using uncatalyzed room temperature amine-vinyl sulfone reactions. Previously, research into this reaction has focused on monofunctional reactants and has largely ignored its potential in polymerization reactions. Thermoset materials can be synthesized by rapid reactions in which a vinyl sulfone can react with both primary and secondary amines. Because amine-vinyl sulfone chemistry has not been well reported in polymerization literature, its use as a fast-reacting alternative to polyurethanes still requires additional investigation. Future studies are needed to explore the stoichiometries and structures of reactants to reveal the full extent of properties and applications of this reaction. Investigation into the use of a catalyst with this system could be beneficial to the synthesis of highly crosslinked materials that can achieve complete conversion at room temperature.

APPENDIX A

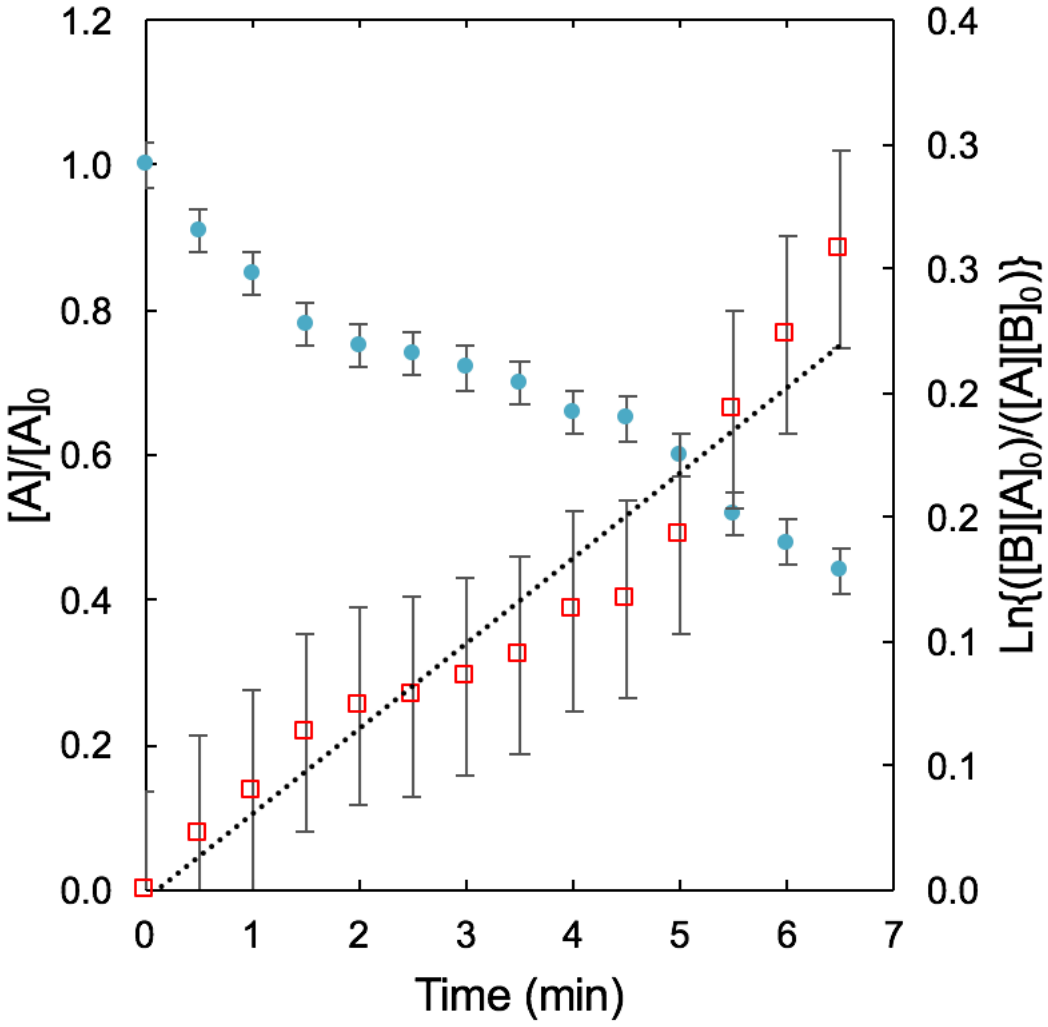

Figure A.1. Normalized vinyl group conversion (circle) for a bulk room temperature reaction between DVS, PTMO and phenyl with imbalanced stoichiometry of 1.0:1.3 A:B. On the second axis, amine (NH, B) and vinyl group (C=C, A) conversions fit to an integrated second-order rate equation (square) with imbalanced stoichiometry of 1.0:1.3 A:B. Slope of the dotted line provides $([B]_0\text{-}[A]_0)k$ values for the reaction. Calculated $k_{app} = 0.11$ M^{-1} min^{-1}.

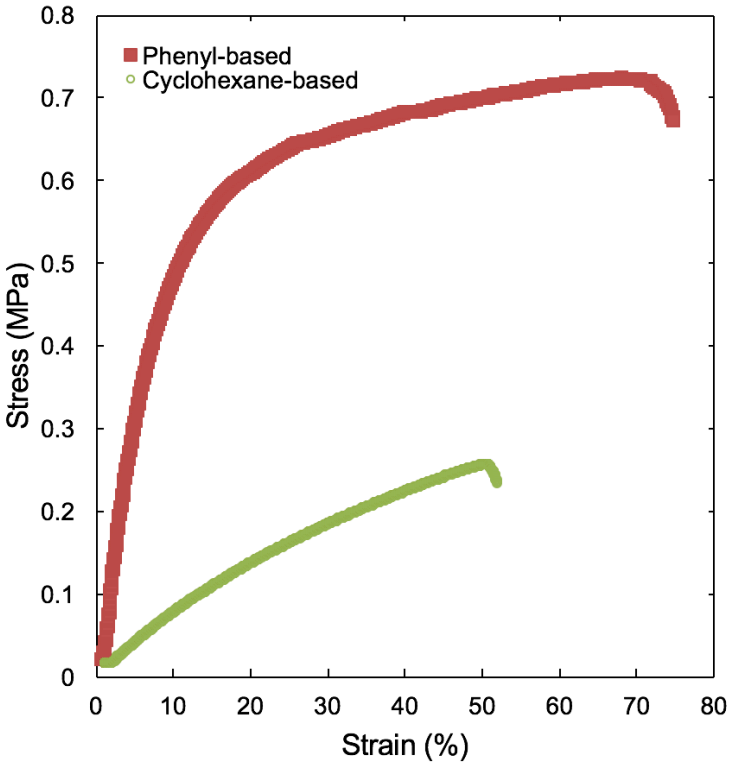

Figure A.2. Stress-strain curves for phenyl- and cyclohexane-based networks synthesized with a 1.0:1.0 A:B stoichiometry.

III. INVESTIGATION INTO AROMATIC INTERACTIONS BY FLUORESCENCE SPECTROSCOPY IN SEGMENTED POLYURETHANES

CHAPTER 6

ANALYSIS OF AROMATIC INTERACTIONS IN SEGMENTED POLYURETHANES USING INTRINSIC FLUORESCENCE

6.1. Introduction

Polyurethanes are versatile materials that are used in a wide range of applications such as building materials, furniture, and automotive interiors (Engels 2013, Nohra 2013, Oertel 1993). Segmented polyurethanes are a type of multi-block copolymer that can undergo phase separation into hard-segment domains and a soft-segment matrix, thereby yielding elastomeric behavior (Woo 1985). In order to be useful as elastomers, the phases must be well phase-separated. Mechanical properties are determined by the molecular structure of the phases, as well as the degree to which they are separated and the resulting morphologies (Petrović 1998, Pukánszky 2008). In polyurethanes, the degree of phase separation is often enhanced by the extent of hydrogen bonding between urethane linkages located in the hard segments (Elwell 1996a, 1996b, Sung 1974, Tang 2011, Zhang 2014a). Although hydrogen bonding interactions are extremely important, the role of aromatic interactions in the extent of phase separation has not been described in detail in current polyurethane literature.

Several techniques are commonly used to quantify phase separation or to qualitatively show phase separation in polyurethanes. One technique that is often used to examine phase separation in polyurethanes is Fourier-transform infrared spectroscopy (FTIR) (Garrett 2003, Hoyle 1986, Wang 1994, Yilgör 2000, Yilgör 2006, 2007, Zhang 2014b). FTIR allows for the examination of hydrogen bonding of functional groups in polyurethanes. Hydrogen bonds in urethane linkages act as physical crosslinks between hard segments. Therefore, the extent of hydrogen bonding can be correlated with the extent of phase separation. Important stretches are the amide hydrogen and the urethane carbonyl, which participate in the hard-segment hydrogen bonding. Information can be extracted from both peak intensities as well as frequency shifts (Lee 1987). At best, this method can be semi-quantitative in addressing degree of phase separation.

Differential scanning calorimetry (DSC) has long been used to characterize phase separation in polymer samples (Camberlin 1983, Kwei 1982, Leung 1986). The most common approach involves the use of the glass transition temperature (T_g) and its sensitivity to molecular structure. The purity of each phase can be estimated by using equations derived from Fox and Flory (Fox 1956, 1950) as well as Couchman (Couchman 1978, Pinal 2008, Velankar 1998) for miscible polymer blends and block copolymers. For qualitative determination of purity, the ΔT, defined as the temperature difference between T_g of the soft segment in the polyurethanes and T_g of the neat soft segment diol, can be assessed (Gedde 1999). More quantitative analysis can be done by calculations with the heat capacities of these two segments (Chen 1997). This analysis is usually performed on the soft-segment matrix in high wt % soft-segment polyurethanes.

As previously studied, the importance of hydrogen bonding between hard segments in polyurethanes has been established as a key factor in phase separation. In research literature, it is well known that polybutadiene, polyether and polyesters as soft segments produce varying degrees of phase separation because of the different interactions between the hard and soft segments (Bagdi 2011, Berezkin 2013, Castagna 2012, Cuvé 1992, Kojio 2010, Kultys 2011, Martin 1996, Pukánszky 2008, Schneider 1979, Yilgör 2000, Yilgör 2015, Zou 2016). When used as a soft segment, polybutadiene produces extremely well phase-separated polyurethanes because there are no secondary bonding interactions between the butadiene units in the soft segment and the urethane linkages. When polyesters are used as the soft segment, such as polycaprolactone, the ester groups can hydrogen bond with the amide hydrogens in the urethane linkage. With such secondary bonding interactions between the soft and hard segments, there is a degree of phase mixing that occurs. Polyether soft segments, such as poly(tetramethylene oxide), have ether linkages that can undergo hydrogen bonding to a lesser degree with the hard segment amide hydrogens and therefore typically have degrees of phase separation that fall above polyesters but below polybutadiene.

Here, intrinsic fluorescence is explored as a novel method for examining phase-separated polyurethanes. In particular, with aromatic-ring containing polyurethanes, intrinsic fluorescence

has the ability to show how the hard-segment aromatic rings are aligning or interacting (Huang 2015, Sun 1996, Wang 2002). Aromatic rings can intrinsically fluoresce in two ways, as monomer or excimer emission (Berlman 2012, Guilbault (Ed.) 1990). Monomer emission occurs from the isolated excited state of a single phenyl ring or disubstituted benzene ring whereas excimer emission occurs from two phenyl rings or disubstituted benzene rings in a parallel, sandwich-like configuration with a separation distance of 3–4 Å (Hirayama 1965). Excimer fluorescence can be further divided into two pathways of dimer formation: static and dynamic (Aladekomo 1965, Birks 1963b, 1965, Winnik 1993). If two rings are able to interact in the ground state and are excited as a dimer, they will fluoresce as static excimer. However, if an excited-state monomer interacts with a ground-state monomer, they will fluoresce as dynamic excimer. An excitation spectrum, similar to an absorption spectrum, can distinguish between the two pathways as each has a distinct formation species, excited-state monomer for dynamic excimer emission and excited-state dimer for static excimer emission (Birks 1964). In short, monomer and dynamic excimer will have the same excitation spectra as the emission of both originates from an excited-state monomer. In contrast, monomer and static excimer will have different excitation spectra.

Up to the present, no experimental study of polyurethanes has analyzed any pi-pi interactions between disubstituted benzene rings that are common to many polyurethane hard segments. This work explores the use of intrinsic fluorescence emission spectra involving both monomer and excimer emission to analyze polyurethanes with varying degrees of phase separation and excitation spectra to gain insight on how the aromatic interactions originate within phase-separated polyurethanes.

6.2. Experimental Section

6.2.1. Synthesis

Five polyurethanes were synthesized using the following two-step procedure. In a typical synthesis, 2,4-toluene diisocyanate (8.25 mmol) was charged into a round bottom flask equipped

with a dry N_2 purge, overhead stirring, and an addition funnel. Following the isocyanate addition, one of the selected 2000 g/mol dried diols (3.75 mmol) was added dropwise through the addition funnel as the limiting reagent. After complete addition of diol, the material was mixed for 30 min. After this stir, dibutyltin dilaurate (0.01 wt%) was added, and the round bottom flask was placed in an oil bath at 80 °C. The reaction proceeded for 2 h, and the resultant prepolymer was poured into a Flacktek max 20 mixing cup. For the chain extension reaction, the prepolymer was mixed with dry 1,4-butanediol (5.4 mmol) and dibutyltin dilaurate (0.01 wt%) using a FlackTek DAC 150.1 FVZ-K SpeedMixer™ at 3500 rpm for 30 sec. This reaction resulted in a polyurethane with a ~ 20 wt % hard segment content after 1 h at 80 °C. The chosen diols were polybutadiene (Krasol LBH P 2000, average Mn ~2000, Cray Valley), poly(tetramethylene oxide) (average Mn ~2000, Aldrich), polycaprolactone (average Mn ~2000, Aldrich), and poly(propylene oxide) (Voranol 220-056, average Mn ~2000, The Dow Chemical Company). Soft segment wt % is calculated as follows:

$$\text{Soft Segment wt \%} = (M_{SS}) / (M_{SS} + RM_{Iso} + (R\text{-}1)M_{CE}) \qquad \text{(Eq. 6.1)}$$

where R is the molar ratio of diisocyanate to soft segment, M_{Iso} is the molar mass of the diisocyanate, M_{CE} is the molar mass of the chain extender and M_{SS} is the molar mass of the soft segment.

6.2.2. Spin Coating of Films

Bulk films of polyurethane materials were spin coated onto glass slides from toluene (Sigma Aldrich) solutions containing 5 wt % polymer with spin speeds of 2000 rpm. Glass slides were thoroughly cleaned by etching in 1.0 M hydrochloric acid, rinsed with water, and dried prior to submerging in base solution (10 wt % sodium hydroxide/20 wt % water/70 wt % ethanol). Substrates were then rinsed with water and dried prior to use.

6.2.3. Film Thickness by Ellipsometry

Measurements were performed at room temperature using spectroscopic ellipsometry (J. A. Woollam Co. M-2000D over a range of wavelengths from 400 to 1000 nm). The ellipsometric

angles (ψ and Δ) of incident light reflected off silica-supported polyurethane films were measured and fitted to a Cauchy layer model to determine thickness. The Cauchy layer model included a PS layer atop a silicon substrate containing a 2-nm-thick silicon oxide surface layer. Film thickness was determined by fitting ψ and Δ to the PS layer in the Cauchy model.

6.2.4. Fluorescence Spectroscopy

After spin coating, emission spectra were collected (Photon Technology International fluorimeter in front-face geometry) at wavelengths from 280 to 550 nm, with excitation at 255 nm. Excitation and emission slit widths were 1 mm (2 nm bandpass). Peak intensities were calculated from an average of ten data points spanning 4 nm around the peak: Monomer intensity was an average of ten data points around 320 nm and excimer intensity an average of ten data points around 418 nm. Steady-state fluorescence excitation spectra, for which emission wavelength (λ_{em}) is held constant and the excitation wavelength (λ_{exc}) is varied, were measured with $\lambda_{em,monomer}$ = 315 nm ($\lambda_{em,excimer}$ = 407 nm) for monomer (excimer) at 30 °C. Fluorescence emission spectra were taken at 30 °C at two times: immediately after spin coating the films and after the anneal process described below.

6.2.5. Film Annealing

Films were spin coated onto glass slides. The films were heated to 130 °C at 25 °C/min. Films were held at this temperature for 130 min and subsequently quenched to 30 °C at -40 °C/min.

6.2.6. Differential Scanning Calorimetry

Samples were characterized using a Mettler-Toledo DSC822e. A sample of ~8 mg was placed into a 40 µl aluminum pan and annealed for 10 min at 150 °C to erase thermal history. After cooling at –40 °C/min to –100 °C, the heat flow was measured upon heating at 10 °C/min to 120 °C. The reported T_g is by the half-ΔC_p method. Extent of phase separation can be quantified through the comparison of the heat capacities for the soft segment phase and pure soft segment measured by DSC. Phase separation % is estimated by the following equation (Couchman 1978):

$$\% \text{ Pure Soft Segment Phase} = [(Cp_{SoftPhase}/x_{SoftPhase})/Cp_{SoftSegment}] \times 100\ \% \qquad \text{(Eq. 6.2)}$$

where $Cp_{SoftPhase}$ is the heat capacity of the soft phase in the polyurethane, $x_{SoftPhase}$ is the theoretical weight fraction of diol-containing phase and $Cp_{SoftSegment}$ is the pure diol heat capacity.

6.2.7. Fourier-transform Infrared Spectroscopy

Attenuated total reflectance FTIR spectra were taken on a Bruker Tensor 37 FTIR spectrometer. The resolution for all infrared spectra was 4 cm^{-1}; there were 32 scans for each spectrum. To measure hydrogen bonding qualitatively, the urethane carbonyl (C=O, wavenumber 1710 cm^{-1}) and the urethane amide (NH, 3400 cm^{-1}) peaks were used. The measurements were made from polymer films at room temperature (23 °C).

6.2.8. Nomenclature

Because of the use of distinct soft segments with identical hard segments, polyurethanes are distinguished based on soft segment backbone and wt % soft segment. Two-phase polyurethanes synthesized with 80 wt % polybutadiene, polycaprolactone, poly(tetramethylene oxide) and poly(propylene oxide) are designated PBD80-PU, PCL80-PU, PTMO80-PU and PPO80-PU, respectively. The single phase polyurethane synthesized with 88 wt % poly(propylene oxide) is designated PPO88-PU. In each polyurethane system, the hard segment consisted of 2,4-toluene diisocyanate and 1,4-butanediol.

6.3. Results and Discussion

Here, the synthesized polyurethanes were designed to be either one-phase or two-phase materials. Figure 6.1 shows the selected starting materials for polyurethane synthesis. Excess 2,4-toluene diisocyanate was reacted with a ~ 2000 g/mol diol (soft segment) to produce a prepolymer. The prepolymer was then chain extended with 1,4-butanediol to yield a segmented polyurethane with soft and hard segments. Depending on the thermodynamic incompatibility of these segments, the covalently linked segments may undergo phase separation.

To characterize the phase behavior of these materials, DSC was used to indicate the number of phases as well as the purity of the soft-segment phase. Table 6.1 displays heat capacity and T_g

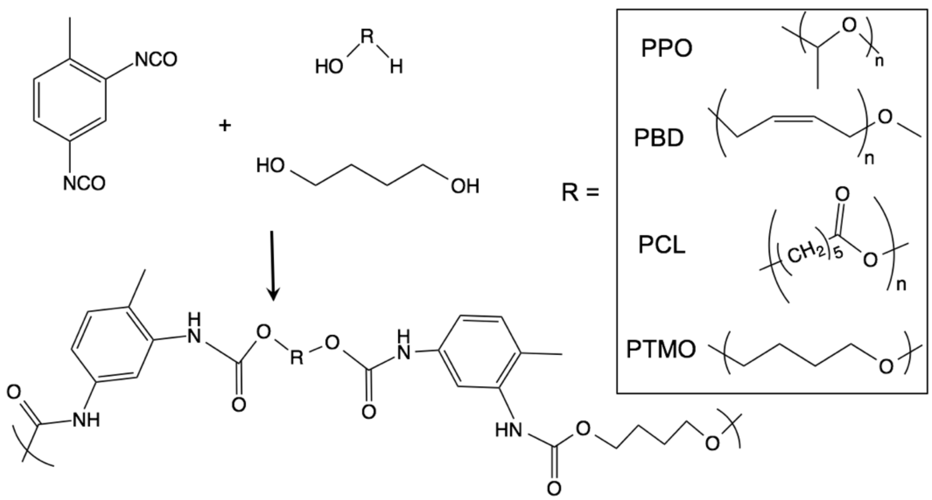

Figure 6.1. Monomer selection for polyurethane synthesis. 2,4-toluene diisocyanate (TDI) is reacted in excess with a ~ 2000 g/mol oligomeric diol (with different R-groups). When chain extended with 1,4-butanediol, a segmented polyurethane results with aromatic hard segments and diol-containing segments. R-groups: poly(propylene oxide) (PPO), polybutadiene (PBD), polycaprolactone (PCL), poly(tetramethylene oxide) (PTMO).

Table 6.1. Thermal analysis of polyurethanes and their respective soft segments.

	Glass Transition Temp (°C)		Heat Capacity (J/K)		
	Pure Soft Segment	Soft Segment	Pure Soft Segment	Soft Segment	% Pure Soft Segment Phase
Polybutadiene	-44		6.62E-03		
PBD80-PU		-43		5.21E-03	98%
Poly(tetramethylene oxide)	-76		2.09E-03		
PTMO80-PU		-68		1.37E-03	82%
Polycaprolactone	-67		9.33E-04		
PCL80-PU		-59		5.77E-04	77%
Poly(propylene oxide)	-69		1.52E-02		
PPO80-PU		-63		1.01E-02	83%
PPO88-PU		-53		N/A	N/A

data for each polymer and its respective soft-segment diol. Glass transition temperature is often used as a qualitative statement on extent of phase separation. The material synthesized with 12 wt % toluene diisocyanate/butanediol hard segment, PPO88-PU, was apparently one-phase, as the low hard-segment content was insufficient to induce phase separation (at a level that was apparent by DSC characterization). Here, the single-phase PPO88-PU shows a single glass transition of -53 °C, which is in accordance with the Fox equation for a miscible polymer blend in which the low T_g component has a T_g of -69 °C (See Table 6.1). This material also exhibited no elastomeric behavior as it was a fluid at room temperature.

If a polymer is sufficiently phase separated, two T_g's, representative of each phase's T_g, may be present. Because the detection of hard segment transitions is difficult with low hard segment wt % polyurethanes (here, a hard-segment T_g was not observed in heat flow or first derivative heat flow curves), the soft-segment transition is used to determine the extent of phase separation. Between PBD-diol and PBD80-PU, the ΔT_g is 1 °C. This indicates an extremely well phase-separated system, which is also evidenced by the calculated 98% pure soft segment. For PCL-diol and PCL80-PU, the ΔT_g is 8 °C, which is close to that expected for a two-phase polyurethane that is ~77 % pure soft segment (based on eq. 6.2). The calculation for % pure soft segment is also an estimate based on literature values for rigid amorphous fraction of the semi-crystalline polymer (Zhuravlev 2011). All phase-separated materials (PCL80-PU, PTMO80-PU, PPO80-PU, and PBD80-PU) were solid and exhibited qualitatively elastomeric behavior at room temperature.

Figure 6.2 shows the FTIR spectra for the one-phase and two-phase polyurethanes synthesized in this study. In Figure 6.2a, N-H stretches from the urethane linkages (centered around 3350 cm^{-1}) are shown (Irusta 2005). With H-bonded stretches at 3300 cm^{-1} and free N-H stretches at 3450 cm^{-1}, it is possible to distinguish the extent of hydrogen bonding that is occurring in each polymer using peak position, peak intensity and peak area. The most phase separated, PBD80-PU, shows a broad peak positioned in the hydrogen bonded region. This qualitatively

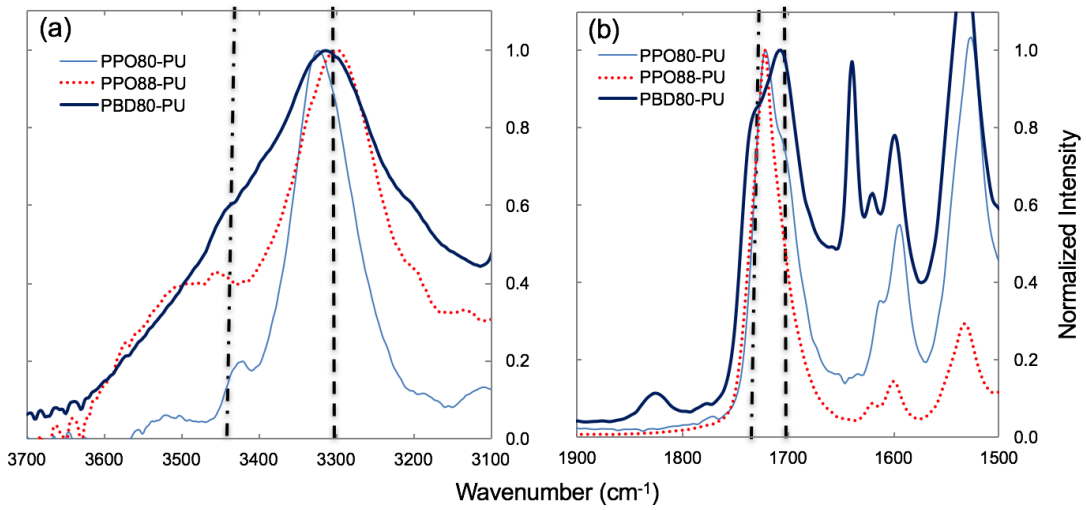

Figure 6.2. FTIR spectra of one-phase and two-phase polyurethane samples of two soft segments: (a) N-H stretches centered around 3350 cm^{-1} with H-bonded stretches at 3300 cm^{-1} and free N-H stretches at 3450 cm^{-1} (b) C=O stretch centered around 1710 cm^{-1} with H-bonded C=O stretches at 1705 cm^{-1} and free C=O stretches at 1725 cm^{-1}. These spectra have been normalized to the maximum peak intensity at (a) 3300 cm^{-1} and (b) 1700 cm^{-1}.

shows the response when N-H groups are hydrogen bonded to other hard segments (as there is no soft segment functional groups to interact with). The spectrum for PPO80-PU, a phase separated material, shows many NH groups participating in hydrogen bonding with a small shoulder that is representative of non-bonded hydrogens. The single phase material, PPO88-PU, has two distinct peaks in this region, with intensities suggesting that ~ 30% of the N-H groups are free. In Figure 6.2b, the carbonyl stretches are shown for both one-phase and two-phase materials. The two polyurethanes synthesized with PPO show a free carbonyl stretch whereas PBD80-PU qualitatively shows that most of the carbonyl functional groups are participating in hydrogen bonding. With the information gained from FTIR and DSC on these polymers, the relative comparison of phase separation extents is observed in the following order: PCL80-PU < PTMO80-PU < PPO80-PU < PBD80-PU.

Fluorescence emission spectra are shown for the apparently one-phase system in Figure 6.3 and the four phase-separated polyurethane systems in Figure 6.4. Figure 6.3 shows the normalized emission spectrum at 30 °C of the apparently single-phase PPO88-PU after spin coating. This material exhibits only monomer emission, centered around 320 nm, and no excimer emission, which would be expected at higher wavelengths if present. Although the apparently one-phase material shows evidence of hydrogen bonding, excimer emission is not present. The monomer peak location is red-shifted relative to monomer emission in polystyrene. This shift is because the urethane units are covalently attached to the aromatic ring in polyurethane. Also shown in Figure 6.3 is the 30 °C emission spectrum for the polymer after a two hour anneal at 130 °C. This annealing procedure led to no change in the emission spectrum, with all fluorescence coming from excited-state monomer.

Figure 6.4 shows the normalized emission spectra for the two-phase polyurethanes: PCL80-PU, PTMO80-PU, PPO80-PU, and PBD80-PU. In each of the spectra, an excimer peak can be observed with peak intensity at ~ 420 nm, in addition to the presence of the monomer peak. In Figure 6.4a, PCL80-PU displays a very small excimer intensity compared to monomer intensity.

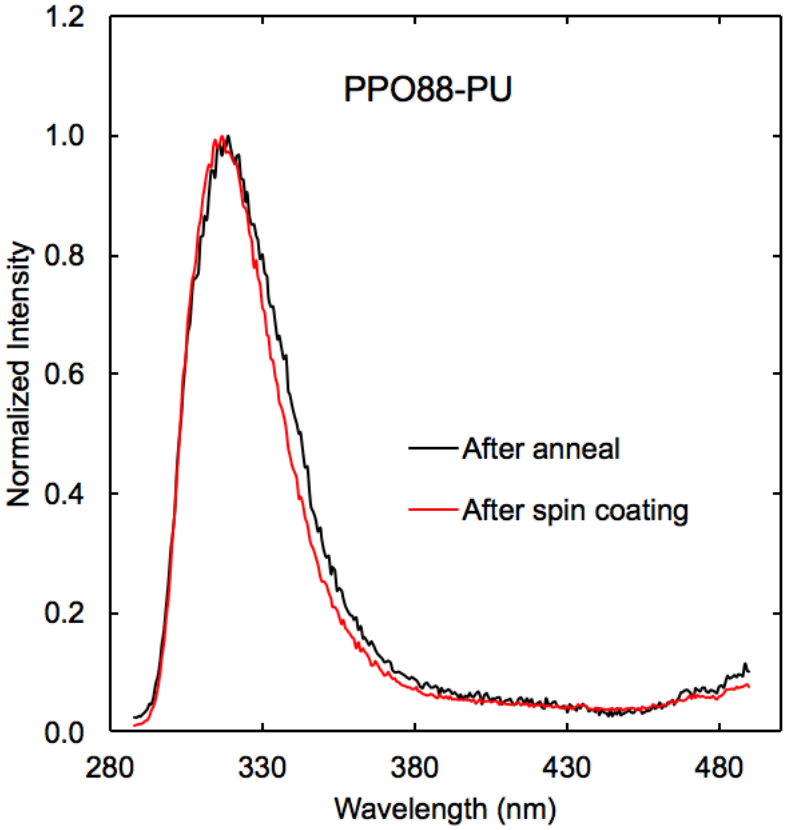

Figure 6.3. Normalized emission spectra on one-phase PPO88-PU bulk films (λ_{exc} = 255 nm) at 30 °C before and after annealing at 130 °C. These spectra have been normalized by maximum monomer peak intensity.

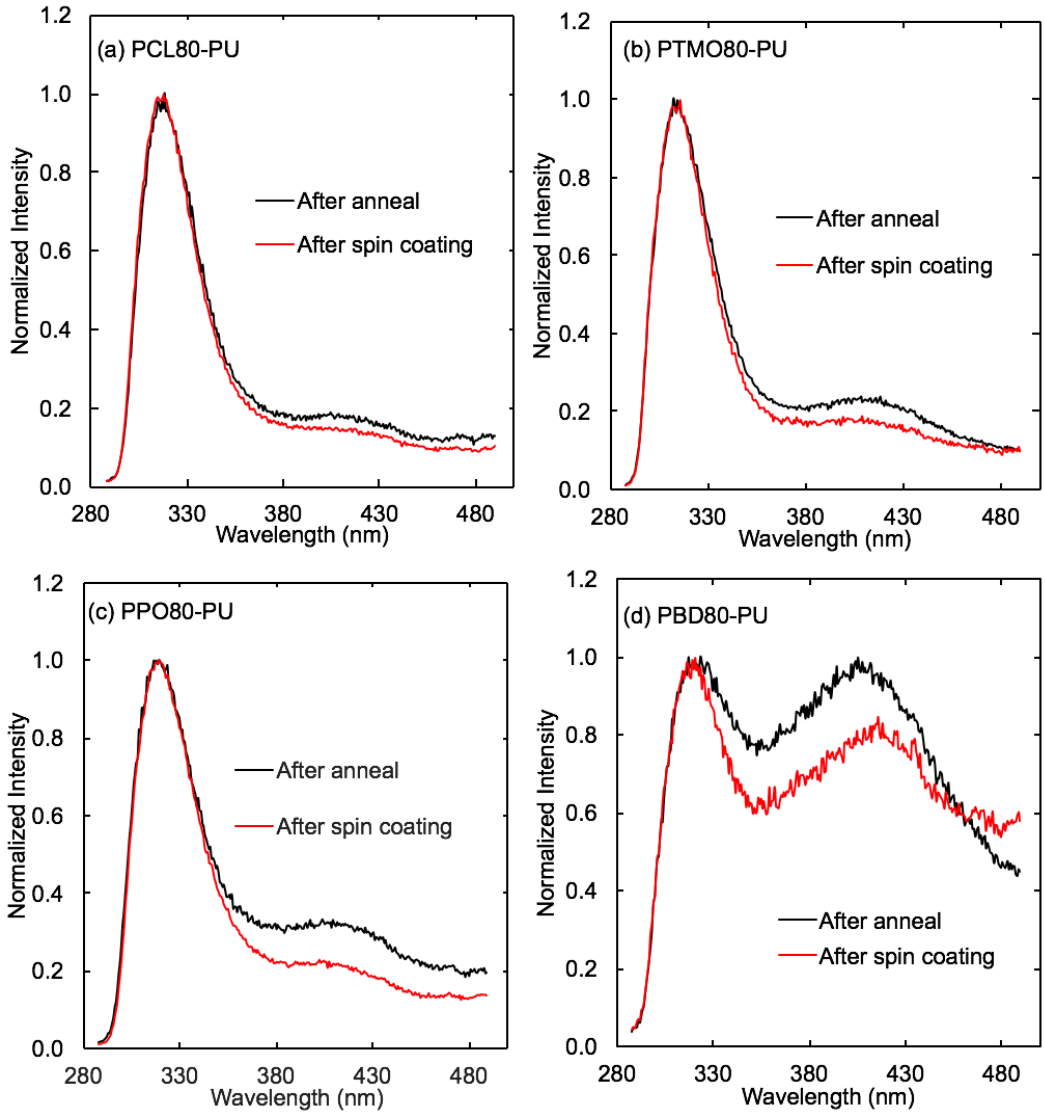

Figure 6.4. Normalized emission spectra of two-phase polyurethane bulk films (λ_{exc} = 255 nm) at 30 °C before and after annealing at 130 °C with different soft segments: (a) PCL80-PU, (b) PTMO80-PU, (c) PPO80-PU, (d) PBD80-PU. These spectra have been normalized by maximum monomer peak intensity.

Figures 6.4b and 6.4c reveal an increased excimer intensity for PTMO80-PU and PPO80-PU with increasing extent of phase separation. In Figure 6.4d, PBD80-PU shows a dramatic increase in the ratio of excimer intensity to monomer intensity (I_E/I_M) when compared to the other polyurethanes. Thus, I_E/I_M increases with increasing polyurethane phase separation from a near zero value in apparently one-phase PPO88-PU to ~ 0.8 in PBD80-PU when excimer and monomer intensities are taken at the peak intensity values. Because of the specific requirements for excimer formation, excimer emission is used to gain insight into the proximity and molecular orientation of the aromatic rings in hard segments of polyurethanes. In a well-phase separated system, the excimer intensity will be greater than that observed in a phase-mixed system due to the presence of the fluorophore in a local environment that is rich in aromatic rings. Also shown in Figure 6.4, the excimer intensities of each polyurethane increase after an anneal for 130 min at 130 °C. After spin coating, the room-temperature, phase-separated structures are frozen in a non-equilibrium state. During a sufficiently high-temperature anneal, further phase separation toward an equilibrium can occur.

Figure 6.5 shows the fluorescence excitation spectra for each phase-separated polymer at 30 ºC (before annealing) and 130 ºC (several minutes after heating from 30 ºC) with emission wavelengths set at both monomer and excimer emission. The excitation spectra for the monomer emission reveal excitation peaks centered at ~ 298 nm for both high and low temperatures. If excimer formation occurred dynamically via interaction of a ground-state monomer with an excited-state monomer, then the excitation spectra from excimer emission would be very similar (identical within error) to the excitation spectra from monomer emission. However, the excitation peak for excimer emission shifts toward lower wavelengths. This shift is indicative of the presence of ground-state dimer, which fluoresces as static excimer. With further analyses of the subtle details of the spectra, more can be understood about each polymer. In Figure 6.5a, PCL80-PU displays the least shifted excimer excitation peak, centered at ~ 278 nm. This shift could arise from

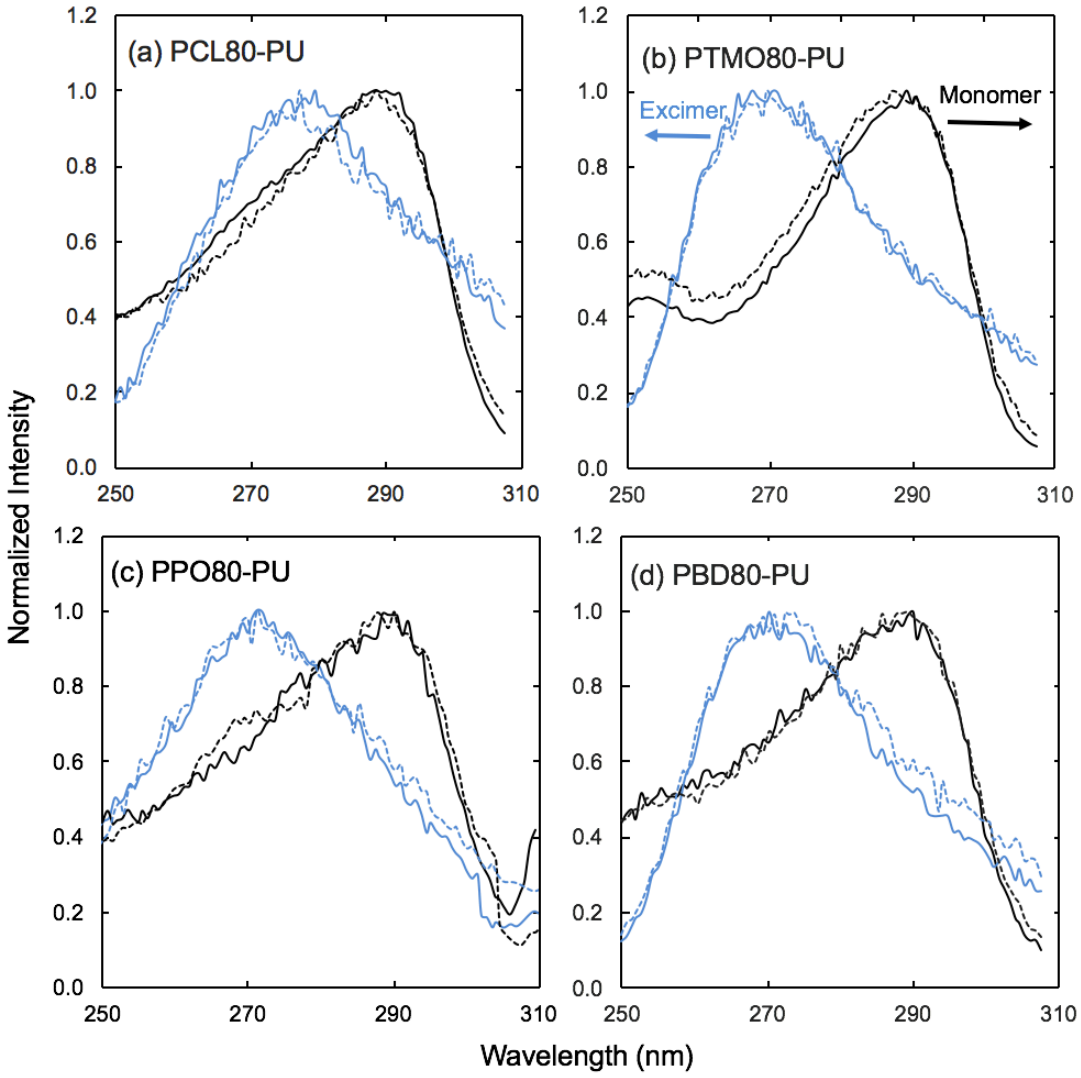

Figure 6.5. Normalized excitation spectra of two-phase polyurethane films monitored at monomer emission wavelength, 318 nm (black), and excimer emission wavelength, 407 nm (blue) at T=30 °C (line) and T=130 °C (dotted). (a) PCL80-PU, (b) PTMO80-PU, (c) PPO80-PU, and (d) PBD80-PU. These spectra have been normalized by maximum monomer and excimer excitation peak intensities.

the increased phase-mixing behavior seen in polyurethanes that contain more interphase due to the hard segment interactions with the polyester soft segments. With less interphase, PTMO80-PU, PPO80-PU and PBD80-PU give the excitation spectra with the fixed excimer emission that are further shifted and centered at ~ 270 nm. The distinct shifts of the excimer excitation peaks relative to monomer excitation peaks reveal that static excimer is responsible for the excimer emission.

In all of the four phase-separated polyurethanes, measurement temperature does not have a significant impact on the origin of the excimer, with all excitation spectra for excimer emission being little changed upon increasing temperature from 30 °C to 130 °C. In literature, it has been observed via FTIR spectroscopy that hydrogen bonding in polyurethanes is dramatically decreased at temperatures above 100 °C when compared to the hydrogen bonding present at room temperature (Koberstein 1986, Pongkitwitoon 2009, Teo 1997, Wang 1994). (Unfortunately, the FTIR equipment at Northwestern University does not allow for spectra to be obtained at 130 °C.) For the excimer excitation spectra to remain relatively constant with major depletion of hydrogen bonding at 130 °C, aromatic association must be a strong influence in the alignment of the aromatic rings in the phase-separated hard segments. The static dimers present in the films are oriented and aligned both at 30 °C and 130 °C, with the static dimers consisting of two aromatic rings (originating from the 2,4-toluene diisocyanate reactant) being 3-4 Å apart in a parallel, sandwich-like arrangement. Although hydrogen bonding could assist in the alignment and orientation of the aromatic rings, it is not necessary for the presence of static dimer, as evidenced by the presence of static dimers at 130 °C. The concept that aromatic interactions play a role in phase behavior is not common in the polyurethane literature. However, the combination of fluorescence emission and excitation spectra is able to detect the nature of aromatic interactions between aromatic rings in hard segments of polyurethanes and has revealed that these aromatic interactions exist in phase-separated polyurethanes with and without the presence of hydrogen bonding. However, in the absence of phase-separated hard segment domains, as with PPO88-PU, there is not excimer fluorescence and thus no static dimers.

6.4. Conclusion

Although discussed in polyurethane literature, aromatic interactions in hard segments have not been experimentally determined or characterized. In this work, intrinsic fluorescence was employed to examine the nature of aromatic interactions in segmented polyurethanes. Emission spectra were utilized to detect the presence of aromatic rings in the specific requirement for excimer fluorescence: a parallel, sandwich-like configuration with an inter-ring distance of 3-4 Å. Excimer emission was present in phase-separated polyurethanes and absent in apparently one-phase polyurethanes that do not have distinct hard-segment domains. Excimer emission also revealed information on the extent of aromatic alignment in the hard segments of polyurethanes with varying degrees of phase separation. Excitation spectra showed the presence of these ground-state dimers in phase-separated polyurethanes. Through analysis of phase-separated polyurethanes at different temperatures, it was found that hydrogen bonding does not influence the presence of these ground-state dimers. This study presented evidence of the importance of aromatic interactions in the organization of these segmented polymers.

CHAPTER 7

MOLECULAR ALIGNMENT OF PHASE-SEPARATED, SEGMENTED POLYURETHANES IN THIN FILMS USING INTRINSIC FLUORESCENCE

7.1. Introduction

Over the past decade, greater interest in self-organized nanostructures in areas such as nanotechnology or smart materials has led to research into the fundamentals of molecular self assembly (Dudowicz 2009, Whitesides 2002). Organization of molecules is most often driven by non-covalent interactions (e.g. van der Waals, electrostatic, hydrophobic, aromatic or hydrogen bonding) (Dudowicz 2009, Gutzler 2009, Krausch 1995, Wojtecki 2015). These molecular interactions are important for polymer properties on both macroscopic and nanoscopic scales. For example, the elastomeric behavior of phase-separated polyurethanes is enhanced by hydrogen bonding between urethane groups (Pukánszky 2008, Sung 1974, Wang 1994). In a nanoconfined system, hydrogen bonding can also influence properties dramatically (Kojio 2009). Recently, in addition to their applications as coatings, polyurethane thin films have been investigated for mechanical, electronic and optical properties, as well as morphological behavior (Harvey 2011, Kim 2003, Lupu 2007, Podsiadlo 2009, Suzuki 2012). However, there are few studies that investigate the behavior of polyurethanes when confined to the nanoscale (Huang 2015, Kojio 2009, Tao 1994).

Polymers under confinement have been observed to perform differently than their bulk counterparts (Ellison 2003, Keddie 1994, 2007, Priestley 2005, 2007). In confined geometries, properties are influenced by interfacial interactions between the polymer and both the substrate and free surface. Interfacial effects on polymer thin films have been widely studied and have been observed to impact a variety of polymer characteristics such as glass transition temperature (T_g), crystallization, morphology, conductivity, and diffusion. In literature, a three-layer model is often used to describe the regions of a polymer thin film including free surface, bulk, and substrate

layers. Near the free surface, the polymer chain mobility is enhanced and the observed perturbations can propagate tens of nanometers into the film. The polymer-substrate interface can also influence polymer properties through the increased requirement for cooperative segmental motion or decreased mobility if attractive interactions are present between the polymer and substrate (i.e. PMMA on silica) (Ellison 2002, Kim 2002, Priestley 2007).

Phase separation in polymer thin films has been extensively studied for polymer blends as well as block copolymers. The free surface and substrate layers have also been observed to influence thin film morphology through differences in block interfacial energies in copolymer thin films (Fasolka 2001, Li 2013, Napolitano 2011, Stewart-Sloan 2011). Because there are numerous variables that can influence thin film morphology (e.g. interaction parameter, substrate, anneal process, energetic preferences, etc.), only relatively simple systems have been studied and reported in literature, such as symmetric diblock copolymers. Few studies have been performed on phase-separated polyurethane thin films as the structures of multi-block polymers with polydisperse segments are complex. Kojio et al. (Kojio 2007, 2009) investigated the morphology of a microphase-separated polyurethane in both bulk and thin films using X-ray photoelectron spectroscopy and Fourier-transform infrared spectroscopy. It was found that the free surface was enriched by the soft segment in the bulk film. In addition, it was observed that as the film thickness decreased, there was a greater extent of phase mixing in the films.

Fluorescence is a technique that can be used to characterize polymer properties in thin films (Ben 1991, Gashgari 1988, Kim 2002, Kriisa 2012, Mundra 2007, Torkelson 1984, Tsai 1988). Fluorescence can be measured extrinsically, with the use of a fluorescent label, or intrinsically, if the molecule contains a fluorophore (Guilbault (Ed.) 1990, Lakowicz 2006). Intrinsic fluorescence is ideal for measurement of phase behavior or molecular alignment as the introduction of a large fluorescent probe can potentially introduce non-native interactions and influence polymer movement if present at high concentrations. Aromatic rings are able to intrinsically fluoresce, as polymer backbones or side groups, due to π–π^* transitions (Dawson 1968). Polymers with

aromatic rings are able to emit two types of fluorescence: monomer and excimer emission (Winnik 1993). Monomer emission occurs from the excited state of a single phenyl ring whereas excimer emission occurs from two phenyl rings in a parallel, sandwich-like configuration with a separation distance of 3–4 Å (Hirayama 1965). Excimers are further divided into two formation pathways: dynamic and static. A dynamic excimer is a dimer which is associated in the excited state and is dissociated in the ground state. A static excimer is a dimer species that is associated in both the excited and ground states. As described in the research literature, the combination of monomer and excimer fluorescence has been employed to analyze morphology, phase separation or probe how molecules interact in solution (Gelles 1982a, 1982b, Kim 2002, Torkelson 1984).

Here, we apply fluorescence to investigate the molecular orientation of aromatic rings in phase-separated polyurethanes in thin film geometries. Using the intrinsic fluorescence of segmented polyurethanes with 2,4-toluene diisocyanate-containing hard segments, both monomer and excimer emission of the aromatic rings are observed. From the excitation and emission spectra of these films as a function of film thickness, it is possible to discern how the aromatic rings orient and align in specific excimer configurations. By modifying the substrate, we can infer the roles of interfacial secondary bonding interactions in molecular alignment. With the fundamental understanding of chain structure and alignment of aromatic rings in segmented polymers, nanomaterial design can become more efficient and effective.

7.2. Experimental Section

7.2.1. Materials

Tolylene-2,4-diisocyanate (TDI; Sigma-Aldrich, 95 %), 1,4-butanediol (Sigma-Aldrich, 99 %) and dibutyltin dilaurate (Sigma-Aldrich, 95 %) were used as received. The diols, Voranol 220-056, a 2000 g mol^{-1} poly(propylene oxide) diol (The Dow Chemical Company) and Krasol LBH P 2000, a 2000 g mol^{-1} polybutadiene diol (Cray Valley), were heated to 110 ºC in an oil bath under a dry N_2 purge for 12 h to remove water.

7.2.2. Polyurethane Synthesis

Traditional polyurethane prepolymers were synthesized by reacting excess TDI with each diol in a 3-neck round-bottom flask equipped with overhead stirring, a N_2 inlet, and an addition funnel. For example, the diol (15.0 g, 7.5 mmol) was added dropwise to TDI (2.3 g, 13.5 mmol) from an addition funnel. The mixture was stirred at room temperature for 30 min. Dibutyltin dilaurate was added to the mixture (0.05 wt%, 4.5 μL), and the components were stirred at 80 °C for 2 h. 1,4-Butanediol (0.54 g, 6.0 mmol) was added to the prepolymer mixture. The reactants were cured between two aluminum plates at 60 °C for 1 h. The poly(propylene oxide)-based polyurethane was synthesized with 16 wt % hard segment (designed to be weakly phase separated based on information in Chapter 6 of this thesis), and the polybutadiene-based polyurethane was synthesized with 20 wt % hard segment (designed to be strongly phase separated).

7.2.3. Film Preparation

Thin films were prepared by spin coating polymer solutions (dissolved in tetrahydrofuran (Aldrich)) onto silicon wafers for ellipsometry measurements or glass slides for fluorescence measurements. Different thicknesses were obtained by adjusting solution concentration and spin speed. After spin coating, films were annealed in vacuum oven at 130 °C for 1 h. Glass slides were pretreated with basic KOH solution for 20 min and acidic HCl solution for 20 min before spin coating. Methylated glass slides were prepared in a similar manner with an additional silanization reaction step with dichlorodimethylsilane. Contact angles were used to confirm surface chemistry of glass slides (~ 77° for quartz and ~ 95° for methyl-functionalized glass).

7.2.4. Film Thickness by Ellipsometry

Measurements were performed at room temperature using spectroscopic ellipsometry (J. A. Woollam Co. M-2000D) over a range of wavelengths from 400 to 1000 nm. The ellipsometric angles (ψ and Δ) of incident light reflected off silica-supported polyurethane films were measured and fitted to a Cauchy layer model to determine thickness. The Cauchy layer model included a PS layer atop a silicon substrate containing a 2-nm-thick silicon oxide surface layer. Film thickness

was determined by fitting ψ and Δ to the PS layer in the Cauchy model.

7.2.5. Fluorescence Spectroscopy

Steady-state fluorescence emission spectra were used to characterize molecular alignment in polymer films as well as determine T_g. The film samples were annealed at 130 °C for 1 h after spin-casting. After annealing, emission spectra were collected (Photon Technology International fluorimeter in front-face geometry) at wavelengths from 280 to 500 nm, with excitation at 255 nm. Excitation and emission slit widths were 1 mm (2 nm bandpass). Peak intensities were calculated from an average of five data points spanning 2 nm around the peak: Monomer intensity was an average of five data points around 305 nm and excimer intensity an average of five data points around 420 nm. Steady-state fluorescence excitation spectra, for which emission wavelength (λ_{em}) is held constant and the excitation wavelength (λ_{exc}) is varied, were measured with $\lambda_{em,monomer}$ = 315 nm ($\lambda_{em,excimer}$ = 407 nm) for monomer (excimer) at 30 °C.

7.3. Results and Discussion

Using intrinsic fluorescence of aromatic rings in the hard segments of a phase-separated polyurethane (structures shown in Figure 7.1), it is possible to investigate the hard-segment behavior at a molecular level. When studying interfacial interactions in thin films, it is important to consider the effect of the three regions in the film: bulk, free surface and substrate interface. In this work, we examine polyurethane thin films of varied thicknesses on a quartz substrate (with hydroxyl groups on the surface that can undergo attractive interactions by hydrogen bonding to the carboxyl units in the urethane linkage) and a methylated-glass substrate (with methyl groups on the surface that are unable to interact with the polymer). With all other variables equal, fluorescence measurements of films on these substrates will show the impact of polymer-substrate attractive interactions or lack thereof on aromatic ring alignment within hard segment domains.

Figure 7.2 shows the emission spectra of polyurethane thin films made from a ~2000 g/mol poly(propylene oxide) (PPO) reacted with excess 2,4-toluene diisocyanate and 1,4-butanediol

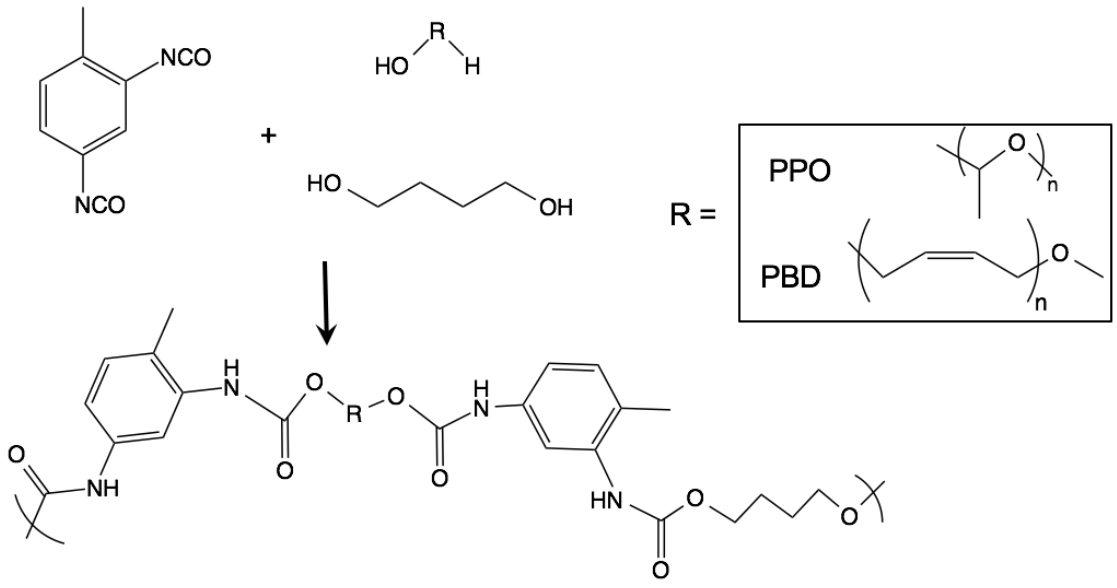

Figure 7.1. Monomer selection for polyurethane synthesis. 2,4-toluene diisocyanate (TDI) is reacted in excess with an oligomeric diol (with different R groups). When chain extended with 1,4-butanediol, a segmented polyurethane results with aromatic hard segments and diol-containing segments. PPO = 2000 g/mol poly(propylene oxide) and PBD = 2000 g/mol polybutadiene.

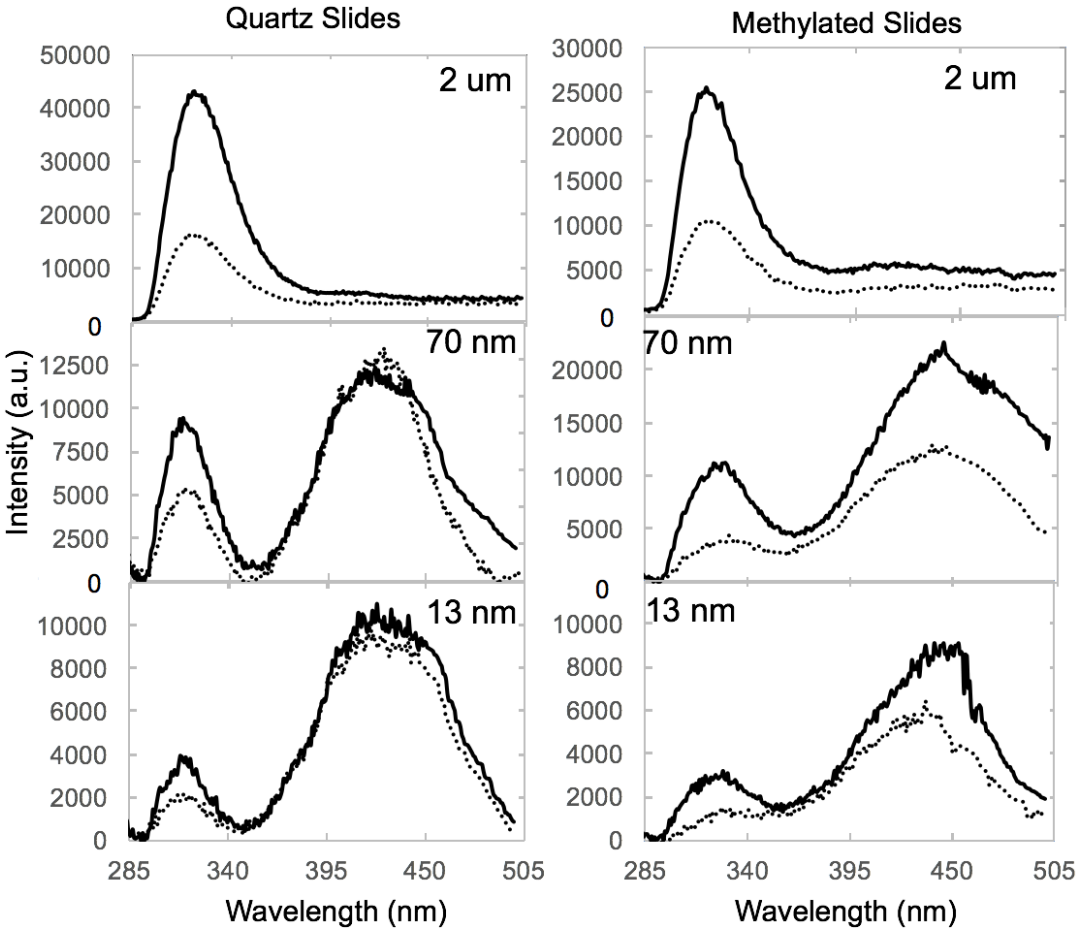

Figure 7.2. Intrinsic fluorescence emission of PPO84-PU polyurethane films (λ_{exc}: 255 nm) of 2 μm, 70 nm, and 13 nm thicknesses on both quartz and methylated substrates. Measurements were first taken at 30 °C (solid curve). Films were heated rapidly to 130 °C (dotted curve) and measured after 5 min at temperature to ensure film thermal equilibrium.

(called PPO84-PU based on soft-segment wt % nomenclature from Chapter 6) on both the quartz and methylated substrates. This PPO-based polyurethane is 16 wt % hard segment. Based on information in Chapter 6, the PPO-based polyurethane synthesized in an identical manner except for being 12 wt % hard segment was apparently one-phase and the PPO-based polyurethane with 20 wt % hard segment was phase separated. As a result, we can consider the PPO84-PU to be weakly phase separated. In the bulk state (2 μm thick film), the spectra on both substrates are similar with one main peak (centered at ~320 nm) that can be attributed to monomer emission of an aromatic ring. When compared to polystyrene (Khan 2005), the monomer emission from the aromatic ring is red-shifted due to the electronic interactions with the neighboring urethane units.

As film thickness decreases to the nanoscale, similarities as well as differences become evident as a function of the substrate. For all polyurethane films with thicknesses below 500 nm, excimer emission is clearly evident in the spectra as a broad peak centered at ~ 420 nm. In the thinnest films studied, with albeit noisy data, the excimer peaks strongly dominate the spectra. The differences between substrate surface chemistry are highlighted when examining the temperature dependence of each film. On the methylated substrate, the monomer and excimer intensities decrease with increasing temperature, which is the typical response of a fluorophore as the radiative pathway is suppressed with increasing temperature. In contrast, on the quartz substrate, the excimer intensities show little to no dependence on temperature. It is rare that excimer intensity does not decrease as a function of temperature as the formation of excimer is typically dependent on excited-state monomer, which undergoes increasing levels of non-radiative decay with increasing temperature.

The unusual features associated with the temperature dependences of the emission spectra in Figure 7.2 cannot be explained if the excimer formation occurs in a strictly dynamic manner, which is the typical pathway observed for excimer forming polymer systems, including polystyrene. Excimer has two formation pathways as shown in Figure 7.3. In the ground state, an aromatic ring can exist as a single chromophore (M). The excitation of this ring produces excited-

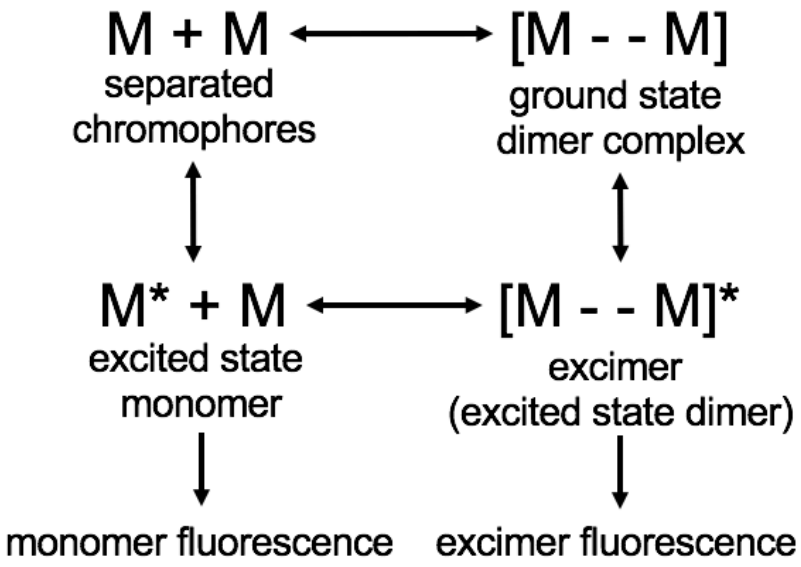

Figure 7.3. Pathways for the formation and emission of static and dynamic excimers in aromatic systems.

state monomer (M*) which can either decay in a radiative (through fluorescence) or non-radiative (through vibration, etc.) pathway. Once in the excited state, it is also possible for the M* to associate with another M to form an excited-state dimer. Dimers created through this pathway are referred to as dynamic excimers. The second pathway to excimer formation is the direct excitation of a preformed ground-state dimer complex, which has the appropriate parallel, sandwich-like configuration with an inter-ring separation distance of 3-4 Å. When excited, this ground-state dimer complex forms static excimer.

Because static and dynamic excimers originate from different ground-state entities, they absorb light differently and show distinctive absorption and excitation spectra. (If all excimer formed dynamically from excited-state monomer, then the excitation spectra for excimer and monomer emission would be identical within error.) Figure 7.4 shows the excitation spectra of PPO84-PU thin films on quartz and methylated substrates. In the bulk film emission spectrum shown in Figure 7.2, there is very little excimer compared to monomer. However, the excitation spectra of the 2 μm film reveals a difference between the monomer and excimer profiles. The excimer excitation spectra for films on both substrates are similarly blue-shifted relative to the monomer excitation spectra (with relatively little noise in the data). This shift is indicative of a ground-state entity that is different from that of a single monomer. Because the aromatic rings are the only fluorescent species in this polymer, excimer fluorescence must be caused by the excitation of a ground-state dimer complex.

As we confine the films to 200 nm and below, differences develop between the excitation spectra for films on the different substrates. With films on quartz substrates, the peak locations for the monomer and excimer excitation spectra remain unchanged within error as a function of confinement. In contrast, with the methylated substrates, the excimer excitation spectrum becomes much broader with confinement. This broadening is suggestive of the formation of both static and dynamic excimers upon confinement, with the peak breadth reflecting a combination of the two distinct peak shapes seen in bulk on the methylated substrate.

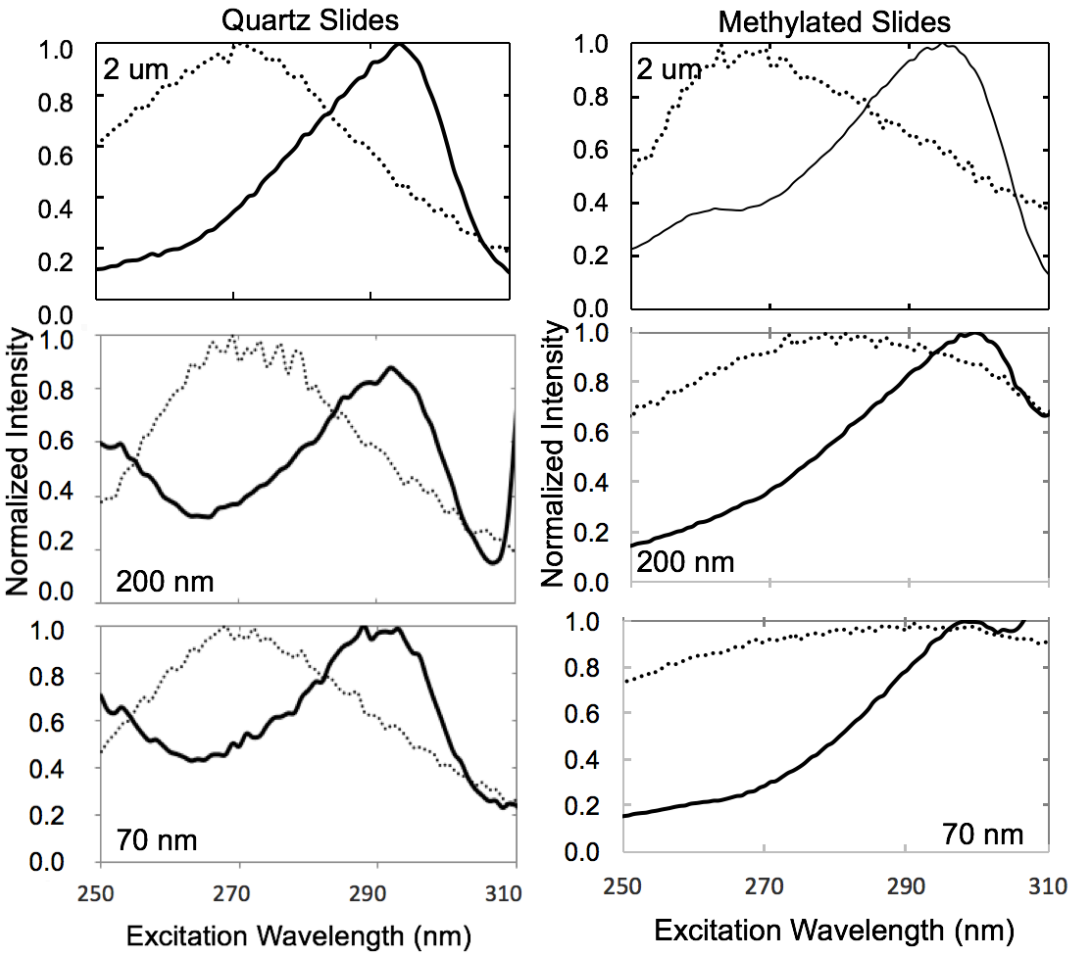

Figure 7.4. Excitation spectra of PPO84-PU films with thicknesses of 2 μm, 200 nm, 70 nm monitored at monomer emission wavelength, 318 nm (solid line), and excimer emission wavelength, 407 nm (dotted line) on a quartz substrate and a methylated substrate.

With the understanding of the different origins of excimer fluorescence, the temperature dependence on the two substrates can be explained through impact of attractive polymer-substrate interactions on the polymer rigidity. On the quartz substrate, the surface hydroxyl groups can hydrogen bond with the carbonyl groups contained in the urethane linkages of the polyurethane. No such hydrogen bonding interactions are present on the methylated substrate. As a result, the interfacial zone at the polymer-substrate interface is more rigid when the polyurethane films are on quartz. On the quartz substrate, ground-state dimer is formed and can fluoresce as static excimer. In the absence of hydrogen bonding, the polymer-substrate interface is comparatively less rigid, as is the case of the methylated substrate. This decrease in rigidity accommodates for the formation of dynamic excimer in addition to the static excimer. Therefore, with increasing temperature, the radiative pathway for dynamic excimer is suppressed and a temperature dependence of excimer emission is observed on the methylated substrate, as shown in Figure 7.2.

In order to quantify the alignment of the aromatic rings on interacting and non-interacting substrates, we use the excimer to monomer intensity ratio (I_E/I_M) to show the relationship between single aromatic rings and aromatic rings that align according to the specific excimer orientation and distance requirements. Figure 7.5 shows the ratio of these intensities over a wide range of film thicknesses at 30 °C on both quartz and methylated substrates. Both substrates show similar trends of increasing I_E/I_M with confinement. Using information gained from the excitation spectra of films on each substrate (Figure 7.4), the increase in I_E/I_M with confinement indicates that the aromatic rings are able to form ground-state dimers more easily upon confinement on both substrates. Notably, with thicknesses below 200 nm, I_E/I_M on the methylated substrate is higher than that on the quartz substrate. The reduced rigidity at the polymer-substrate interface on the methylated substrate allows for dynamic excimer in combination with the static excimer, which gives an increased I_E/I_M relative to that on the quartz substrate. The rigidity at the polymer-substrate interface can propagate (in a decaying manner) over many tens of nanometers into the interior of the film (Ellison 2003, Evans 2015, Priestley 2005), as is observed here up to ~200 nm.

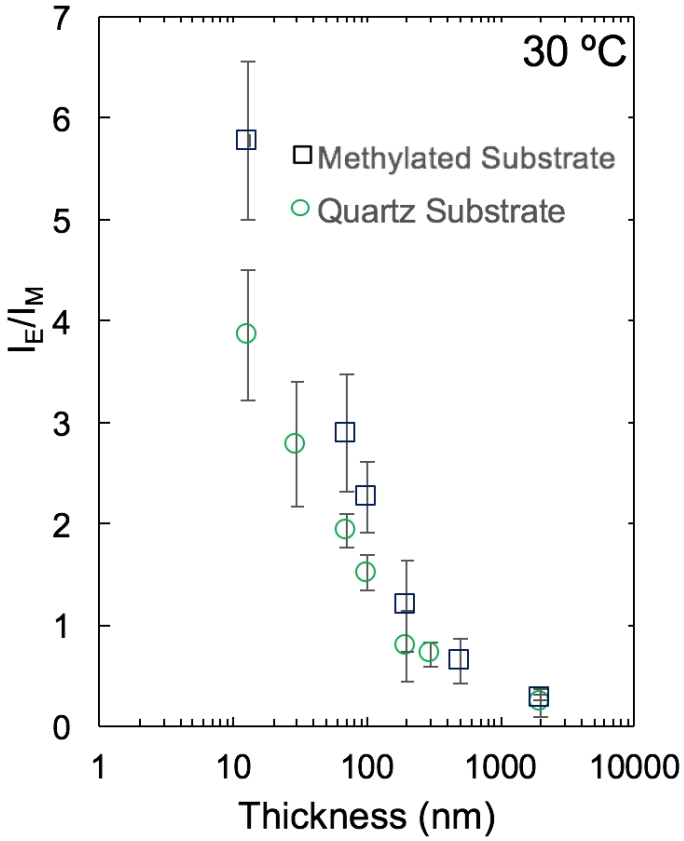

Figure 7.5. Excimer to monomer intensity ratios of PPO84-PU (at 30 °C) as a function of film thickness on quartz (circle) and methylated (square) substrates.

In a bulk layer, polymer behavior should not be influenced by interfacial effects. In the past, it has been observed that fluorescence intensity of a fluorescent label is linearly proportional to the film thickness (t) (when absorbance is less than 0.05) (Hall 1997). Here, in order to more clearly understand the effect of confinement on monomer and excimer behavior, we can divide I_E and I_M of films on the quartz substrate by film thickness, t. In bulk (t = 2 μm), I_E/t is ~ 3 a.u./nm^{-1}. Upon confinement, I_E/t is increased to ~ 170 and ~ 550 a.u./nm^{-1} for 70 and 13 nm, respectively. This increase can be explained through the hypothesis that excimer is formed in the interfacial regions and that dimer formation does not occur in bulk (as confirmed by the bulk emission spectra). As bulk (non-dimer containing polymer) is removed from the system with confinement, there will be an overall increase of intensity divided by thickness. The dramatic increase for excimer intensity of the 13 nm film shows that in the ultra-thin case, the maximum orientation and alignment of aromatic rings occurs. For monomer intensity, a similar trend is observed. In bulk, I_M/t is ~ 13 a.u./nm^{-1}. Upon confinement, I_M/t is increased to ~ 100 and ~ 195 a.u./nm^{-1} for 70 and 13 nm, respectively. Although it may seem counter-intuitive that both monomer and excimer intensities increase upon confinement, it can be reasoned through their distinct formation pathways. Because the excitation spectra show that these are static excimers, not dynamic excimers, the pathways do not compete for excited-state monomers. Upon confinement, the substrate rigidity effects are increased. With increased rigidity and stiffness, the fluorescence intensity increases as the non-radiative pathways for energy decay are suppressed.

Upon confinement, a weakly phase-separated polyurethane shows changes in excimer behavior when compared to bulk. To investigate the behavior of a strongly phase-separated polyurethane, a polymer was synthesized using a polybutadiene-based soft segment with a 20 wt % hard-segment content (named PBD80-PU). Figure 7.6 shows the emission and excitation spectra for this well phase-separated polyurethane. In Figure 7.6a, the emission spectra for three film thicknesses are shown on a quartz substrate. Different from the weakly phase-separated PPO84-PU, the bulk PBD80-PU film shows roughly equal maximum intensities of monomer and excimer

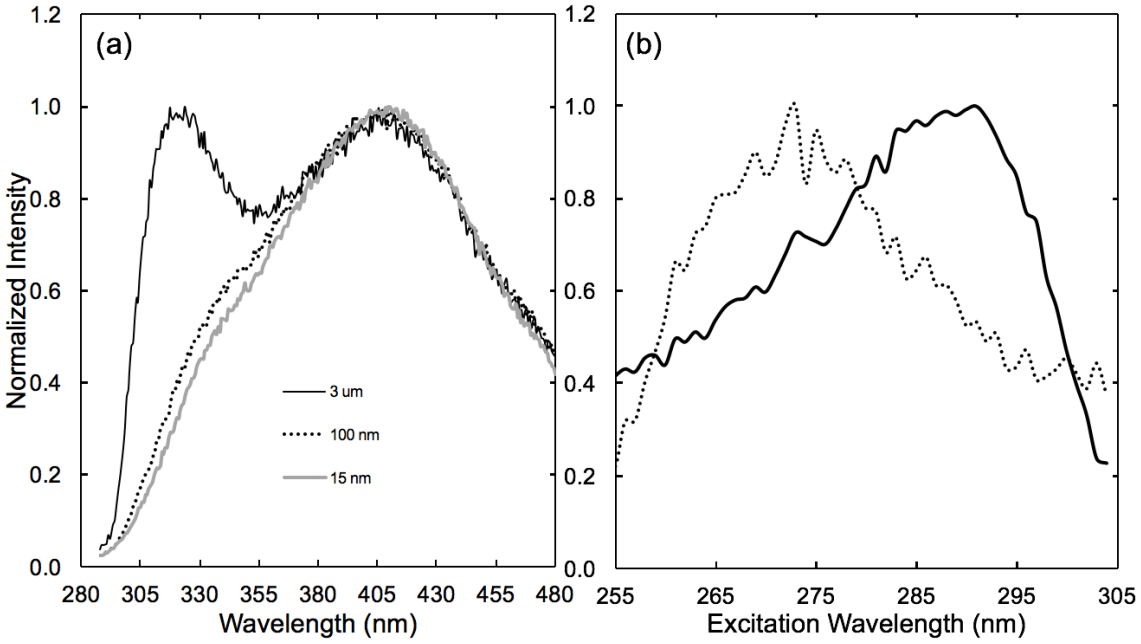

Figure 7.6. (a) Intrinsic fluorescence emission of PBD80-PU (λ_{exc}: 255 nm) of 2 μm, 100 nm and 15 nm thicknesses on quartz substrate. (b) Excitation spectra of 3 μm polyurethane film monitored at monomer emission wavelength, 318 nm (solid line), and excimer emission wavelength, 407 nm (dotted line) on a quartz substrate.

emission. With nanoscale confinement, the monomer emission is strongly reduced to a slight shoulder on the low wavelength side of the broad excimer peak. In a strongly phase-separated polyurethane, the aromatic rings in the hard segment domains are highly aligned in bulk (see Chapter 6). Upon confinement, the rings are further forced into the sandwich-like geometries, with very little interphase that contains isolated rings. In Figure 7.6b, the excitation spectra for monomer and excimer emission are different, indicating that monomer and excimer fluorescence originate from different ground-state species. Upon confinement, the excitation spectra for monomer and excimer emission cannot be well distinguished because the excimer fluorescence so strongly dominates the emission spectra.

7.4. Conclusion

This study employed intrinsic fluorescence to reveal orientation and alignment of aromatic rings in the hard segments of phase-separated polyurethanes upon confinement. With decreasing film thickness, there was an increase in the alignment of aromatic rings in parallel, sandwich-like configurations with inter-ring distances of 3-4 Å as the ground-state dimers were more easily formed along the interfaces. With confinement, it is observed that excimer intensity increases dramatically as the rigidity from the interfaces caused a suppression in the non-radiative pathway. It was observed that the extent of aromatic ring alignment was a function of attractive polymer-substrate interactions, specifically hydrogen bonding. In the absence of polymer-substrate interactions, the mobility at the substrate allowed for both dynamic and static excimer formation. Hydrogen bonding at the substrate was observed to increase the rigidity of the polymer-substrate interfacial zone and only accommodate the formation of ground-state dimers by the aromatic rings. This rigidity from hydrogen bonding at the substrate was observed to propagate into the thin films by many tens of nanometers.

VI. SUMMARY

CHAPTER 8

CONCLUSIONS AND FUTURE WORK

This dissertation focused on the synthesis and characterization of physically and chemically crosslinked polymer networks related to polyurethanes or non-isocyanate polyurethane-like materials. Section I provided an introduction and background to the fundamental concepts explored in this dissertation. Summaries of key findings of Sections II and III are discussed below. In addition, suggested pathways for future work are discussed.

8.1. Section II Conclusions

In Section II, thiol and amine reactants were utilized in polymerizations in order to produce networks with the attributes of click chemistry, such as fast reaction times, high yield, and network uniformity. Chapter 3 presented results of the first study to undertake a one-pot, single-catalyst approach to the synthesis of thiol-acrylate-epoxy polymer networks. In the cases studied here, the network was formed with all three components. With 1,8 diazabicyclo[5.4.0]undec-7-ene (DBU) as a base catalyst, both thiol-acrylate and thiol-epoxide reactions achieved full thiol conversion under ambient conditions during the simultaneous synthesis. We compared the simultaneous synthesis to two types of sequential syntheses in order to demonstrate the benefits of a one-step approach. Characterization associated with each reaction approach included reaction kinetics as well as thermal and mechanical properties of the final polymer. Characterization of reactions kinetics revealed that phase separation was a critical parameter in conversion levels in the sequential syntheses but not in the simultaneous synthesis. Through reaction-induced phase separation, the first phase-separated thiol-acrylate-epoxy polymer was synthesized by simultaneous reactions between thiols, oligomeric diacrylates and aromatic diepoxides. From these phase-separated materials, a novel type of thermally induced shape memory polymer with good thermal and mechanical properties was synthesized and characterized. This material exhibited

shape-fixity values above 95% and shape-recovery values above 99% after multiple cycles.

Reaction-induced phase separation in the hybrid thiol-acrylate-epoxide network produced a spherical morphology that allowed for desired elastomeric and shape memory properties. However, because the study described in Chapter 3 and a study by Jin and Torkelson are the only reports on phase-separated thiol-acrylate-epoxide networks published in the literature, Chapter 4 focused on the morphology of these systems (Dhulst 2016, Jin 2016). Typical polymer systems that undergo reaction-induced phase separation, such as modified epoxy resins, have morphologies that are heavily dependent on cure conditions. In Chapter 4, we observed that the morphology of this hybrid thiol-acrylate-epoxide network is independent of temperature and DBU catalyst loading over a broad range of conditions. This independence of phase-separated morphology with reaction conditions can be understood to arise from the high asymmetry of reaction rates, with the thiol-acrylate reaction being essentially complete before there is much conversion of epoxide. Because the morphology is unaffected by temperature and DBU catalyst loading, the thermal and mechanical properties of these materials are also unaffected. In Chapter 3, room temperature reactions were explored; here, we showed that the typical cure-rate dependence of morphology was largely avoided through the combination of rapid and (comparatively) slow reactions. As a result, when DBU is employed as a catalyst, the thiol-acrylate-epoxide reaction rate can be tuned via temperature and DBU concentration without the need to consider the complexity of the reaction-induced phase separation behavior common in many polymer systems that undergo phase separation during reaction.

In Chapter 5, amine and vinyl sulfone reactants were used toward the development of ambient non-isocyanate polyurethane-like materials for field-use applications. Vinyl sulfone is an electrophile that has commonly been used as an intermediate in click reactions but not as a reactant in polymerizations. The electron withdrawing nature of the sulfone allows for fast reactivity at room temperature with diamines in the absence of external catalyst. Here, novel crosslinked elastomeric materials were produced by oligomeric diamines, divinyl sulfone and diamine chain

extenders. In this chapter, reaction kinetics for these room-temperature polymerizations were reported for the first time and showed this uncatalyzed reaction as second order. With k_{app} = 0.17 M^{-1} min^{-1} for a bulk reaction with balanced stoichiometry, this reaction rate is competitive with (or better than) uncatalyzed polyurethane reactions and reactions of selected polyurethane replacements reported in literature. With the structures employed in this chapter, thermoset elastomers with modest strain at break (73%) and modulus values (5.1 MPa) were obtained.

8.2. Section II Future Work

With the introduction of a simple one-step synthesis for thiol-acrylate-epoxide hybrid systems, the barriers for commercial use, such as complex multi-step, multi-catalyst syntheses, are removed. However, because the focus of the initial study was on reaction kinetics and phase separation, the structure-property relationships in this system were not explored. In Chapter 3, shape memory materials were designed through optimization of electrophile stoichiometry and diacrylate molecular weight. To influence the phase separation, the structure of the oligomeric diacrylate should be changed to a less polar backbone such as PTMO or PBD. To enhance the hard segment T_g, the structure of the epoxide could be adjusted. In exploratory work, different epoxide structures were examined. It was found that the aromatic structure provided greater phase separation and a higher T_g than any aliphatic replacements. However, in our group, there has been work with thiol-maleimide (Jin unpublished) and thiol-norbornene reactions (Leitsch 2015) and we hypothesize that the introduction of these structures as an epoxide replacement could be valuable for enhanced network properties.

Future pathways of research on hybrid morphology can work toward either tuning or maintaining the observed morphology. Because Chapter 4 showed that thiol-acrylate-epoxide systems avoided morphological variability over a wide range of cure conditions due to the use of two distinct reaction rates, tunability of morphology through those parameters is lost. Future work should examine catalyst type as a variable to tune morphology. Based on the literature, if the two

reactions (thiol-acrylate and thiol-epoxide) had similar rates, a cocontinuous morphology could be possible. For example, reaction conditions more favorable for the thiol-epoxide reaction (different catalyst, very high *T*) could equalize the two rates and allow for different morphologies. The second research pathway would involve capitalizing on the morphology control provided by these distinct rates. Future work could explore other hybrid polymers with these rate differences, including amine-acrylate-epoxide, and observe similar control.

With the reaction of primary amines and vinyl groups, crosslinked polymers are formed. In literature, the use of secondary amines is common with vinyl sulfone to produce linear or branched chains. However, largely unexplored is the the use of primary amines to produce thermoplastic elastomers. Besides the impact of its strong electron-withdrawing nature on reactivity, the sulfone group also provides foundation for non-covalent interactions in a polymer backbone, like increased van der Waals interactions with nonpolar atoms, including aromatic rings or hydrophobic segments. Currently, no study has been reported that investigates the effect of sulfone group interactions on the thermal and mechanical behavior of polymers. In preliminary studies, thermoplastic amine-vinyl sulfones were synthesized using similar reactants with adjusted stoichiometry and solvent. However, these materials were single phase up to ~40 wt% hard segment. Future work to investigate the role of structure and non-covalent interactions in phase separation of vinyl sulfone-based thermoplastic elastomers is warranted.

8.3. Section III Conclusions

In Section III, intrinsic fluorescence spectroscopy was employed to examine segmented polyurethanes. In Chapter 6, one-phase and two-phase polyurethanes were synthesized with toluene diisocyanate-containing hard segments and various soft segments to give polymers with a wide range of degrees of phase separation. Using intrinsic fluorescence of the aromatic rings, extents of aromatic alignment and aromatic interactions in the hard segments were characterized. In literature, aromatic interactions between hard segments in polyurethanes have been inferred and

not experimentally determined. With this experimental technique, the nature of aromatic interactions can be discerned. Using emission spectra, excimer intensity revealed the orientation and alignment of aromatic rings in parallel, sandwich-like configurations 3-4 Å apart while monomer intensity revealed aromatic rings that do not have other rings in their local environment. Using excitation spectra, the distinction between aromatic interactions that occur in the ground state and those that occur in the excited state were determined. Here, it was shown that in phase-separated polyurethanes, the formation of these dimers occurred in the ground state, suggesting that aromatic interactions play a role in the hard-segment alignment. It was also found that ground-state dimers were formed at both 30 °C and 130 °C, which demonstrates that these complexes are present with both high and low concentrations of hydrogen bonding. This is the only report in literature that proves aromatic interactions exist (in specific excimer configurations) in the hard segments of polyurethanes and potentially contribute to the stabilization of phase separation.

Chapter 7 discussed the application of this intrinsic fluorescence technique to segmented polyurethanes (with toluene diisocyanate-containing hard segments) in confined geometries. Here, polyurethanes with a low hard-segment content (weakly phase separated) were examined in bulk and thin film geometries. Upon confinement, excimer emission increased relative to monomer emission. Because a larger fraction of polymer chains present are adjacent to the interfaces with decreasing film thickness, we inferred that the dimer formation was dominantly present in the interfacial regions. We hypothesized that rigidity from an interface, such as polymer-substrate interface, can assist in ring alignment. It was observed that alignment perturbations caused by the interface rigidity can propagate in a decaying manner, and effects are observed many tens of nanometers into the film. This study also investigated the impact of hydrogen bonding interactions between polymer and substrate on ring alignment. In the absence of attractive interactions, the aromatic rings formed both dynamic and static excimers. With enhanced rigidity from directional hydrogen bonding, only static excimer was formed as the rings only had the mobility to orient and align in the ground state. This study revealed the importance of polymer-substrate interactions on

polyurethane thin films as well as how rigidity impacts the formation of static and dynamic excimers.

8.4. Section III Future Work

Fluorescence has been widely employed to assess polymer properties in bulk and confined geometries. However, this was the first application of intrinsic fluorescence to characterize hard-segment behavior in segmented polyurethanes. The studies in this dissertation explored polyurethanes synthesized with 2,4-toluene diisocyanate, a commonly used, asymmetric hard segment. Future studies that examine common symmetric diisocyanates, including 2,6-toluene diisocyanate and methylene diphenyl diisocyanate, would advance both academic and industrial research as these segments can crystallize and have different orientation and alignment behavior that has been seen to influence phase separation and orientation of aromatic rings. In addition, the hydrogen bonding between these well-studied hard segments have been explored computationally (Sami 2014, Zhang 2014a). Information relating hydrogen bond angles between hard segments can be useful in determining the underlying mechanism for excimer formation in these systems. Additionally, the use of other techniques commonly applied to polymer thin films can give insight into the confinement behavior of the segmented polyurethanes. For example, X-ray photoelectron spectroscopy can be employed to determine the alignment of soft and hard segments at the substrate at different thicknesses. Understanding this behavior will allow for better mechanistic insight to ground-state dimer formation.

Another pathway of future work with polyurethane intrinsic fluorescence would be to monitor phase separation over the course of a polymerization. Previous studies have shown polyurethane cure characterization by fluorescence (Sun 1996, Vatanparast 2000), but there have been no reports that track phase separation. Combined with other techniques such as DSC or time-resolved SAXS, it would be possible to decouple the roles of structure incompatibilities and aromatic interactions in phase separation. Future work with this technique could also become more

application dependent with focus on enhancing properties through increased aromatic ring alignment. For example, hard-segment alignment is important to polyurethane applications such as electrospinning of nanofibers (Sakamoto 2014). Future work could use this technique as a method for understanding molecular orientation in these fibers. With proper instrumentation, it would also be possible to analyze ring alignment as a function of strain.

For a commercial phase-separated polyurethane, two T_g's are typically present. Depending on the concentration of hard segment in the material, it is often difficult to observe a hard-segment T_g using DSC. Fluorescence has been used as a technique to observe T_g's in multi-component miscible polymer blends (Evans 2012). Because Chapters 6 and 7 show that fluorescence is sensitive molecular orientation of the hard segments in polyurethane, it would likely be useful in quantitatively observing the cooperative motion of aromatic rings in the hard segments. From a preliminary study, Figure 8.1 shows the novel use of intrinsic fluorescence to identify the hard-segment T_g of a polyurethane thin film. Here, in a 1 μm-thick film, the T_g by fluorescence is 79 °C, which is, within error, the same T_g determined by bulk DSC measurements for a well phase-separated polyurethane with identical hard segment structure. This measurement reiterates the hypothesis that fluorescence is sensitive to the local environment of aromatic rings in hard segments of polyurethanes and can be used to observe T_g in systems where DSC and DMA may be insensitive. Future work should explore this sensitivity and apply this technique to the range of materials studied in Chapter 6, as well as examine T_g-confinement behavior from Chapter 7.

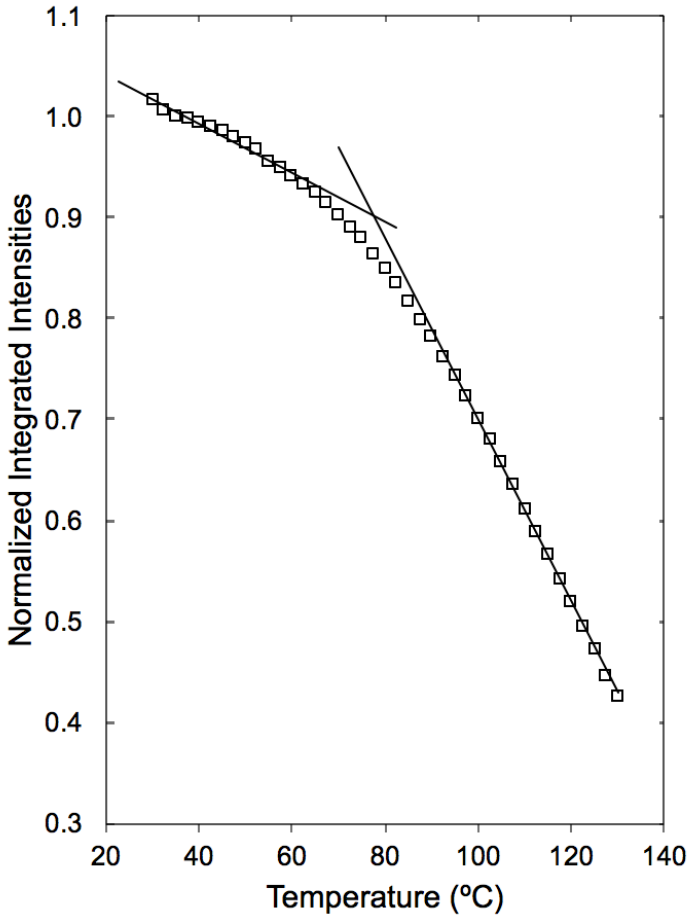

Figure 8.1. Integrated intensity from 280-490 nm as a function of temperature used to determine T_g for a 1000 nm PPO84-PU film. The value of T_g is taken as from the intersection of the rubbery- and glassy-state temperature dependences of the normalized integrated fluorescence intensity (the intensity has been normalized to 30 °C).

V. REFERENCES

Ahmad, M.; Xu, B.; Purnawali, H.; Fu, Y.; Huang, W.; Miraftab, M.; Luo, J. *Applied Sciences*. **2012**, *2*, 535–548.

Ajithkumar, S.; Kansara, S. S.; Patel, N. K. *European Polymer Journal*. **1998**, *34*, 1273–1276.

Aladekomo, J. B.; Birks, J. B. *Proceedings of The Royal Society of London - Series A*. **1965**, *284*, 551–555.

Alleti, R.; Oh, W. S.; Perambuduru, M.; Ramana, C. V.; Prakash Reddy, V. *Tetrahedron Letters*. **2008**, *49*, 3466–3470.

Amantini, D.; Fringuelli, F.; Pizzo, F.; Tortoioli, S.; Vaccaro, L. *Synlett*. **2003**, 2292–2296.

American Chemistry Council Bulletin. *Isocyanate Health Hazards*. **2012**.

Andersson, A.; Lundmark, S.; Magnusson, A.; Maurer, F. H. J. *Journal of Cellular Plastics*. **2010**, *46*, 73–93.

Atli, B.; Gandhi, F.; Karst, G. *Journal of Intelligent Material Systems and Structures*. **2009**, *20*, 87–95.

Bagdi, K.; Molnár, K.; Kállay, M.; Schön, P.; Vancsó, J. G.; Pukánszky, B. *European Polymer Journal*. **2012**, *48*, 1854–1865.

Bagdi, K.; Molnár, K.; Sajó, I.; Pukánszky, B. *Express Polymer Letters*. **2011**, *5*, 417–427.

Baidya, M.; Mayr, H. *Chemical Communications (Cambridge, England)*. **2008**, 1792–1794.

Balzani, V.; Scandola, F. *Supramolecular Photochemistry*. **1991**. Ellis Horwood Limited.

Bates, F. S.; Fredrickson, G. H. *Annual Review of Physical Chemistry*. **1990**, *41*, 525–557.

Bates, F. S.; Fredrickson, G. H. *Physics Today*. **1999**, *52*, 32–38.

Behl, M.; Lendlein, A. *Materials Today*. **2007**, *10*, 20–28.

Beloshenko, V. A.; Varyukhin, V. N.; Voznyak, Y. V. *Russian Chemical Reviews*. **2007**, *74*, 265–283.

Ben, F.; Larbi, C.; Monnerie, L. *Macromolecules*. **1991**, 867–871.

Berezkin, Y.; Urick, M. *ACS Symposium Series*. **2013**, *1148*, 65–81.

Berlman, I. *Handbook of Fluorescence Spectra of Aromatic Molecules*. **2012**. Elsevier.

Besse, V.; Foyer, G.; Auvergne, R.; Caillol, S.; Boutevin, B. *Journal of Polymer Science, Part A: Polymer Chemistry*. **2013**, *51*, 3284–3296.

Binder, S.; Gadwal, I.; Bielmann, A.; Khan, A. *Journal of Polymer Science, Part A: Polymer Chemistry*. **2014**, *52*, 2040–2046.

Birks, J. B.; Aladekomo, J. B. *Spectrochimica Acta*. **1964**, *20*, 15–21.

Birks, J. B.; Braga, C. L.; Lumb, M. D. *Proceedings of The Royal Society of London - Series A*. **1965**, *283*, 83-88.

Birks, J. B.; Christophorou, L. G. *Nature*. **1962**, *194*, 442–444.

Birks, J. B.; Christophorou, L. G. *Spectrochimica Acta*. **1963a**, *19*, 401–410.

Birks, J. B.; Christophorou, L. G. *Nature*. **1963b**, *197*, 1064–1065.

Birks, J. B.; Munro, I. H.; Dyson, D. J. *Proceedings of The Royal Society of London - Series A*. **1963c**, *275*, 575–588.

Bissantz, C.; Kuhn, B.; Stahl, M. *Journal of Medicinal Chemistry*. **2010**, *53*, 5061–5084.

Bonnet, A.; Pascault, J. P.; Sautereau, H.; Camberlin, Y. *Macromolecules*. **1999**, *32*, 8524–8530.

Bosch, P.; Catalina, F.; Corrales, T.; Peinado, C. *Chemistry - A European Journal*. **2005a**, *11*, 4314–4325.

Bosch, P.; Fernández, A.; Salvador, E. F.; Corrales, T.; Catalina, F.; Peinado, C. *Polymer*. **2005b**, *46*, 12200–12209.

Bounds, C. O.; Goetter, R.; Pojman, J. A.; Vandersall, M. *Journal of Polymer Science, Part A: Polymer Chemistry*. **2012**, *50*, 409–422.

Bouyahyi, M.; Pepels, M. P. F.; Heise, A.; Duchateau, R. *Macromolecules*. **2012**, *45*, 3356–3366.

Boyard, N.; Vayer, M.; Sinturel, C.; Seifert, S.; Erre, R. *European Polymer Journal*. **2005**, *41*, 1333–1341.

Brändle, A.; Khan, A. *Polymer Chemistry*. **2012**, *3*, 3224–3227.

Bras, W.; Derbyshire, G. E.; Bogg, D.; Cooke, J.; Elwell, M. J.; Komanschek, B. U.; Naylor, S.;

Ryan, A. J. *Science*. **1995**, *267*, 996–999.

Brazel, C. S.; Rosen, S. L. *Fundamental Principles of Polymeric Materials*. **2012** (2nd ed.). Hoboken: John Wiley and Sons.

Calvo-Castro, J.; Morris, G.; Kennedy, A. R.; McHugh, C. J. *Crystal Growth and Design*. **2016**, *16*, 2371–2384.

Camberlin, Y.; Pascault, J. P. *Journal of Polymer Science: Polymer Chemistry Edition*. **1983**, *21*, 415–423.

Carioscia, J. A.; Schneidewind, L. *Journal of Polymer Science, Part A: Polymer Chemistry*. **2007a**, 5686–5696.

Carioscia, J. A.; Stansbury, J. W.; Bowman, C. N. *Polymer*. **2007b**, *48*, 1526–1532.

Castagna, A. M.; Pangon, A.; Choi, T.; Dillon, G. P.; Runt, J. *Macromolecules*. **2012**, *45*, 8438–8444.

Chan, J. W.; Hoyle, C. E.; Lowe, A. B.; Bowman, M. *Macromolecules*. **2010**, *43*, 6381–6388.

Chan, J. W.; Wei, H.; Zhou, H.; Hoyle, C. E. *European Polymer Journal*. **2009a**, *45*, 2717–2725.

Chan, J. W.; Yu, B.; Hoyle, C. E.; Lowe, A. B. *Polymer*. **2009b**, *50*, 3158–3168.

Chang, M.; Chen, S. *Journal of Polymer Science, Part A: Polymer Chemistry*. **1987**, *25*, 2543–2559.

Chatani, S.; Nair, D. P.; Bowman, C. N. *Polymer Chemistry*. **2013**, *4*, 1048–1055.

Chattopadhyay, D. K.; Sreedhar, B.; Raju, K. *Journal of Polymer Science, Part B: Polymer Physics*. **2006**, *44*, 102–118.

Chattopadhyay, D. K.; Webster, D. C. *Progress in Polymer Science*. **2009**, *34*, 1068–1133.

Chen, T. K.; Chui, J. Y.; Shieh, T. S. *Macromolecules.* **1997**, *9297*, 5068–5074.

Cho, J.; Hwang, J.; Cho, K.; An, J.; Park, C. *Polymer*. **1993**, *34*, 1–5.

Chu, B.; Gao, T.; Li, Y. J.; Wang, J.; Desper, C. R.; Byrne, C. A. *Macromolecules*. **1992**, *25*, 5724–5729.

Clemens, R. J.; Rector, F. D. *Journal of Coatings Technology and Research*. **1989**, *61*, 83–91.

Connor, R.; McClellan, W. R. *Journal of Organic Chemistry*. **1938**, *3*, 570–577.

Cook, W. D.; Moad, G.; Mccarthy, L.; Van Deipen, G.; Zhang, T.; Cser, F.; McCarthy, L. *Journal of Applied Polymer Science*. **1996**, *62*, 1709–1714.

Cook, W. D.; Schiller, T. L.; Chen, F.; Moorho, C.; Thang, S. H.; Bowman, C. N.; Scott, T. F. *Macromolecules*. **2012**, *45*, 9734–9741.

Cornille, A.; Auvergne, R.; Figovsky, O.; Boutevin, B.; Caillol, S. *European Polymer Journal*. **2016**, *87*, 535–552.

Couchman, P. R. *Macromolecules*. **1978**, *11*, 1156–1161.

Cuvé, L.; Pascault, J. P.; Boiteux, G. *Polymer*. **1992**, *33*, 3957–3967.

Dalnoki-Veress, K.; Forrest, J. A.; Dutcher, J. *Physical Review E*. **1998**, *57*, 5811–5817.

Dawson, W. R.; Windsor, M. W. *The Journal of Physical Chemistry*. **1968**, *72*, 3251–3260.

De, S.; Khan, A. *Chemical Communications (Cambridge, England)*. **2012**, *48*, 3130–3132.

de Castries, A.; Escande, A.; Fensterbank, H.; Magnier, E.; Marrot, J.; Larpent, C. *Tetrahedron*. **2007**, *63*, 10330–10336.

Delebecq, E.; Pascault, J.; Boutevin, B. *Chemical Reviews*. **2013**, *113*, 80–118.

Despotopoulou, M. M.; Miller, R. D.; Rabolt, J. F.; Frank, C. W. *Journal of Polymer Science, Part B: Polymer Physics*. **1996**, *34*, 2335–2349.

Dhulst, E. A.; Heath, W. H.; Torkelson, J. M. *Polymer*. **2016**, *96*, 1–7.

Dubey, R.; Lim, D. *Current Organic Chemistry*. **2011**, *15*, 2072–2081.

Dudowicz, J.; Douglas, J. F.; Freed, K. F. *Journal of Chemical Physics*. **2009**, *130*, 84903–84913.

Dušek, K.; Prins, W. *Advances in Polymer Science*. **1969**, *6*, 1–102.

Ellison, C. J.; Kim, S. D.; Hall, D. B.; Torkelson, J. M. *European Physical Journal E*. **2002**, *8*, 155–166.

Ellison, C. J.; Torkelson, J. M. *Nature Materials*. **2003**, *2*, 695–700.

Elwell, M. J.; Ryan, A. J.; Grunbauer, H. J. M.; VanLieshout, H. C. *Polymer*. **1996a**, *37*, 1353–1361.

Elwell, M. J.; Ryan, A. J.; Grunbauer, H. J. M.; VanLieshout, H. C. *Macromolecules*. **1996b**, *29*, 2960–2968.

Engels, H. W.; Pirkl, H. G.; Albers, R.; Albach, R. W.; Krause, J.; Hoffmann, A.; Casselmann, H.; Dormish, J. *Angewandte Chemie - International Edition*. **2013**, *52*, 9422–9441.

Enns, J.; Gillham, J. *Journal of Applied Polymer Science*. **1983**, *28*, 2567–2591.

Esteves, A. P.; Silva, M. E.; Rodrigues, L. M.; Oliveira-Campos, A. M. F.; Hrdina, R. *Tetrahedron Letters*. **2007**, *48*, 9040–9043.

Evans, C. M.; Kim, S.; Roth, C. B.; Priestley, R. D.; Broadbelt, L. J.; Torkelson, J. M. *Polymer*. **2015**, *80*, 180–187.

Evans, C.M.; Torkelson, J.M. *Polymer*. **2012**, *53*, 6118-6124.

Fasolka, M. J.; Mayes, A. M. *Annual Review Materials Research*. **2001**, *31*, 323–355.

Flores, M.; Tomuta, A. M.; Fernández-Francos, X.; Ramis, X.; Sangermano, M.; Serra, A. *Polymer*. **2013**, *54*, 5473–5481.

Flory, J. *Journal of the American Chemical Society*. **1939**, *61*, 3334–3340.

Förster, T. *Angewandte Chemie - International Edition*. **1969**, *8*, 333–343.

Fox, T. G. *American Physical Society*. **1956**, *1*, 123–125.

Fox, T. G.; Flory, P. J. *Journal of Applied Physics*. **1950**, *21*, 581–591.

Fredrickson, G. H.; Helfand, E. *The Journal of Chemical Physics*. **1987**, *87*, 697.

Fringuelli, F.; Pizzo, F.; Tortoioli, S.; Vaccaro, L. *Journal of Organic Chemistry*. **2003**, *68*, 8248–8251.

Gao, C.; Tang, W.; Yan, D. *Macromolecular Chemistry and Physics*. **2001a**, *202*, 2623–2629.

Gao, C.; Tang, W.; Yan, D.; Wang, Z.; Zhu, P.; Tao, P. *Science in China Series B: Chemistry*. **2001b**, *44*, 207–215.

Gao, C.; Tang, W.; Yan, D.; Zhu, P.; Tao, P. *Polymer*. **2001c**, *42*, 3437–3443.

Gao, C.; Yan, D. *Macromolecules*. **2001d**, *34*, 156–161.

Gao, C.; Yan, D.; Tang, W. *Macromolecular Chemistry and Physics*. **2001e**, *202*, 3035–3042.

Gao, C.; Yan, D.; Zhang, B.; Chen, W. *Langmuir*. **2002**, *18*, 3708–3713.

Gao, C.; Yan, D.; Zhu, X.; Huang, W. *Polymer*. **2001f**, *42*, 7603–7610.

Garrett, J. T.; Xu, R.; Cho, J.; Runt, J. *Polymer*. **2003**, *44*, 2711–2719.

Gashgari, M. A.; Frank, C. W. *Macromolecules*. **1988**, *21*, 2782–2790.

Ge, Q.; Luo, X.; Rodriguez, E. D.; Zhang, X.; Mather, P. T.; Dunn, M. L.; Qi, H. J. *Journal of the Mechanics and Physics of Solids*. **2012**, *60*, 67–83.

Gedde, U. *Polymer Physics*. **1999**. Springer.

Gelles, R.; Frank, C. W. *Macromolecules*. **1982a**, *15*, 741–747.

Gelles, R.; Frank, C. W. *Macromolecules*. **1982b**, *15*, 1486–1491.

Giannotti, M.; Mondragon, I.; Galante, M.; Oyanguren, P. *Polymer International*. **2005**, *54*, 897–903.

Girard-Reydet, E.; Riccardi, C. *Macromolecules*. **1995**, *28*, 7608–7611.

Girard-Reydet, E.; Sautereau, H.; Pascault, J. *Polymer*. **1998**, *39*, 2269–2279.

Girard-Reydet, E.; Sautereau, H.; Pascault, J. P. *Polymer*. **1999**, *40*, 1677–1687.

Girard-Reydet, E.; Vicard, V.; Pascault, J. P.; Sautereau, H. *Journal of Applied Polymer Science*. **1997**, *65*, 2433–2445.

Glória, P. M. C.; Gut, J.; Gonalves, L. M.; Rosenthal, P. J.; Moreira, R.; Santos, M. M. M. *Bioorganic and Medicinal Chemistry*. **2011**, *19*, 7635–7642.

Goda, H.; Frank, C. W. *Chemistry of Materials*. **2001**, *13*, 2783–2787.

González-Benito, J.; Mike, F.; Baselga, J.; Lemetyinemm, H. *Journal of Applied Polymer Science*. **2002**, *86*, 2992–3000.

Gordon, M.; Ware, W. R. (Eds.). *The Exciplex*. **1975**. New York: Academic Press.

Grubbs, R. B.; Dean, J. M.; Broz, M. E.; Bates, F. S. *Macromolecules*. **2000**, *33*, 9522–9534.

Guan, J.; Song, Y.; Lin, Y.; Yin, X.; Zuo, M.; Zhao, Y.; Tao, X.; Zheng, Q. *Industrial and*

Engineering Chemistry Research. **2011**, *50*, 6517–6527.

Guilbault, G. G. (Ed.). *Practical Fluorescence*. **1990** (2nd ed.). New York: CRC Press.

Gutzler, R.; Lappe, S.; Mahata, K.; Schmittel, M.; Heckl, W. M.; Lackinger, M. *Chemical Communications (Cambridge, England)*. **2009**, 680–682.

Guzmán, D.; Ramis, X.; Fernández-Francos, X.; Serra, A. *Polymers*. **2015**, *7*, 680–694.

Halimehjani, A. Z.; Mohtasham, R.; Shockravi, A.; Martens, J. *RSC Advances.* **2016**, *6*, 75223–75226.

Hall, D. B.; Miller, R. D.; Torkelson, J. M. *Journal of Polymer Science, Part B: Polymer Physics*. **1997**, *35*, 2795–2802.

Harvey, C. P.; Tovar, J. D. *Journal of Polymer Science, Part A: Polymer Chemistry*. **2011**, *49*, 4861–4874.

Harvison, M. A.; Davis, T. P.; Lowe, A. B. *Polymer Chemistry*. **2011a**, *2*, 1347.

Harvison, M. A.; Lowe, A. B. *Macromolecular Rapid Communications*. **2011b**, *32*, 779–800.

Healy, M. S.; Hanson, J. E. *Journal of Applied Polymer Science*. **2007**, *104*, 360–364.

Hirayama, F. *The Journal of Chemical Physics*. **1965**, *42*, 3163.

Hotze, E. M.; Phenrat, T.; Lowry, G. V. *Journal of Environmental Quality*. **2010**, *39*, 1909–1924.

Houston, P. L. (Ed.). *Chemical Kinetics and Reaction Dynamics*. **2001**. McGraw-Hill.

Hoyle, C. E.; Bowman, C. N. *Angewandte Chemie - International Edition*. **2010a**, *49*, 1540–73.

Hoyle, C. E.; Kim, K. *Journal of Polymer Science, Part A: Polymer Chemistry* **1986**, *24*, 1879–1894.

Hoyle, C. E.; Lee, T. Y.; Roper, T. *Journal of Polymer Science, Part A: Polymer Chemistry*. **2004**, *42*, 5301–5338.

Hoyle, C. E.; Lowe, A. B.; Bowman, C. N. *Chemical Society Reviews*. **2010b**, *39*, 1355–1387.

Huang, W. M.; Ding, Z.; Wang, C. C.; Wei, J.; Zhao, Y.; Purnawali, H. *Materials Today*. **2010**, *13*, 54–61.

Huang, Y.; Zhou, J.; Luo, W. *International Journal of Polymer Analysis and Characterization*. **2015**, *20*, 660–669.

Hunter, C. A.; Sanders, J. K. M. *Journal of the American Chemical Society*. **1990**, *112*, 5525–5534.

Imai, Y.; Shimizu, H.; Sato, Y.; Ueda, M. *Journal of Polymer Science: Polymer Chemistry Edition*. **1981**, *19*, 3031–3034.

Inoue, T. *Progress in Polymer Science*. **1995**, *20*, 119–153.

Irusta, L.; Iruin, J. J.; Mendikute, G.; Fernández-Berridi, M. J. *Vibrational Spectroscopy*. **2005**, *39*, 144–150.

Itoh, H.; Kameyama, A.; Nishikubo, T. *Journal of Polymer Science, Part A: Polymer Chemistry*. **1996**, *34*, 217–225.

Jacobine, A. F. *In Radiation Curing in Polymer Science and Technology III*. **1993**. London: Elsevier.

Jaffrennou, B.; Me, F. *Journal of Polymer Science, Part B: Polymer Physics*. **2006**, 2821–2827.

Jansen, B. J. P.; Rastogi, S.; Meijer, H. E. H.; Lemstra, P. J. *Macromolecules*. **1999**, *32*, 6283–6289.

Javni, I.; Zhang, W.; Petrovic, Z. S. *Journal of Applied Polymer Science*. **2003**, *88*, 2912–2916.

Jian, Y.; He, Y.; Sun, Y.; Yang, H.; Yang, W.; Nie, J. *Journal of Materials Chemistry C*. **2013**, *1*, 4481–4489.

Jin, K.; Heath, W. H.; Torkelson, J. M. *Polymer (United Kingdom)*. **2015**, *81*, 70–78.

Jin, K.; Wilmot, N.; Heath, W. H.; Torkelson, J. M. *Macromolecules*. **2016**, *49*, 4115–4123.

Jung, M. E. In *Comprehensive Organic Synthesis*. **1991** (pp. 1–67).

Kade, M.; Burke, D.; Hawker, C. *Journal of Polymer Science, Part A: Polymer Chemistry*. **2010**, *48*, 743–750.

Karthikeyan, S.; Sijbesma, R. P. *Macromolecules*. **2009**, *42*, 5175–5178.

Kathalewar, M. S.; Joshi, P. B.; Sabnis, A. S.; Malshe, V. C. *RSC Advances*. **2013**, *3*, 4110–

4129.

Keddie, J. L.; Jones, R. A. L.; Cory, R. A. *Faraday Discussions*. **1994**, *98*, 219–230.

Keddie, J. L.; Jones, R. A. L.; Cory, R. A. *Europhysics Letters*. **2007**, *27*, 59–64.

Khan, M.; Khan, W.; Khan, S.; Iqbal, Y. *Journal of the Chemical Society of Pakistan*. **2005**, *27*, 20–23.

Kim, B. S.; Chiba, T.; Inoue, T. *Polymer*. **1993**, *34*, 2809–2815.

Kim, B. S.; Chiba, T.; Inoue, T. *Polymer*. **1995**, *36*, 43–47.

Kim, J.; Cho, J.; Ryba, E.; Bai, J. *Polymer Journal*. **2003**, *35*, 929–937.

Kim, S. D.; Torkelson, J. M. *Macromolecules*. **2002**, *35*, 5943–5952.

Klempner, D.; Frisch, K. C.; Xiao, H. X. *Polymer Engineering and Science*. **1985**, *25*, 488–493.

Koberstein, J. T.; Gancarz, I.; Clarke, T. C. *Journal of Polymer Science, Part B: Polymer Physics*. **1986**, *24*, 2487–2498.

Kojio, K.; Furukawa, M.; Nonaka, Y.; Nakamura, S. *Materials*. **2010**, *3*, 5097–5110.

Kojio, K.; Kugumiya, S.; Uchiba, Y.; Nishino, Y.; Furukawa, M. *Polymer Journal*. **2009**, *41*, 118–124.

Kojio, K.; Uchiba, Y.; Mitsui, Y.; Furukawa, M.; Sasaki, S.; Matsunaga, H.; Okuda, H. *Macromolecules*. **2007**, *40*, 2625–2628.

Kolb, H. C.; Finn, M. G.; Sharpless, K. B. *Angewandte Chemie International Edition*. **2001**, *40*, 2004–2021.

Koretsky, M. *Engineering and Chemical Thermodynamics*. **2004**. John Wiley & Sons.

Krausch, G. *Materials Science and Engineering: Reports*. **1995**, *14*, v–vi.

Kriisa, A.; Park, S. S.; Roth, C. B. *Journal of Polymer Science, Part B: Polymer Physics*. **2012**, *50*, 250–256.

Król, P. *Progress in Materials Science*. **2007a**, *52*, 915–1015.

Król, P.; Pilch-Pitera, B. *Journal of Applied Polymer Science*. **2007b**, *104*, 1464–1474.

Kultys, A.; Rogulska, M.; Głuchowska, H. *Polymer International*. **2011**, *60*, 652–659.

Kwei, T. K. *Journal of Applied Polymer Science*. **1982**, *27*, 2891–2899.

Kwisnek, L.; Nazarenko, S.; Hoyle, C. E. *Macromolecules*. **2009**, *42*, 7031–7041.

Lakowicz, J. R. *Principles of Fluorescence Spectroscopy* **2006**. Springer.

Lee, H. S.; Wang, Y. K.; Hsu, S. L. *Macromolecules*. **1987**, *20*, 2089–2095.

Lee, T. Y.; Smith, Z.; Reddy, S. K.; Cramer, N. B.; Bowman, C. N. *Macromolecules.* **2007**, *40*, 1466–1472.

Leibler, L. *Macromolecules.* **1980**, *13*, 1602–1617.

Leitsch, E. K. **2015**. *Polyurethane and polyurethane-like materials synthesized with a reduced reliance on isocyanate compounds.* Northwestern University.

Leitsch, E. K.; Heath, W. H.; Torkelson, J. M. *International Journal of Adhesion and Adhesives*. **2016**, *64*, 1–8.

Lendlein, A.; Jiang, H.; Junger, O.; Langer, R. *Nature*. **2005**, *434*, 879–882.

Lendlein, A.; Kelch, S. *Angewandte Chemie*. **2002**, *41*, 2043–2057.

Leonards, H.; Engelhardt, S.; Hoffmann, A.; Pongratz, L.; Schriever, S.; Bläsius, J.; Wehner, M.; Gillner, A. *Proceedings of the National Academy of Sciences of the United States of America*. **2015**, *9353*, 30–37.

Leung, L. M.; Koberstein, J. T. *Macromolecules*. **1986**, *19*, 706–713.

Li, G.; Randev, R. K.; Soeriyadi, A. H.; Rees, G.; Boyer, C.; Tong, Z.; Davis, T. P.; Becer, C. R.; Haddleton, D. M. *Polymer Chemistry*. **2010**, *1*, 1196.

Li, L.; Tsai, S. W.; Anderson, A. L.; Keire, D. A.; Raubitschek, A. A.; Shively, J. E. *Bioconjugate Chemistry*. **2002a**, *13*, 110–115.

Li, W.; Liu, M.; Qiu, F.; Shi, A. C. *Journal of Physical Chemistry B*. **2013**, *117*, 5280–5288.

Li, W.; Ryan, A. J.; Meier, I. K. *Macromolecules*. **2002b**, *35*, 5034–5042.

Li, Z.; Shen, W.; Liu, X.; Liu, R. *Polymer Chemistry* **2017**, 1579–1588.

Lipatov, Y. S.; Alekseeva, T. In K. Dusek (Ed.), *Advances in Polymer Science*. **2007** (208th ed.). Springer.

Liu, C.; Qin, H.; Mather, P. T. *Journal of Materials Chemistry*. **2007**, *17*, 1543–1558.

Liu, J.; Thompson, Z. J.; Sue, H. J.; Bates, F. S.; Hillmyer, M. A.; Dettloff, M.; Jacob, G.; Verghese, N.; Pham, H. *Macromolecules*. **2010**, *43*, 7238–7243.

Liu, M.; Tan, B. H.; Burford, R. P.; Lowe, A. B. *Polymer Chemistry*. **2013a**, *4*, 3300–3311.

Liu, Y. *Journal of Applied Polymer Science*. **2013b**, *127*, 3279–3292.

Liu, Y.; Sun, H.; Tan, H.; Du, X. *Journal of Applied Polymer Science*. **2013**, *127*, 3152–3158.

Lombardo, V. M.; Dhulst, E. A.; Leitsch, E. K.; Wilmot, N.; Heath, W. H.; Gies, A. P.; Miller, M. D.; Torkelson, J. M.; Scheidt, K. A. *European Journal of Organic Chemistry*. **2015**, 2791–2795.

Lopez-Jaramillo, F. J.; Ortega-Munõz, M.; Megia-Fernandez, A.; Hernandez-Mateo, F.; Santoyo-Gonzalez, F. *Bioconjugate Chemistry*. **2012**, *23*, 846–855.

Loureiro, R. M.; Amarelo, T. C.; Abuin, S. P.; Soulé, E. R.; Williams, R. J. J. *Thermochimica Acta*. **2015**, *616*, 79–86.

Lowe, A. B. *Polymer Chemistry*. **2010**, *1*, 17–36.

Lowe, A. B.; Bowman, C. N. (Eds.). *Thiol-X Chemistries in Polymer and Materials Science*. **2013**. Royal Society of Chemistry.

Lowe, A. B.; Harvison, M. A. *Australian Journal of Chemistry*. **2010**, *63*, 1251–1266.

Lu, Q. W.; Hoye, T. R.; Macosko, C. W. *Journal of Polymer Science, Part A: Polymer Chemistry*. **2002**, *40*, 2310–2328.

Luo, X.; Mather, P. T. *Current Opinion in Chemical Engineering*. **2013**, *2*, 103–111.

Lupu, M.; Epure, V.; Mococinschi, D.; Ioan, S. *Journal of Optoelectronics and Advancaed Materials*. **2007**, *9*, 985–989.

Lutolf, M. P.; Tirelli, N.; Cerritelli, S.; Cavalli, L.; Hubbell, J. A. *Bioconjugate Chemistry*. **2001**, *12*, 1051–1056.

Magnier-Bouvier, C.; Blazejewski, J. C.; Larpent, C.; Magnier, E. *Tetrahedron Letters*. **2006**, *47*, 9121–9124.

Martin, D. J.; Meijs, G. F.; Renwick, G. M.; Gunatillake, P. A.; McCarthy, S. J. *Journal of Applied Polymer Science*. **1996**, *60*, 557–571.

Martinez, C. R.; Iverson, B. L. *Chemical Science*. **2012**, *3*, 2191–2201.

Masri, M. S.; Friedman, M. *Journal of Protein Chemistry*. **1988**, *7*, 49–54.

Mather, B. D.; Viswanathan, K.; Miller, K. M.; Long, T. E. *Progress in Polymer Science*. **2006**, *31*, 487–531.

Mather, P. T.; Luo, X.; Rousseau, I. A. *Annual Review of Materials Research*. **2009**, *39*, 445–471.

Matsushima, H.; Shin, J.; Bowman, C. N.; Hoyle, C. E. *Journal of Polymer Science, Part A: Polymer Chemistry*. **2010**, *48*, 3255–3264.

McEwan, K. A.; Slavin, S.; Tunnah, E.; Haddleton, D. M. *Polymer Chemistry*. **2013**, *4*, 2608–2614.

McNair, O. D.; Sparks, B. J.; Janisse, A. P.; Brent, D. P.; Patton, D. L.; Savin, D. A. *Macromolecules*. **2013**, *46*, 5614–5621.

Meadows, D. C.; Gervay-Hague, J. *Medicinal Research Reviews*. **2006**, *26*, 793–814.

Mei, X.; Wolf, C. *Journal of Organic Chemistry*. **2005**, *70*, 2299–2305.

Meier-Westhues, U. *Polyurethanes: Coatings, Adhesives and Sealants*. **2007**. Hannover: Vincentz Network.

Meng, F.; Zheng, S.; Li, H.; Liang, Q.; Liu, T. *Macromolecules.* **2006**, *39*, 5072–5080.

Mijovic, J.; Wijayat, J. *Macromolecules.* **1992**, *25*, 979–985.

Mimura, K.; Ito, H.; Fujioka, H. *Polymer*. **2000**, *41*, 4451–4459.

Moghaddam, F. M.; Bardajee, G. R.; Chadorneshine Veranlou, R. O. *Synthetic Communications*. **2005**, *35*, 2427–2433.

Morales-Sanfrutos, J.; Lopez-Jaramillo, J.; Ortega-Muñoz, M.; Megia-Fernandez, A.; Perez-Balderas, F.; Hernandez-Mateo, F.; Santoyo-Gonzalez, F. *Organic & Biomolecular Chemistry*. **2010**, *8*, 667–675.

Morgan, C. R.; Magnotta, F.; Ketley, A. D. *Journal of Polymer Science, Part A: Polymer Chemistry*. **1977**, *15*, 627–645.

Morpurgo, M.; Veronese, F. M.; Kachensky, D.; Harris, J. M.; Farmaceutiche, S. *Bioconjugate Chemistry*. **1996**, *7*, 363–368.

Morris, C.; Ryder, A. G. In C. D. Geddes (Ed.), *Reviews in Fluorescence*. **2016,** 97–126. Springer International Publishing.

Mundra, M. K.; Donthu, S. K.; Dravid, V. P.; Torkelson, J. M. *Nano Letters*. **2007**, *7*, 713–718.

Nair, D. P.; Cramer, N. B.; Gaipa, J. C.; McBride, M. K.; Matherly, E. M.; McLeod, R. R.; Shandas, R.; Bowman, C. N. *Advanced Functional Materials*. **2012**, *22*, 1502–1510.

Nair, D. P.; Podgórski, M.; Chatani, S.; Gong, T.; Xi, W.; Fenoli, C. R.; Bowman, C. N. *Chemistry of Materials*. **2014**, *26*, 724–744.

Napolitano, S.; Wübbenhorst, M. *Nature Communications*. **2011**, *2*, 260.

Narayanan, J.; Jungman, M. J.; Patton, D. L. *Reactive and Functional Polymers*. **2012**, *72*, 799–806.

Nguyen, L.-T. T.; Gokmen, M. T.; Du Prez, F. E. *Polymer Chemistry* **2013**, *4*, 5527–5536.

Nohra, B.; Candy, L.; Blanco, J. F.; Guerin, C.; Raoul, Y.; Mouloungui, Z. *Macromolecules*. **2013**, *46*, 3771–3792.

Odian, G. *Principles of Polymerization*. **2004** (Fourth). John Wiley & Sons.

Oertel, G. *Polyurethane Handbook*. **1993** (2nd ed.). Munich: Hanser.

Ortiz, R. A.; García Valdez, A. E.; Navarro Tovar, A. G.; Hilario de la Cruz, A. A.; González Sánchez, L. F.; García Trejo, J. H.; Espinoza Muñoz, J. F.; Sangermano, M. *Journal of Polymer Research*. **2014**, *21*, 504.

Ortiz, R. A.; Urbina, B. A. P. *Journal of Polymer Science, Part A: Polymer Chemistry*. **2007**, *45*, 4829–4843.

Ortiz, R. A.; Urbina, B. A. P.; Santos, R. G.; Duarte, L. B.; Valdez, A. E. G.; Soucek, M. D. *Macromolecular Materials and Engineering*. **2008a**, *293*, 731–739.

Ortiz, R. A.; Valdéz, A. E. G.; Duarte, L. B.; Santos, R. G.; Flores, L. R. O.; Soucek, M. D. *Macromolecular Chemistry and Physics*. **2008b**, *209*, 2157–2168.

Park, J. M.; Mauri, R.; Anderson, P. D. *Chemical Engineering Science*. **2012**, *80*, 270–278.

Pascault, J. P.; Williams, R. J. J. *Epoxy Polymers*. **2010**. Weinheim, Germany: Wiley.

Patai, S. *The Chemistry of the Thiol Group*. **1974**. London: Wiley.

Petrovic, Z. S. *Polymer Reviews*. **2008**, *48*, 109–155.

Petrović, Z. S.; Javni, I.; Divjaković, V. *Journal of Polymer Science, Part B: Polymer Physics*. **1998**, *36*, 221–235.

Pinal, R. *Entropy*. **2008**, *10*, 207–223.

Podgórski, M.; Chatani, S.; Bowman, C. N. *Macromolecular Rapid Communications*. **2014**, *35*, 1497–1502.

Podsiadlo, P.; Qin, M.; Cuddihy, M.; Zhu, J.; Critchley, K.; Kheng, E.; Kaushik, A. K.; Qi, Y.; Kim, H. S.; Noh, S. T.; Arruda, E. M.; Waas, A. M.; Kotov, N. A. *Langmuir*. **2009**, *25*, 14093–14099.

Pongkitwitoon, S.; Hernández, R.; Weksler, J.; Padsalgikar, A.; Choi, T.; Runt, J. *Polymer*. **2009**, *50*, 6305–6311.

Priestley, R. D.; Ellison, C. J.; Broadbelt, L. J.; Torkelson, J. M. *Science (New York, N.Y.)*. **2005**, *309*, 456–459.

Priestley, R. D.; Mundra, M. K.; Barnett, N. J.; Broadbelt, L. J.; Torkelson, J. M. *Australian Journal of Chemistry*. **2007**, *60*, 765–771.

Prisacariu, C. *Polyurethane Elastomers*. **2011**. New York: Springer-Verlag

Procházka, K. In *Fluorescence Studies of Polymer Containing Systems*. **2016** (pp. 151–202). Springer International Publishing.

Pukánszky, B.; Bagdi, K.; Tóvölgyi, Z.; Varga, J.; Botz, L.; Hudak, S.; Dóczi, T. *European Polymer Journal*. **2008**, *44*, 2431–2438.

Rahane, S. B.; Hensarling, R. M.; Sparks, B. J.; Stafford, M.; Patton, D. L. *Journal of Materials*

Chemistry. **2012**, *22*, 932–943.

Ratna, D.; Karger-Kocsis, J. *Journal of Materials Science*. **2008**, *43*, 254–269.

Ritzenthaler, S.; Court, F.; David, L.; Girard-Reydet, E.; Leibler, L.; Pascault, J. P. *Macromolecules*. **2002**, *35*, 6245–6254.

Rizzi, S. C.; Hubbell, J. A. *Biomacromolecules*. **2005**, *6*, 1226–38.

Rozenberg, B. A. *Epoxy Resins and Composites II*. **1986**, 115–161.

Ruiz-Pérez, L.; Royston, G. J.; Fairclough, J. P. A.; Ryan, A. J. *Polymer*. **2008**, *49*, 4475–4488.

Rydholm, A. E.; Held, N. L.; Benoit, D. S. W.; Bowman, C. N.; Anseth, K. S. *Journal of Biomedical Materials Research Part A*. **2008**, *86*, 23–30.

Saidi, M. R.; Pourshojaei, Y.; Aryanasab, F. *Synthetic Communications*. **2009**, *39*, 1109–1119.

Saito, H.; Tsutsumi, D.; Inoue, T. *Polymer Journal*. **1990**, *2*, 128–134.

Sakamoto, H.; Asakawa, H.; Fukuma, T.; Fujita, S.; Suye, S.-I. *Science and Technology of Advanced Materials*. **2014**, *15*, 1–6.

Sami, S.; Yildirim, E.; Yurtsever, M.; Yurtsever, E.; Yilgör, E.; Yilgör, I.; Wilkes, G. L. *Polymer (United Kingdom)*. **2014**, *55*, 4563–4576.

Sangermano, M.; Cerrone, M.; Colucci, G.; Roppolo, I.; Ortiz, R. A. *Polymer International*. **2010**, *59*, 1046–1051.

Sangermano, M.; Colucci, G.; Fragale, M.; Rizza, G. *Reactive and Functional Polymers*. **2009**, *69*, 719–723.

Sangermano, M.; Roppolo, I.; Ortiz, R. A.; Tovar, A. G. N.; Valdez, A. E. G.; Duarte, M. L. B. *Progress in Organic Coatings*. **2015**, *78*, 244–248.

Schneider, N. S.; Matton, R. W. *Polymer Engineering and Science*. **1979**, *19*, 1122–1128.

Schreck, K. M.; Leung, D.; Bowman, C. N. *Macromolecules*. **2011**, *44*, 7520–7529.

Seefried, C. G.; Koleske, J. V.; Critchfield, F. E. *Journal of Applied Polymer Science*. **1975**, *19*, 2493–2502.

Sheth, J. P.; Klinedinst, D. B.; Wilkes, G. L.; Iskender, Y.; Yilgör, I. *Polymer*. **2005**, *46*, 7317–

7322.

Shibanov, Y. D.; Godovsky, Y. K. *Colloid & Polymer Science*. **1985**, *263*, 202–216.

Shin, J.; Matsushima, H.; Comer, C. M.; Bowman, C. N.; Hoyle, C. E. *Chemistry of Materials*. **2010**, *22*, 2616–2625.

Shin, J.; Nazarenko, S.; Hoyle, C. E. *Macromolecules*. **2009**, *42*, 6549–6557.

Shultz, A. R.; Flory, P. J. *Journal of the American Chemical Society*. **1952**, *74*, 4760–4767.

Simpkins, N. S. *Tetrahedron*. **1990**, *46*, 6951–6984.

Slavin, S.; Khoshdel, E.; Haddleton, D. M. *Polymer Chemistry*. **2012**, *3*, 1461–1466.

Sperling, L. H.; Mishra, V. *Polymers for Advanced Technologies*. **1996**, *7*, 197–208.

Stewart-Sloan, C. R.; Thomas, E. L. *European Polymer Journal*. **2011**, *47*, 630–646.

Stuparu, M. C.; Khan, A. *Journal of Polymer Science, Part A: Polymer Chemistry*. **2016**, *54*, 3057–3070.

Sun, X.-D. D.; Sung, C. S. P. *Macromolecules*. **1996**, *29*, 3198–3202.

Sung, C. S. P.; Schneider, N. S. *Macromolecules*. **1974**, *8*, 68–73.

Suthar, B.; Xiao, H. X.; Klempner, D.; Frisch, K. C. *Polymers for Advanced Technologies.* **1995**, *7*, 221–233.

Sutton, D.; Stanford, J. L.; Ryan, A. *Journal of Macromolecular Science, Part B*. **2004**, *43*, 219–232.

Suzuki, M.; Takahashi, T.; Aoyagi, S. *Micromachines*. **2012**, *3*, 315–324.

Szczepanskia, C. R.; Pfeiferb, C. S.; Stansbury, J. W. *Polymer*. **2012**, *53*, 4694–4701.

Tang, C. N.; Nulwala, H. B.; Damodaran, K.; Kaur, P.; Luebke, D. R. *Journal of Polymer Science, Part A: Polymer Chemistry*. **2011**, *49*, 2024–2032.

Tao, H. J.; Meuse, C. W.; Yang, X. Z.; Macknight, W. J.; Hsu, S. L. *Macromolecules*. **1994**, *27*, 7146–7151.

Tcharkhtchi, A.; Abdallah-Elhirtsi, S.; Ebrahimi, K.; Fitoussi, J.; Shirinbayan, M.; Farzaneh, S. *Polymers*. **2014**, *6*, 1144–1163.

Teo, L.-S.; Chen, C.-Y.; Kuo, J.-F. *Macromolecules*. **1997**, *30*, 1793–1799.

Teyssot, M.-L.; Fayolle, M.; Philouze, C.; Dupuy, C. *European Journal of Organic Chemistry*. **2003**, *2003*, 54–62.

Torkelson, J. M.; Tirrell, M.; Frank, C. W. *Macromolecules*. **1984**, *17*, 1505–1512.

Tosatti, S.; De Paul, S. .; Askendal, A.; VandeVondele, S.; Hubbell, J. A.; Tengvall, P.; Textor, M. *Biomaterials*. **2003**, *24*, 4949–4958.

Tsai, F. J. *Macromolecules*. **1988**, *21*, 1026–1033.

Tsai, Y.-M.; Yu, T.-L.; Tseng, Y.-H. *Polymer International*. **1998**, *47*, 445–450.

Tunca, U. *Journal of Polymer Science, Part A: Polymer Chemistry*. **2014**, *52*, 3147–3165.

Uygun, M.; Tasdelen, M. A.; Yagci, Y. *Macromolecular Chemistry and Physics*. **2010**, *211*, 103–110.

Varley, R. J.; Hodgkin, J. H.; Hawthorne, D. G.; Simon, G. P. *Journal of Applied Polymer Science*. **1996**, *60*, 2251–2263.

Vatanparast, R.; Li, S.; Hakala, K.; Lemmetyinen, H. *Macromolecules*. **2000**, *33*, 438–443.

Velankar, S.; Cooper, S. L. *Macromolecules*. **1998**, *31*, 9181–9192.

Wabnitz, T. C.; Spencer, J. B. *Organic Letters*. **2003**, *5*, 2141–2144.

Wabnitz, T. C.; Yu, J. Q.; Spencer, J. B. *Chemistry - A European Journal*. **2004**, *10*, 484–493.

Wang, C.; Qi, C. *Tetrahedron*. **2013**, *69*, 5348–5354.

Wang, F. C.; Feve, M.; Lam, T. M.; Pascault, J. P. *Journal of Polymer Science, Part B: Polymer Physics*. **1994**, *32*, 1305–1313.

Wang, H.; Cheng, F.; Li, M.; Peng, W.; Qu, J. *Langmuir*. **2015**, *31*, 3413–3421.

Wang, R.; Wang, L.; Zhou, L.; Su, Y.; Qiu, F.; Wang, D.; Wu, J.; Zhu, X.; Yan, D. *Journal of Materials Chemistry*. **2012**, *22*, 15227–15234.

Wang, S.; Sook, C.; Sung, P. *Macromolecules.* **2002**, 883–888.

Waters, M. L. *Biopolymers*. **2004**, *76*, 435–445.

Watts, W. E.; Knipe, A.C. *Organic Reaction Mechanisms: An Annual Survey.* **2001,** (Vol. 6).

New York: John Wiley & Sons.

Wei, H.; Li, Q.; Ojelade, M.; Madbouly, S.; Otaigbe, J. U.; Hoyle, C. E. *Macromolecules*. **2007**, *40*, 8788–8793.

Whitesides, G. M.; Grzybowski, B. *Science (New York, N.Y.)*. **2002**, *295*, 2418–21.

Wicks, D. A.; Wicks, Z. W. *Progress in Organic Coatings*. **1999**, *36*, 148–172.

Williams, R. J. J.; Rozenberg, B. A.; Pascault, J. P. In *Advances in Polymer Science.* **1997** (Vol. 128). Berlin: Springer Verlag.

Winnik, F. M. *Chem. Rev.* **1993**, *93*, 587–614.

Wojtecki, R. J.; Nelson, A. *Journal of Polymer Science, Part A: Polymer Chemistry*. **2015**, *54*, 457–472.

Woo, E. J.; Farber, G.; Farris, R. J.; Lillya, C. P.; Chienf, J. C. W. *Polymer Engineering and Science*. **1985**, *25*, 834–840.

Wu, D.; Liu, Y.; He, C.; Chung, T.; Goh, S. *Macromolecules*. **2004**, *37*, 6763–6770.

Xie, T. *Polymer*. **2011**, *52*, 4985–5000.

Yamanaka, K.; Takagi, Y.; Inoue, T. *Polymer.* **1989**, *60*, 1839–1844.

Yan, D.; Gao, C. *Macromolecules*. **2000**, *33*, 7693–7699.

Yan, X.; Wang, F.; Zheng, B.; Huang, F. *Chemical Society Reviews*. **2012**, *41*, 6042.

Ye, S.; Cramer, N. B.; Smith, I. R.; Voigt, K. R.; Bowman, C. N. *Macromolecules*. **2011**, *44*, 9084–9090.

Yilgör, E.; Burgaz, E.; Yurtsever, E.; Yilgör, I. *Polymer*. **2000**, *41*, 849–857.

Yilgör, I.; Yilgör, E. *Polymer Reviews*. **2007**, *47*, 487–510.

Yilgör, I.; Yilgör, E.; Guler, I. G.; Ward, T. C.; Wilkes, G. L. *Polymer*. **2006**, *47*, 4105–4114.

Yilgör, I.; Yilgör, E.; Wilkes, G. L. *Polymer*. **2015**, *58*, A1–A36.

Yu, R.; Zheng, S.; Li, X.; Wang, J. *Macromolecules*. **2012**, *45*, 9155–9168.

Zacharaisse, K. A.; Duveneck, G.; Kuhnle, W.; Leinhos, U.; Reynders, P. In K. Honda (Ed.), *Photochemical Processes in Organized Molecular Systems*. **1991** (pp. 83–100).

Amsterdam: Elsevier.

Zhang, C.; Hu, J.; Chen, S.; Ji, F. *Journal of Molecular Modeling*. **2010**, *16*, 1391–1399.

Zhang, C.; Hu, J.; Li, X.; Wu, Y.; Han, J. *Journal of Physical Chemistry A*. **2014a**, *118*, 12241–12255.

Zhang, C.; Hu, J.; Wu, Y. *Journal of Molecular Structure*. **2014b**, *1072*, 13–19.

Zhang, X.; Yi, X.; Xu, Y. *Frontiers of Chemical Engineering in China*. **2008**, *2*, 276–285.

Zheng, Z.; Pan, C.; Wang, D.; Liu, Y. *Macromolecular Chemistry and Physics*. **2005**, *206*, 2182–2189.

Zhuravlev, E.; Schmelzer, J. W. P.; Wunderlich, B.; Schick, C. *Polymer*. **2011**, *52*, 1983–1997.

Zou, R.; Tan, J.; Liu, K.; Liang, L.; Cheng, X.; Zhang, X.; Zhang, L.; Yue, D. *RSC Advances*. **2016**, *6*, 20198–20201.